

Drivers of plant nutrient acquisition and allocation strategies and their influence  
on plant responses to environmental change

by

Evan A. Perkowski, B.S.

A Dissertation

In

Biological Sciences

Submitted to the Graduate Faculty  
of Texas Tech University in  
Partial Fulfillment of  
the Requirements for  
the Degree of

Doctor of Philosophy

Approved

Nicholas G. Smith, Ph.D.  
Chair of Committee

Aimée T. Classen, Ph.D.

Natasja van Gestel, Ph.D.

Lindsey C. Slaughter, Ph.D.

Dylan W. Schwilk, Ph.D.

Mark Sheridan, Ph.D.  
Dean of the Graduate School

May 2023

Copyright 2023, Evan A. Perkowski

## Acknowledgements

Placeholder for text

## Table of Contents

<b>Acknowledgements . . . . .</b>	ii
<b>Abstract . . . . .</b>	vii
<b>List of Tables . . . . .</b>	viii
<b>List of Figures . . . . .</b>	x
<b>1. Introduction . . . . .</b>	1
<b>2. Structural carbon costs to acquire nitrogen are determined by nitrogen and light availability in two species with different nitrogen acquisition strategies . . . . .</b>	8
2.1    Introduction . . . . .	8
2.2    Methods . . . . .	12
2.2.1 <i>Experiment setup</i> . . . . .	12
2.2.2 <i>Plant measurements and calculations</i> . . . . .	13
2.2.3 <i>Statistical analyses</i> . . . . .	14
2.3    Results . . . . .	16
2.3.1 <i>Carbon costs to acquire nitrogen</i> . . . . .	16
2.3.2 <i>Whole plant nitrogen biomass</i> . . . . .	19
2.3.3 <i>Root carbon biomass</i> . . . . .	21
2.3.4 <i>Root nodule biomass</i> . . . . .	23
2.4    Discussion . . . . .	27
<b>3. Soil nitrogen availability modifies leaf nitrogen economies in mature temperate deciduous forests: a direct test of photosynthetic least-cost theory . . . . .</b>	35
3.1    Introduction . . . . .	35
3.2    Methods . . . . .	39
3.2.1 <i>Study site description</i> . . . . .	39
3.2.2 <i>Experimental design</i> . . . . .	40
3.2.3 <i>Leaf gas exchange and trait measurements</i> . . . . .	40
3.2.4 <i><math>A_{net}/C_i</math> curve-fitting and parameter estimation</i> . . . . .	43

3.2.5 <i>Proportion of leaf nitrogen allocated to photosynthesis and structure</i> . . . . .	45
3.2.6 <i>Tradeoffs between nitrogen and water use</i> . . . . .	46
3.2.7 <i>Soil nitrogen availability and pH</i> . . . . .	47
3.2.8 <i>Statistical analyses</i> . . . . .	49
3.3 Results . . . . .	51
3.3.1 <i>Leaf N content</i> . . . . .	51
3.3.2 <i>Net photosynthesis and leaf biochemistry</i> . . . . .	54
3.3.3 <i>Leaf N allocation</i> . . . . .	57
3.3.4 <i>Tradeoffs between nitrogen and water use</i> . . . . .	60
3.4 Discussion . . . . .	63
3.4.1 <i>Soil nitrogen availability modifies tradeoffs between nitrogen and water use</i> . . . . .	64
3.4.2 <i>Soil pH did not modify tradeoffs between nitrogen and water usage</i> . . . . .	66
3.4.3 <i>Species identity explains a large amount of variation in leaf and whole plant traits</i> . . . . .	67
3.4.4 <i>Implications for photosynthetic least-cost theory model development</i> . . . . .	68
3.4.5 <i>Conclusions</i> . . . . .	70
4. The relative cost of resource use for photosynthesis drives variance in leaf nitrogen content across climate and soil resource availability gradients . . . . .	71
4.1 Introduction . . . . .	71
4.2 Methods . . . . .	73
4.2.1 <i>Site descriptions and sampling methodology</i> . . . . .	73
4.2.2 <i>Leaf trait measurements</i> . . . . .	73
4.2.3 <i>Site climate data</i> . . . . .	79
4.2.4 <i>Site edaphic characteristics</i> . . . . .	79
4.2.5 <i>Plant functional group assignments</i> . . . . .	81
4.2.6 <i>Data analysis</i> . . . . .	82

4.3 Results . . . . .	84
4.3.1 Cost to acquire nitrogen relative to water ( $\beta$ ) . . . . .	84
4.3.2 Leaf $C_i:C_a$ . . . . .	88
4.3.3 Leaf nitrogen content . . . . .	91
4.3.4 Structural equation model . . . . .	95
4.4 Discussion . . . . .	98
<b>5. Optimal resource investment to photosynthetic capacity maximizes nutrient allocation to whole plant growth under elevated CO<sub>2</sub> . . . . .</b>	<b>99</b>
5.1 Introduction . . . . .	99
5.2 Methods . . . . .	104
5.2.1 Seed treatments and experimental design . . . . .	104
5.2.2 Growth chamber conditions . . . . .	105
5.2.3 Leaf gas exchange measurements . . . . .	107
5.2.4 Leaf trait measurements . . . . .	108
5.2.5 $A/C_i$ curve fitting and parameter estimation . . . . .	110
5.2.6 Stomatal limitation . . . . .	110
5.2.7 Proportion of leaf nitrogen allocated to photosynthesis and structure . . . . .	111
5.2.8 Whole plant traits . . . . .	113
5.2.9 Statistical analyses . . . . .	115
5.3 Results . . . . .	117
5.3.1 Leaf nitrogen content, chlorophyll content, and mass per area . . . . .	117
5.3.2 Leaf biochemistry and stomatal conductance . . . . .	121
5.3.3 Leaf nitrogen allocation . . . . .	125
5.3.4 Whole plant growth and total leaf area . . . . .	129
5.3.5 Carbon costs to acquire nitrogen . . . . .	129
5.3.6 Nitrogen fixation . . . . .	133
5.4 Discussion . . . . .	137

5.4.1	<i>Soil nitrogen fertilization has divergent effects on leaf and whole plant acclimation responses to CO<sub>2</sub></i>	138
5.4.2	<i>Implications for future model development</i>	142
5.4.3	<i>Study limitations and future directions</i>	143
5.4.4	<i>Conclusions</i>	145
6.	<b>Conclusions</b>	147
	<b>References</b>	149

**Abstract**

## List of Tables

2.1 Analysis of variance results exploring species-specific effects of light availability, nitrogen fertilization, and their interactions on carbon costs to acquire nitrogen, whole-plant nitrogen biomass, and root carbon biomass . . . . .	17
2.2 Analysis of variance results exploring effects of light availability, nitrogen fertilization, and their interactions on <i>G. max</i> root nodule biomass and the ratio of root nodule biomass to root biomass* . . . . .	24
2.3 Slopes of the regression line describing the relationship between each dependent variable and nitrogen fertilization at each light level* . . . . .	25
3.1 Effects of soil N availability, soil pH, and species on leaf N content per unit leaf area ( $N_{\text{area}}$ ), leaf N content per unit leaf mass ( $N_{\text{mass}}$ ), and leaf mass per unit leaf area ( $M_{\text{area}}$ ) . . . . .	52
3.2 Effects of soil N availability, soil pH, species, and $N_{\text{area}}$ on leaf biochemistry . . . . .	55
3.3 Effects of soil N availability, soil pH, and species on the proportion of leaf nitrogen content allocated to photosynthesis, Rubisco, bioenergetics, and structure . . . . .	58
3.4 Effects of soil N availability, soil pH, species, and $N_{\text{area}}$ on tradeoffs between nitrogen and water use . . . . .	61

5.1 Effects of soil nitrogen fertilization, inoculation, and CO <sub>2</sub> treatments on $N_{\text{area}}$ , $N_{\text{mass}}$ , $M_{\text{area}}$ , and $Chl_{\text{area}}$ . . . . .	119
5.2 Effects of soil nitrogen fertilization, inoculation, and CO <sub>2</sub> on leaf biochemistry . . . . .	123
5.3 Effects of soil N availability, soil pH, species, and $N_{\text{area}}$ on leaf nitrogen allocation . . . . .	127
5.4 Effects of soil N availability, soil pH, species, and $N_{\text{area}}$ on total leaf area, whole plant biomass, and costs of nitrogen acquisition . . . . .	131
5.5 Effects of soil N availability, soil pH, species, and $N_{\text{area}}$ on leaf biochemistry . . . . .	135

## List of Figures

2.1 Relationships between soil nitrogen fertilization and light availability on carbon costs to acquire nitrogen in <i>G. hirsutum</i> and <i>G. max</i> . . . . .	18
2.2 Relationships between soil nitrogen fertilization and light availability on whole-plant nitrogen biomass in <i>G. hirsutum</i> and <i>G. max</i> . . . . .	20
2.3 Relationships between soil nitrogen fertilization and light availability on root carbon biomass in <i>G. hirsutum</i> and <i>G. max</i> . . . . .	22
2.4 Effects of shade cover and nitrogen fertilization on root nodule biomass and the ratio of root nodule biomass to root biomass in <i>G. max</i> . . . . .	26
3.1 Effects of soil N availability and species on leaf N content per unit leaf area, leaf nitrogen content per unit leaf biomass, and leaf mass per leaf area . . . . .	53
3.2 Effects of soil N availability, species, and leaf N content leaf biochemistry . . . . .	56
3.3 Effects of soil N availability, species, and leaf N content on the fraction of leaf nitrogen allocated to photosynthesis and structure	59
3.4 Effects of soil N availability, species, and leaf N content on tradeoffs between nitrogen and water use . . . . .	62

4.1	Maps that detail site locations along 2006-2020 mean annual precipitation (panel A) and mean annual temperature (panel B) gradients in Texas, USA. . . . .	78
4.2	Effects of soil nitrogen availability and soil moisture on the unit cost ratio $\beta$ . . . . .	87
4.3	Effects of 4-day mean vapor pressure deficit, 2-day soil moisture (per water holding capacity), and soil nitrogen availability on $\chi$ . . . . .	90
4.4	Effects of $\chi$ , soil nitrogen availability, and soil moisture on leaf nitrogen content per unit leaf area, leaf nitrogen content per unit leaf biomass, and leaf mass per area. . . . .	94
4.5	Structural equation model results exploring direct and indirect drivers of $N_{\text{area}}$ . . . . .	97
5.1	Effects of CO <sub>2</sub> , fertilization, and inoculation on leaf nitrogen per unit leaf area, leaf nitrogen content, leaf mass per unit leaf area, and chlorophyll content per unit leaf area. . . . .	120
5.2	Effects of CO <sub>2</sub> , fertilization, and inoculation on maximum rate of Rubisco carboxylation, the maximum rate of RuBP regeneration, and the ratio of the maximum rate of RuBP regeneration to the maximum rate of Rubisco carboxylation leaf mass per unit leaf area, dark respiration, stomatal conductance, and stomatal limitation. . .	124
5.3	Effects of CO <sub>2</sub> , fertilization, and inoculation on the relative fraction of leaf nitrogen allocated to photosynthesis and the fraction of leaf nitrogen allocated to structure. . . . .	128

5.4 Effects of CO <sub>2</sub> , fertilization, and inoculation on total leaf area, total biomass, and structural carbon costs to acquire nitrogen. . . . .	132
5.5 Effects of CO <sub>2</sub> , fertilization, and inoculation on nodule biomass, nodule: root biomass, and percent nitrogen fixed from the atmosphere. . . . .	136

1                   **Chapter 1**  
2                   **Introduction**

3       Photosynthesis represents the largest carbon flux between the atmosphere  
4   and biosphere, and is regulated by complex ecosystem carbon and nutrient cy-  
5   cles (Hungate et al. 2003; IPCC 2021). As a result, the inclusion of robust,  
6   empirically tested representations of photosynthetic processes is critical in order  
7   for terrestrial biosphere models to accurately and reliably simulate carbon and  
8   nutrient fluxes between the atmosphere and terrestrial biosphere (Wieder et al.  
9   2015; Smith and Dukes 2013; Prentice et al. 2015; Oreskes et al. 1994). Despite  
10   evidence that the inclusion of coupled carbon and nutrient cycles can improve  
11   model uncertainty, widespread divergence in predicted carbon and nutrient fluxes  
12   is still apparent across model products (Arora et al. 2020; Friedlingstein et al.  
13   2014; Davies-Barnard et al. 2020). Divergence in predicted carbon and nutrient  
14   fluxes across terrestrial biosphere models may be due to an incomplete under-  
15   standing of how plants acclimate to changing environments (Smith and Dukes  
16   2013; Davies-Barnard et al. 2020), as terrestrial biosphere models are sensitive to  
17   the formulation of photosynthetic processes (Ziehn et al. 2011; Bonan et al. 2011;  
18   Booth et al. 2012; Smith et al. 2016; Smith et al. 2017; Rogers et al. 2017).

19       Many terrestrial biosphere models predict leaf-level photosynthesis through  
20   linear relationships between area-based leaf nitrogen content and the maximum  
21   rate of Ribulose-1,5-bisphosphate carboxylase/oxygenase ("Rubisco"), following  
22   from the idea that large fractions of nitrogen allocated to leaf tissue are allocated  
23   to the construction and maintenance of Rubisco (Evans 1989). The inclusion of

24 coupled carbon and nutrient cycles in terrestrial biosphere models (Shi et al. 2016;  
25 Braghieri et al. 2022) allows for the prediction of leaf nitrogen content through  
26 soil nitrogen availability, which causes models to indirectly predict photosynthetic  
27 processes through shifts in soil nitrogen availability (Smith et al. 2014; Lawrence  
28 et al. 2019). While these patterns are commonly observed in ecosystems globally  
29 (Brix 1971; Evans 1989; Liang et al. 2020; Firn et al. 2019), this formulation of  
30 photosynthetic processes does not allow for the prediction of leaf and whole plant  
31 acclimation responses to changing environments (Smith and Dukes 2013; Rogers  
32 et al. 2017; Harrison et al. 2021). Incorporating leaf and whole plant acclimation  
33 schemes in terrestrial biosphere models is important (Smith and Dukes 2013),  
34 particularly because recent work indicates that variance in leaf nitrogen content  
35 and leaf photosynthesis across environmental gradients may be better explained  
36 as an integrated product of leaf acclimation responses to changing climates and  
37 soil nitrogen availability than soil nitrogen availability alone (Dong et al. 2017;  
38 Dong et al. 2020; Smith et al. 2019; Querejeta et al. 2022; Dong et al. 2022;  
39 Westerband et al. 2023).

40 Photosynthetic least-cost theory (Prentice et al. 2014; Wang et al. 2017;  
41 Smith et al. 2019; Scott and Smith 2022; Harrison et al. 2021) provides a con-  
42 temporary framework for predicting leaf and whole plant acclimation responses  
43 to environmental change. The theory, which unifies photosynthetic optimal coor-  
44 dination (Chen et al. 1993; Maire et al. 2012) and least-cost (Wright et al. 2003)  
45 theories, posits that plants optimize photosynthetic processes by minimizing the  
46 summed cost of nitrogen and water use (referred to here and in the rest of this  
47 dissertation as  $\beta$ ). Photosynthetic processes are optimized such that nitrogen is

48 allocated to photosynthetic enzymes in to allow net photosynthesis rates to be  
49 equally co-limited by the maximum rate of Rubisco carboxylation and the max-  
50 imum rate of Ribulose-1,5-bisphosphate (RuBP) regeneration (Chen et al. 1993;  
51 Maire et al. 2012). The theory indicates that costs of nitrogen and water use  
52 are substitutable such that, in a given environment, optimal photosynthesis rates  
53 can be achieved by sacrificing inefficient use of a relatively more abundant (and  
54 less costly to acquire) resource for more efficient use of a relatively less abundant  
55 (and more costly to acquire) resource. These predictions imply that acclimation  
56 responses to changing environments may be partially driven by tradeoffs between  
57 nitrogen and water use, though empirical tests of the theory are sparse.

58 Optimality models leveraging patterns expected from photosynthetic least-  
59 cost theory have been developed for both C<sub>3</sub> (Wang et al. 2017; Smith et al. 2019;  
60 Stocker et al. 2020) and more recently for C<sub>4</sub> species (Scott and Smith 2022). Such  
61 models show broad agreement with patterns observed across environmental gradi-  
62 ents (Paillassa et al. 2020; Querejeta et al. 2022; Smith et al. 2019; Westerband  
63 et al. 2023), and are capable of reconciling dynamic leaf nitrogen-photosynthesis  
64 relationships and acclimation responses to elevated CO<sub>2</sub>, temperature, light avail-  
65 ability, and vapor pressure deficit (Dong et al. 2017; Dong et al. 2020; Dong et al.  
66 2022; Dong et al. 2022; Smith and Keenan 2020; Luo et al. 2021; Peng et al. 2021;  
67 Querejeta et al. 2022; Westerband et al. 2023). Current versions of optimality  
68 models that invoke patterns expected from photosynthetic least-cost theory hold  
69  $\beta$  constant across growing environments. As growing evidence suggests that costs  
70 of nitrogen use change across resource availability and climatic gradients in species  
71 with different nutrient acquisition strategies (Fisher et al. 2010; Brzostek et al.

72 2014; Allen et al. 2020; Terrer et al. 2018), one might expect that  $\beta$  should  
73 dynamically change across environments and in species with different acquisition  
74 strategies. However, manipulative experiments that test mechanisms underlying  
75 nitrogen-water use tradeoffs and leaf nitrogen-photosynthesis relationships pre-  
76 dicted from theory are rare, and no study has related these patterns to shifts in  $\beta$   
77 or across species with different nutrient acquisition strategies. Understanding the  
78 dynamicism of  $\beta$  across different environmental contexts and impacts of  $\beta$  on pat-  
79 terns expected from theory are critical for further optimality model development,  
80 and is the central motivation for the experiments presented in this dissertation.

81 In this dissertation, I use four experiments to quantify nutrient acquisition  
82 and allocation responses under different environmental conditions and in species  
83 with different nutrient acquisition strategies. These experiments provide impor-  
84 tant empirical data needed to evaluate patterns expected from photosynthetic  
85 least-cost theory and test mechanisms that drive such patterns. In the first ex-  
86 perimental chapter, I re-analyze data from a greenhouse experiment that grew  
87 *Glycine max* L. (Merr) and *Gossypium hirsutum* seedlings under full-factorial  
88 combinations of four light treatments and four fertilization treatments. This re-  
89 analysis examined the effect of soil nitrogen availability and light availability on  
90 structural carbon costs to acquire nitrogen in a species capable of forming associ-  
91 ations with symbiotic nitrogen-fixing bacteria (*G. max*) and a species not capable  
92 of forming such associations (*G. hirsutum*). I find strong evidence suggesting that  
93 increasing light availability increases structural carbon costs to acquire nitrogen  
94 and that increasing soil nitrogen fertilization decreases structural carbon costs to  
95 acquire nitrogen.

96        In the second experimental chapter, I measure leaf physiological traits in  
97    the upper canopy of mature trees growing in a 9-year nitrogen-by-pH field manip-  
98    ulation experiment to assess whether changes in soil nitrogen availability or soil  
99    pH modify nitrogen-water use tradeoffs expected from photosynthetic least-cost  
100   theory. I find strong nitrogen-water use tradeoffs in response to increasing soil ni-  
101   trogen availability, indicated by a strong negative relationship between leaf  $C_i:C_a$   
102   (referred to here and in the rest of this dissertation as  $\chi$ ) and leaf nitrogen content,  
103   as well as a strong increase in leaf nitrogen content per unit leaf  $\chi$  with increas-  
104   ing soil nitrogen availability. Interestingly, I also find a null effect of soil pH on  
105   nitrogen-water use tradeoffs. These patterns provide strong support for patterns  
106   expected from photosynthetic least-cost theory across soil nitrogen availability  
107   gradients, and indicate that previous studies which note strong nitrogen-water  
108   use tradeoffs in response to soil pH may be driven by covariation between soil  
109   nitrogen availability and soil pH (Paillassa et al. 2020; Westerband et al. 2023).

110        In the third experimental chapter, I leverage a broad precipitation and soil  
111   nutrient availability gradient in Texan grasslands to investigate primary drivers of  
112   leaf nitrogen content. In this chapter, I directly quantify  $\beta$  and  $\chi$  using leaf  $\delta^{13}\text{C}$  to  
113   examine primary drivers of leaf nitrogen content and find that leaf nitrogen content  
114   is driven through a negative relationship with  $\chi$ . I also show that soil nitrogen  
115   availability is negatively associated with  $\beta$ , and that  $\beta$  is positively associated  
116   with  $\chi$ . I show strong support for patterns expected from theory, showing for  
117   the first time that positive effects of increasing soil nitrogen availability on leaf  
118   nitrogen content are mediated by changes in  $\beta$ .

119        In the fourth experimental chapter, I use reach-in growth chambers to

120 quantify leaf and whole plant acclimation responses to CO<sub>2</sub> across a soil nitro-  
121 gen fertilization gradient, while also manipulating nutrient acquisition strategy  
122 by controlling whether seedlings were able to form associations with symbiotic  
123 nitrogen-fixing bacteria. Specifically, I measure leaf physiological and whole plant  
124 growth responses of 7-week *G. max* seedlings grown under one of two CO<sub>2</sub> treat-  
125 ments, one of nine fertilization treatments, and one of two inoculation treatments  
126 in a full factorial design. I find a downregulation in leaf nitrogen content and  
127 leaf photosynthesis under elevated CO<sub>2</sub>, a pattern that is not modified across  
128 the fertilization gradient or between inoculation treatments. However, I also find  
129 strong stimulations in total leaf area and whole plant growth under elevated CO<sub>2</sub>  
130 that are enhanced with increasing fertilization. There was no observable effect  
131 of inoculation in modifying whole plant growth responses to CO<sub>2</sub>, which I spec-  
132 ulate is the result of a downregulation in plant investments to nitrogen fixation  
133 with increasing fertilization. Results from this experiment provide strong evidence  
134 suggesting that leaf acclimation responses to CO<sub>2</sub> were controlled by optimal re-  
135 source investment to photosynthetic capacity, following patterns expected from  
136 theory, and suggest divergent roles of soil nitrogen fertilization in modifying leaf  
137 and whole plant acclimation responses to CO<sub>2</sub>.

138 Throughout the four experimental chapters, I find strong and consistent  
139 patterns that are supportive of patterns expected from photosynthetic least-cost  
140 theory. Specifically, I find strong nitrogen-water use tradeoffs in response to chang-  
141 ing climates and soil resources, and that shifts in soil nitrogen availability have  
142 strong negative impacts on costs of nitrogen acquisition, and therefore tend to  
143 increase  $\beta$ . In a final conclusion chapter, I summarize major findings from each of

**144** the four experimental chapters and synthesize common mechanisms that drive leaf  
**145** and whole plant responses to changing environmental conditions. I conclude this  
**146** dissertation with brief dialogue on lessons learned throughout the experimental  
**147** chapters, and propose future experiments that will target additional uncertainties  
**148** in photosynthetic least-cost theory responses across environmental gradients.

149

## Chapter 2

150

Structural carbon costs to acquire nitrogen are determined by  
151 nitrogen and light availability in two species with different nitrogen  
152 acquisition strategies

153 2.1 Introduction

154

Carbon and nitrogen cycles are tightly coupled in terrestrial ecosystems.

155

This tight coupling influences photosynthesis (Walker et al. 2014; Rogers et al.

156

2017), net primary productivity (LeBauer and Treseder 2008; Thomas et al. 2013),

157

decomposition (Cornwell et al. 2008; Bonan et al. 2013; Sulman et al. 2019), and

158

plant resource competition (Gill and Finzi 2016; Xu-Ri and Prentice 2017). Ter-

159

restrial biosphere models are beginning to include connected carbon and nitrogen

160

cycles to improve the realism of their simulations (Fisher et al. 2010; Brzostek

161

et al. 2014; Wieder et al. 2015; Shi et al. 2016; Zhu et al. 2019). Simula-

162

tions from these models indicate that coupling carbon and nitrogen cycles can

163

drastically influence future biosphere-atmosphere feedbacks under global change,

164

such as elevated carbon dioxide or nitrogen deposition (Thornton et al. 2007;

165

Goll et al. 2012; Wieder et al. 2015; Wieder et al. 2019). Nonetheless, there

166

are still limitations in our quantitative understanding of connected carbon and

167

nitrogen dynamics (Thomas et al. 2015; Meyerholt et al. 2016; Rogers et al.

168

2017; Exbrayat et al. 2018; Shi et al. 2019), forcing models to make potentially

169

unreliable assumptions.

170

Plant nitrogen acquisition is a process in terrestrial ecosystems by which

171

carbon and nitrogen are tightly coupled (Vitousek and Howarth 1991; Delaire

172

et al. 2005; Brzostek et al. 2014). Plants must allocate photosynthetically de-

173 rived carbon belowground to produce and maintain root systems or exchange with  
174 symbiotic soil microbes in order to acquire nitrogen (Högberg et al. 2008; Hög-  
175 berg et al. 2010). Thus, plants have an inherent carbon cost associated with  
176 acquiring nitrogen, which can include both direct energetic costs associated with  
177 nitrogen acquisition and indirect costs associated with building structures that  
178 support nitrogen acquisition (Gutschick 1981; Rastetter et al. 2001; Vitousek  
179 et al. 2002; Menge et al. 2008). Model simulations (Fisher et al. 2010; Brzostek  
180 et al. 2014; Shi et al. 2016; Allen et al. 2020) and meta-analyses (Terrer et al.  
181 2018) suggest that these carbon costs vary between species, particularly those  
182 with different nitrogen acquisition strategies. For example, simulations using iter-  
183 ations of the Fixation and Uptake of Nitrogen (FUN) model indicate that species  
184 that acquire nitrogen from non-symbiotic active uptake pathways (e.g. mass flow)  
185 generally have larger carbon costs to acquire nitrogen than species that acquire  
186 nitrogen through symbiotic associations with nitrogen-fixing bacteria (Brzostek  
187 et al. 2014; Allen et al. 2020).

188 Carbon costs to acquire nitrogen likely vary in response to changes in soil  
189 nitrogen availability. For example, if the primary mode of nitrogen acquisition  
190 is through non-symbiotic active uptake, then nitrogen availability could decrease  
191 carbon costs to acquire nitrogen as a result of increased per-root nitrogen up-  
192 take (Franklin et al. 2009; Wang et al. 2018). However, if the primary mode of  
193 nitrogen acquisition is through symbiotic active uptake, then nitrogen availabil-  
194 ity may incur additional carbon costs to acquire nitrogen if it causes microbial  
195 symbionts to shift toward parasitism along the parasitism–mutualism continuum  
196 (Johnson et al. 1997; Hoek et al. 2016; Friel and Friesen 2019) or if it reduces

197 the nitrogen acquisition capacity of a microbial symbiont (van Diepen et al. 2007;  
198 Soudzilovskaia et al. 2015; Muñoz et al. 2016). Species may respond to shifts in  
199 soil nitrogen availability by switching their primary mode of nitrogen acquisition  
200 to a strategy with lower carbon costs to acquire nitrogen in order to maximize  
201 the magnitude of nitrogen acquired from a belowground carbon investment and  
202 outcompete other individuals for soil resources (Rastetter et al. 2001; Menge et al.  
203 2008).

204 Environmental conditions that affect demand to acquire nitrogen to sup-  
205 port new and existing tissues could also be a source of variance in plant carbon  
206 costs to acquire nitrogen. For example, an increase in plant nitrogen demand could  
207 increase carbon costs to acquire nitrogen if this increases the carbon that must be  
208 allocated belowground to acquire a proportional amount of nitrogen (Kulmatiski  
209 et al. 2017; Noyce et al. 2019). This could be driven by a temporary state of  
210 diminishing return associated with investing carbon toward building and main-  
211 taining structures that are necessary to support enhanced nitrogen uptake, such  
212 as fine roots (Matamala and Schlesinger 2000; Norby et al. 2004; Arndal et al.  
213 2018), mycorrhizal hyphae (Saleh et al. 2020), or root nodules (Parvin et al. 2020).  
214 Alternatively, if the environmental factor that increases plant nitrogen demand  
215 causes nitrogen to become more limiting in the system (e.g. atmospheric CO<sub>2</sub>;  
216 Luo et al. (2004), LeBauer and Treseder (2008), Vitousek et al. (2010), Liang  
217 et al. (2016)), species might switch their primary mode of nitrogen acquisition to  
218 a strategy with lower relative carbon costs to acquire nitrogen in order to gain a  
219 competitive advantage over species with either different or more limited modes of  
220 nitrogen acquisition (Ainsworth and Long 2005; Taylor and Menge 2018).

221        Using a plant economics approach, we examined the influence of plant  
222    nitrogen demand and soil nitrogen availability on plant carbon costs to acquire  
223    nitrogen. This was done by growing a species capable of forming associations  
224    with nitrogen-fixing bacteria (*Glycine max* L. (Merr)) and a species not capable  
225    of forming these associations (*Gossypium hirsutum* L.) under four levels of light  
226    availability (plant nitrogen demand proxy) and four levels of soil nitrogen fertil-  
227    ization (soil nitrogen availability proxy) in a full-factorial, controlled greenhouse  
228    experiment. We used this experimental set-up to test the following hypotheses:

- 229        1. An increase in plant nitrogen demand due to increasing light availability will  
230        increase carbon costs to acquire nitrogen through a proportionally larger  
231        increase in belowground carbon than whole-plant nitrogen acquisition. This  
232        will be the result of an increased investment of carbon toward belowground  
233        structures that support enhanced nitrogen uptake, but at a lower nitrogen  
234        return.
- 235        2. An increase in soil nitrogen availability will decrease carbon costs to acquire  
236        nitrogen as a result of increased per root nitrogen uptake in *G. hirsutum*.  
237        However, soil nitrogen availability will not affect carbon costs to acquire  
238        nitrogen in *G. max* because of the already high return of nitrogen supplied  
239        through nitrogen fixation.

**240** 2.2 Methods

**241** 2.2.1 *Experiment setup*

**242** *Gossypium hirsutum* and *G. max* were planted in individual 3 liter pots  
**243** (NS-300; Nursery Supplies, Orange, CA, USA) containing a 3:1 mix of unfertil-  
**244** ized potting mix (Sungro Sunshine Mix #2, Agawam, MA, USA) to native soil  
**245** extracted from an agricultural field most recently planted with *G. max* at the  
**246** USDA-ARS Laboratory in Lubbock, TX, USA (33.59°N, -101.90°W). The field  
**247** soil was classified as Amarillo fine sandy loam (75% sand, 10% silt, 15% clay).  
**248** Upon planting, all *G. max* pots were inoculated with *Bradyrhizobium japonicum*  
**249** (Verdesian N-Dure™ Soybean, Cary, NC, USA) to stimulate root nodulation. In-  
**250** dividuals of both species were grown under similar, unshaded, ambient greenhouse  
**251** conditions for 2 weeks to germinate and begin vegetative growth. Three blocks  
**252** were set up in the greenhouse, each containing four light treatments created us-  
**253** ing shade cloth that reduced incoming radiation by either 0 (full sun), 30, 50,  
**254** or 80%. Two weeks post-germination, individuals were randomly placed in the  
**255** four light treatments in each block. Individuals received one of four nitrogen fer-  
**256** tilization doses as 100ml of a modified Hoagland solution (Hoagland and Arnon  
**257** 1950) equivalent to either 0, 70, 210, or 630 ppm N twice per week within each  
**258** light treatment. Nitrogen fertilization doses were received as topical agents to  
**259** the soil surface. Each Hoagland solution was modified to keep concentrations of  
**260** other macro- and micronutrients equivalent (Supplementary Table S1). Plants  
**261** were routinely well watered to eliminate water stress.

**262** 2.2.2 *Plant measurements and calculations*

**263** Each individual was harvested after 5 weeks of treatment, and biomass  
**264** was separated by organ type (leaves, stems, and roots). Nodules on *G. max*  
**265** roots were also harvested. With the exception of the 0% shade cover and 630  
**266** ppm N treatment combination, all treatment combinations in both species had  
**267** lower average dry biomass:pot volume ratios than the 1:1 ratio recommended by  
**268** Poorter et al. (2012) to minimize the likelihood of pot volume-induced growth  
**269** limitation (Supplementary Tables S2, S3; Supplementary Fig. S1). All harvested  
**270** material was dried, weighed, and ground by organ type. Carbon and nitrogen  
**271** content ( $\text{g g}^{-1}$ ) was determined by subsampling from ground and homogenized  
**272** biomass of each organ type using an elemental analyzer (Costech 4010; Costech,  
**273** Inc., Valencia, CA, USA). We scaled these values to total leaf, stem, and root  
**274** carbon and nitrogen biomass (g) by multiplying dry biomass of each organ type  
**275** by carbon or nitrogen content of each corresponding organ type. Whole-plant  
**276** nitrogen biomass (g) was calculated as the sum of total leaf (g), stem (g), and  
**277** root (g) nitrogen biomass. Root nodule carbon biomass was not included in the  
**278** calculation of root carbon biomass; however, relative plant investment toward root  
**279** or root nodule standing stock was estimated as the ratio of root biomass to root  
**280** nodule biomass ( $\text{g g}^{-1}$ ), following similar metrics to those adopted by Dovrat et al.  
**281** (2018) and Dovrat et al. (2020).

**282** Carbon costs to acquire nitrogen ( $\text{gC gN}^{-1}$ ) were estimated as the ratio of  
**283** total root carbon biomass (gC) to whole-plant nitrogen biomass (gN). This cal-  
**284** culation quantifies the relationship between carbon spent on nitrogen acquisition  
**285** and whole-plant nitrogen acquisition by using root carbon biomass as a proxy for

286 estimating the magnitude of carbon allocated toward nitrogen acquisition. This  
287 calculation therefore assumes that the magnitude of root carbon standing stock is  
288 proportional to carbon transferred to root nodules or mycorrhizae, or lost through  
289 root exudation or turnover. This assumption has been supported in species that  
290 associate with ectomycorrhizal fungi (Hobbie 2006; Hobbie and Hobbie 2008), but  
291 is less clear in species that acquire nitrogen through non-symbiotic active uptake  
292 or symbiotic nitrogen fixation. It is also unclear whether relationships between  
293 root carbon standing stock and carbon transfer to root nodules are similar in mag-  
294 nitude to carbon lost through exudation or when allocated toward other active  
295 uptake pathways. Thus, because of the way we performed our measurements, our  
296 proximal values of carbon costs to acquire nitrogen are underestimates.

297 2.2.3 *Statistical analyses*

298 We explored the effects of light and nitrogen availability on carbon costs to  
299 acquire nitrogen using separate linear mixed-effects models for each species. Mod-  
300 els included shade cover, nitrogen fertilization, and interactions between shade  
301 cover and nitrogen fertilization as continuous fixed effects, and also included block  
302 as a random intercept term. Three separate models for each species were built  
303 with this independent variable structure for three different dependent variables: (i)  
304 carbon costs to acquire nitrogen ( $\text{gC gN}^{-1}$ ); (ii) whole-plant nitrogen biomass (de-  
305 nominator of carbon cost to acquire nitrogen;  $\text{gN}$ ); and (iii) root carbon biomass  
306 (numerator of carbon cost to acquire nitrogen;  $\text{gC}$ ). We constructed two additional  
307 models for *G. max* with the same model structure described above to investigate  
308 the effects of light availability and nitrogen fertilization on root nodule biomass

309 (g) and the ratio of root nodule biomass to root biomass (unitless).

310 We used Shapiro–Wilk tests of normality to determine whether species-  
311 specifc linear mixed-effects model residuals followed a normal distribution. None  
312 of our models satisfied residual normality assumptions when models were fit using  
313 untransformed data (Shapiro–Wilk:  $P<0.05$  in all cases). We attempted to satisfy  
314 residual normality assumptions by first fitting models using dependent variables  
315 that were natural-log transformed. If residual normality assumptions were still  
316 not met (Shapiro–Wilk:  $P>0.05$ ), then models were fit using dependent variables  
317 that were square root transformed. All residual normality assumptions were satis-  
318 fied when models were fit with either a natural-log or square root transformation  
319 (Shapiro–Wilk:  $P>0.05$  in all cases). Specifically, we natural-log transformed *G.*  
320 *hirsutum* carbon costs to acquire nitrogen and *G. hirsutum* whole-plant nitrogen  
321 biomass. We also square root transformed *G. max* carbon costs to acquire nitro-  
322 gen, *G. max* whole-plant nitrogen biomass, root carbon biomass in both species,  
323 *G. max* root nodule biomass, and the *G. max* ratio of root nodule biomass to root  
324 biomass. We used the ‘lmer’ function in the ‘lme4’ R package (Bates et al. 2015)  
325 to fit each model and the ‘Anova’ function in the ‘car’ R package (Fox and Weis-  
326 berg 2019) to calculate Wald’s  $\chi^2$  to determine the significance ( $\alpha = 0.05$ ) of each  
327 fixed effect coefficient. Finally, we used the ‘emmeans’ R package (Lenth 2019)  
328 to conduct post-hoc comparisons of our treatment combinations using Tukey’s  
329 tests. Degrees of freedom for all Tukey’s tests were approximated using the Ken-  
330 ward–Roger approach (Kenward and Roger 1997). All analyses and plots were  
331 conducted in R version 4.0.1 (R Core Team 2021).

**332** 2.3 Results

**333** 2.3.1 *Carbon costs to acquire nitrogen*

**334** Carbon costs to acquire nitrogen in *G. hirsutum* increased with increasing  
**335** light availability ( $p < 0.001$ ; Table 2.1; Fig. 2.1) and decreased with increasing  
**336** nitrogen fertilization ( $p < 0.001$ ; Table 2.1; Fig. 2.1). There was no interaction  
**337** between light availability and nitrogen fertilization ( $p = 0.486$ , Table 2.1; Fig.  
**338** 2.1).

**339** Carbon costs to acquire nitrogen in *G. max* also increased with increasing  
**340** light availability ( $p < 0.001$ , Table 2.1; Fig. 2.1) and decreased with increasing  
**341** nitrogen fertilization ( $p < 0.001$ ; Table 2.1; Fig. 2.1). There was no interaction  
**342** between light availability and nitrogen fertilization ( $p = 0.261$ , Table 2.1; Fig.  
**343** 2.1).

**Table 2.1.** Analysis of variance results exploring species-specific effects of light availability, nitrogen fertilization, and their interactions on carbon costs to acquire nitrogen, whole-plant nitrogen biomass, and root carbon biomass

	df	Carbon costs to acquire nitrogen			Whole-plant nitrogen biomass			Root carbon biomass		
		Coefficient	$\chi^2$	p	Coefficient	$\chi^2$	p	Coefficient	$\chi^2$	p
<i>G. hirsutum</i>										
Intercept		1.594	-	-	-3.232	-	-	0.432	-	-
Light (L)	1	-1.09E-02	56.494	<0.001	-6.41E-03	91.275	<0.001	-2.62E-03	169.608	<0.001
Nitrogen (N)	1	-1.34E-03	54.925	<0.001	1.83E-03	118.784	<0.001	1.15E-04	2.901	0.089
L*N	1	3.88E-06	0.485	0.486	-1.34E-05	10.721	0.001	-1.67E-06	3.140	0.076
<i>G. max</i>										
Intercept		1.877	-	-	0.239	-	-	0.438	-	-
Light (L)	1	-7.67E-03	174.156	<0.001	-6.72E-04	39.799	<0.001	-2.55E-03	194.548	<0.001
Nitrogen (N)	1	-2.35E-04	21.948	<0.001	1.55E-04	70.771	<0.001	2.52E-04	19.458	<0.001
L*N	1	-2.89E-06	1.262	0.261	-6.32E-07	1.435	0.231	-3.16E-06	10.803	0.001

\*Significance determined using Wald's  $\chi^2$  tests ( $P=0.05$ ).  $P$ -values<0.05 are in bold and  $p$ -values between 0.05 and 0.1 are italicized. Negative coefficients for light treatments indicate a positive effect of increasing light availability on all response variables, as light availability is treated as percent shade cover in all linear mixed-effects models.

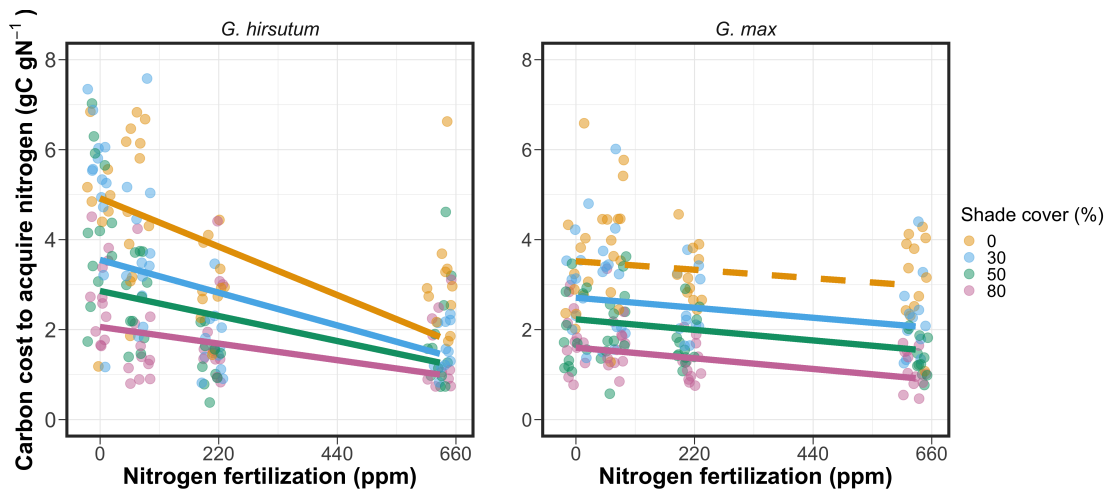


**Figure 2.1.** Relationships between soil nutrient fertilization and light availability on carbon costs to acquire nitrogen in *G. hirsutum* and *G. max*. Nitrogen fertilization treatments are represented on the x-axis. Shade cover treatments are represented through colored points and trendlines. Trendlines were created by back-transforming marginal mean slopes and intercepts from species-specific linear mixed-effects models. These values were calculated using the ‘emtrends’ and ‘emmmeans’ functions in the ‘emmeans’ R package (Lenth, 2019). Points are jittered for visibility. Yellow points and trendlines represent the 0% shade cover treatment, blue points and trendlines represent the 30% shade cover treatment, green points and trendlines represent the 50% shade cover treatment, and purple points and trendlines represent the 80% shade cover treatment. Solid trendlines indicate slopes that are significantly different from zero (Tukey:  $p < 0.05$ ), while dashed trendlines indicate slopes that are not statistically different from zero.

**344** 2.3.2 *Whole plant nitrogen biomass*

**345** Whole-plant nitrogen biomass in *G. hirsutum* was driven by an interaction  
**346** between light availability and nitrogen fertilization ( $p = 0.001$ ; Table 2.1; Fig.  
**347** 2.2). This interaction indicated a greater stimulation of whole-plant nitrogen  
**348** biomass by nitrogen fertilization as light levels increased (Table 2.1; Fig. 2.2).

**349** Whole-plant nitrogen biomass in *G. max* increased with increasing light  
**350** availability ( $p < 0.001$ ) and nitrogen fertilization ( $p < 0.001$ ), with no interaction  
**351** between light availability and nitrogen fertilization ( $p = 0.231$ ; Table 2.1; Fig.  
**352** 2.2).

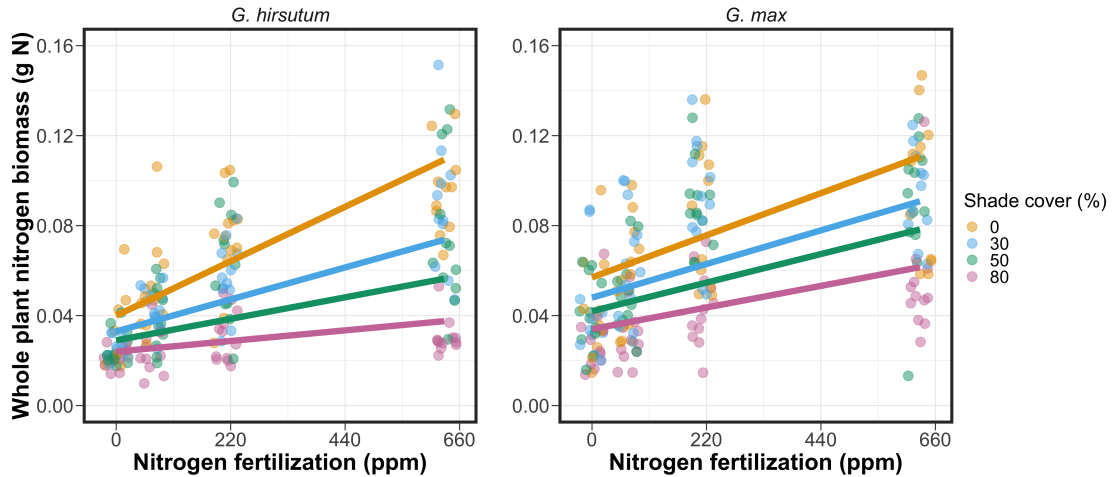


**Figure 2.2.** Relationships between soil nutrient fertilization and light availability on whole-plant nitrogen biomass in *G. hirsutum* and *G. max*. Whole-plant nitrogen biomass is the denominator of the carbon cost to acquire nitrogen calculation. Nitrogen fertilization treatments are represented on the x-axis. Shade cover treatments are represented through colored points and trendlines. Trendlines were created by back-transforming marginal mean slopes and intercepts from species-specific linear mixed-effects models. These values were calculated using the ‘emtrends’ and ‘emmmeans’ functions in the ‘emmeans’ R package (Lenth 2019). Points are jittered for visibility. Yellow points and trendlines represent the 0% shade cover treatment, blue points and trendlines represent the 30% shade cover treatment, green points and trendlines represent the 50% shade cover treatment, and purple points and trendlines represent the 80% shade cover treatment. Solid trendlines indicate slopes that are significantly different from zero (Tukey:  $P < 0.05$ ), while dashed trendlines indicate slopes that are not statistically different from zero.

**353** 2.3.3 *Root carbon biomass*

**354** Root carbon biomass in *G. hirsutum* significantly increased with increasing  
**355** light availability ( $p < 0.001$ ; Table 2.1; Fig. 2.3) and marginally increased with  
**356** nitrogen fertilization ( $p = 0.089$ ; Table 2.1; Fig. 2.3). There was also a marginal  
**357** interaction between light availability and nitrogen fertilization ( $p = 0.076$ ; Table  
**358** 2.1), driven by an increase in the positive response of root carbon biomass to  
**359** increasing nitrogen fertilization as light availability increased. This resulted in  
**360** significantly positive trends between root carbon biomass and nitrogen fertilization  
**361** in the two highest light treatments (Tukey:  $p < 0.05$  in both cases; Table 2.3;  
**362** Fig. 2.3) and no effect of nitrogen fertilization in the two lowest light treatments  
**363** (Tukey:  $p > 0.05$  in both cases; Table 2.3; Fig. 2.3).

**364** There was an interaction between light availability and nitrogen fertiliza-  
**365** tion on root carbon biomass in *G. max* ( $p = 0.001$ ; Table 2.1; Fig. 2.3). Post-hoc  
**366** analyses indicated that the positive effects of nitrogen fertilization on *G. max* root  
**367** carbon biomass increased with increasing light availability (Table 2.3; Fig. 2.3).  
**368** There were also positive individual effects of increasing nitrogen fertilization ( $p <$   
**369**  $0.001$ ) and light availability ( $p < 0.001$ ) on *G. max* root carbon biomass (Table  
**370** 2.1; Fig. 2.3).

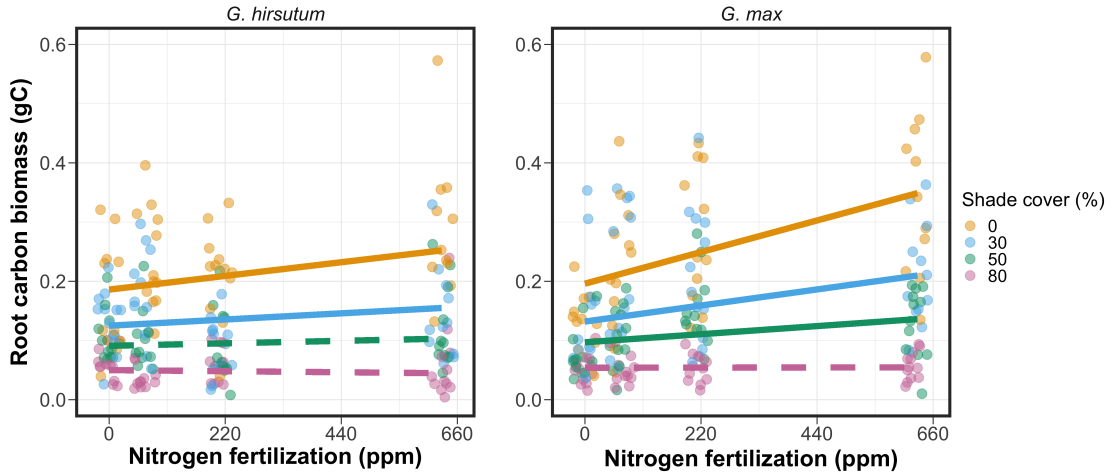


**Figure 2.3.** Relationships between soil nutrient fertilization and light availability on root carbon biomass in *G. hirsutum* and *G. max*. Root carbon biomass is the numerator of the carbon cost to acquire nitrogen calculation. Nitrogen fertilization treatments are represented on the x-axis. Shade cover treatments are represented through colored points and trendlines. Trendlines were created by back-transforming marginal mean slopes and intercepts from species-specific linear mixed-effects models. These values were calculated using the ‘emtrends’ and ‘emmmeans’ functions in the ‘emmeans’ R package (Lenth 2019). Points are jittered for visibility. Yellow points and trendlines represent the 0% shade cover treatment, blue points and trendlines represent the 30% shade cover treatment, green points and trendlines represent the 50% shade cover treatment, and purple points and trendlines represent the 80% shade cover treatment. Solid trendlines indicate slopes that are significantly different from zero (Tukey:  $p < 0.05$ ), while dashed trendlines indicate slopes that are not statistically different from zero.

**371** 2.3.4 *Root nodule biomass*

**372** Root nodule biomass in *G. max* increased with increasing light availability  
**373** ( $p < 0.001$ ; Table 2.2; Fig. 2.4A) and decreased with increasing nitrogen fertiliza-  
**374** tion ( $p < 0.001$ ; Table 2.2; Fig. 2.4A). There was no interaction between nitrogen  
**375** fertilization and light availability ( $p = 0.133$ ; Table 2.2; Fig. 2.4A). The ratio of  
**376** root nodule biomass to root biomass did not change in response to light avail-  
**377** ability ( $p = 0.481$ ; Table 2.2; Fig. 2.4B) but decreased with increasing nitrogen  
**378** fertilization ( $p < 0.001$ ; Table 2.2; Fig. 2.4B). There was no interaction between  
**379** nitrogen fertilization and light availability on the ratio of root nodule biomass to  
**380** root biomass ( $p = 0.621$ ; Table 2.2; Fig. 2.4B).

**Table 2.2.** Analysis of variance results exploring effects of light availability, nitrogen fertilization, and their interactions on *G. max* root nodule biomass and the ratio of root nodule biomass to root biomass\*

	Nodule biomass			Nodule biomass: root biomass			
	df	Coefficient	$\chi^2$	p	coefficient	$\chi^2$	p
(Intercept)		0.302	-	-	0.448	-	-
Light (L)	1	-1.81E-03	72.964	<b>&lt;0.001</b>	-8.76E-05	0.496	0.481
Nitrogen (N)	1	-2.83E-04	115.377	<b>&lt;0.001</b>	-5.09E-04	156.476	<b>&lt;0.001</b>
L*N	1	1.14E-06	2.226	0.133	-7.30E-07	0.244	0.621

\*Significance determined using Wald's  $\chi^2$  tests ( $\alpha = 0.05$ ). *p*-values less than 0.05 are in bold. Negative coefficients for light treatments indicate a positive effect of increasing light availability on all response variables, as light availability is treated as percent shade cover in all linear mixed-effects models. Root nodule biomass and nodule biomass: root biomass models were only constructed for *G. max* because *G. hirsutum* was not inoculated with *B. japonicum* and is not capable of forming root nodules.

**Table 2.3.** Slopes of the regression line describing the relationship between each dependent variable and nitrogen fertilization at each light level\*

Shade cover	Carbon cost to acquire nitrogen	Whole-plant nitrogen biomass	Root carbon biomass	Root nodule biomass	Nodule biomass root biomass
<i>G. hirsutum</i>					
0%	<b>-1.34E-03<sup>a</sup></b>	<b>1.83E-03<sup>a</sup></b>	<b>1.15E-04<sup>b</sup></b>	-	-
30%	<b>-1.22E-03<sup>a</sup></b>	<b>1.43E-03<sup>a</sup></b>	<b>1.17E-04<sup>b</sup></b>	-	-
50%	<b>-1.14E-03<sup>a</sup></b>	<b>1.17E-03<sup>a</sup></b>	3.12E-05 <sup>b</sup>	-	-
80%	<b>-1.02E-03<sup>a</sup></b>	<b>7.66E-04<sup>a</sup></b>	-1.89E-06 <sup>b</sup>	-	-
<i>G. max</i>					
0%	-2.35E-04 <sup>b</sup>	<b>1.55E-05<sup>b</sup></b>	<b>2.51E-04<sup>b</sup></b>	<b>-2.83E-04<sup>b</sup></b>	<b>-5.09E-04<sup>b</sup></b>
30%	<b>-3.22E-04<sup>b</sup></b>	<b>1.35E-05<sup>b</sup></b>	<b>1.57E-04<sup>b</sup></b>	<b>-2.49E-04<sup>b</sup></b>	<b>-5.31E-04<sup>b</sup></b>
50%	<b>-3.80E-04<sup>b</sup></b>	<b>1.23E-05<sup>b</sup></b>	<b>9.37E-05<sup>b</sup></b>	<b>-2.26E-04<sup>b</sup></b>	<b>-5.45E-04<sup>b</sup></b>
80%	<b>-4.66E-04<sup>b</sup></b>	<b>1.04E-05<sup>b</sup></b>	-9.95E-07 <sup>b</sup>	<b>-1.92E-04<sup>b</sup></b>	<b>-5.67E-04<sup>b</sup></b>

\*Slopes represent estimated marginal mean slopes from linear mixed-effects models described in the Methods. Slopes were calculated using the ‘emmeans’ R package (Lenth 2019). Superscripts indicate slopes fit to natural-log (<sup>a</sup>) or square root (<sup>b</sup>) transformed data. Slopes statistically different from zero (Tukey:  $p < 0.05$ ) are indicated in bold. Marginally significant slopes (Tukey:  $0.05 < p < 0.1$ ) are italicized.

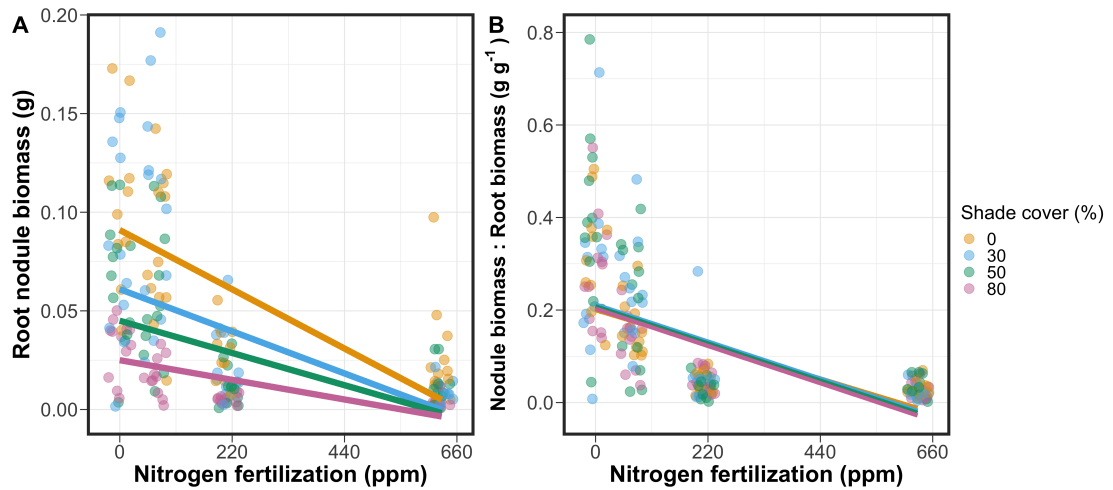


**Figure 2.4.** Effects of shade cover and nitrogen fertilization on root nodule biomass (A) and the ratio of root nodule biomass to root biomass (B) in *G. max*. Nitrogen fertilization treatments are represented on the x-axis. Shade cover treatments are represented through colored points and trendlines. Trendlines were created by back-transforming marginal mean slopes and intercepts from species-specific linear mixed-effects models. These values were calculated using the ‘emtrends’ and ‘emmeans’ functions in the ‘emmeans’ R package (Lenth 2019). Points are jittered for visibility. Yellow points and trendlines represent the 0% shade cover treatment, blue points and trendlines represent the 30% shade cover treatment, green points and trendlines represent the 50% shade cover treatment, and purple points and trendlines represent the 80% shade cover treatment. Solid trendlines indicate slopes that are significantly different from zero (Tukey:  $p < 0.05$ ), while dashed trendlines indicate slopes that are not statistically different from zero.

**381** 2.4 Discussion

**382** In this chapter, we determined the effects of light availability and soil ni-  
**383** trogen fertilization on root mass carbon costs to acquire nitrogen in *G. hirsutum*  
**384** and *G. max*. In support of our hypotheses, we found that carbon costs to acquire  
**385** nitrogen generally increased with increasing light availability and decreased with  
**386** increasing soil nitrogen fertilization in both species. These findings suggest that  
**387** carbon costs to acquire nitrogen are determined by factors that influence plant  
**388** nitrogen demand and soil nitrogen availability. In contrast to our second hypothe-  
**389** sis, root nodulation data suggested that *G. max* and *G. hirsutum* achieved similar  
**390** directional carbon cost responses to nitrogen fertilization despite a likely shift in  
**391** G.!max allocation from nodulation to root biomass along the nitrogen fertilization  
**392** gradient (Fig. 2.4B).

**393** Both *G. max* and *G. hirsutum* experienced an increase in carbon costs to  
**394** acquire nitrogen due to increasing light availability. These patterns were driven by  
**395** a larger increase in root carbon biomass than whole-plant nitrogen biomass. In-  
**396** creases in root carbon biomass due to factors that increase plant nitrogen demand  
**397** are a commonly observed pattern, as carbon allocated belowground provides sub-  
**398** strate needed to produce and maintain structures that satisfy aboveground plant  
**399** nitrogen demand (Nadelhoffer and Raich 1992; Giardina et al. 2005; Raich et al.  
**400** 2014). Our findings suggest that plants allocate relatively more carbon for acquir-  
**401** ing nitrogen when demand increases over short temporal scales, which may cause  
**402** a temporary state of diminishing return due to asynchrony between belowground  
**403** carbon and whole-plant nitrogen responses to plant nitrogen demand (Kulmatiski  
**404** et al. 2017; Noyce et al. 2019). These responses might be attributed to a temporal

lag associated with producing structures that enhance nitrogen acquisition. For example, fine roots (Matamala and Schlesinger 2000; Norby et al. 2004; Arndal et al. 2018) and root nodules (Parvin et al. 2020) take time to build and first require the construction of coarse roots. Thus, full nitrogen returns from these investments may not occur immediately (Kayler et al. 2010; Kayler et al. 2017), and may vary by species acquisition strategy. We speculate that increases in nitrogen acquisition from a given carbon investment may occur beyond the 5 week scope of this experiment. A similar study conducted over a longer temporal scale would address this.

Increasing soil nitrogen fertilization generally decreased carbon costs to acquire nitrogen in both species. These patterns were driven by a larger increase in whole-plant nitrogen biomass than root carbon biomass. In *G. hirsutum*, reductions in carbon costs to acquire nitrogen may have been due to an increase in per-root nitrogen uptake, allowing individuals to maximize the amount of nitrogen acquired from a belowground carbon investment. Interestingly, increased soil nitrogen fertilization increased whole-plant nitrogen biomass in *G. max* despite reductions in root nodule biomass that likely reduced the nitrogen-fixing capacity of *G. max* (Andersen et al. 2005; Muñoz et al. 2016). While reductions in root nodulation due to increased soil nitrogen availability are commonly observed (Gibson and Harper 1985; Fujikake et al. 2003), our responses were observed in tandem with increased root carbon biomass, implying that *G. max* shifted relative carbon allocation from nitrogen fixation to soil nitrogen acquisition (Markham and Zekveld 2007; Dovrat et al. 2020). This was likely because there was a reduction in the carbon cost advantage of acquiring fixed nitrogen relative to soil nitrogen, and

429 suggests that species capable of associating with symbiotic nitrogen-fixing bacte-  
430 ria shift their relative nitrogen acquisition pathway to optimize nitrogen uptake  
431 (Rastetter et al. 2001). Future studies should further investigate these patterns  
432 with a larger quantity of phylogenetically related species, or different varieties  
433 of a single species that differ in their ability to form associations with symbiotic  
434 nitrogen-fixing bacteria to more directly test the impact of nitrogen fixation on  
435 the patterns observed in this study.

436 Carbon costs to acquire nitrogen are subsumed in the general discussion of  
437 economic analogies to plant resource uptake (Bloom et al. 1985; Rastetter et al.  
438 2001; Vitousek et al. 2002; Phillips et al. 2013; Terrer et al. 2018; Henneron et al.  
439 2020). Despite this, terrestrial biosphere models rarely include these carbon costs  
440 within their framework for predicting plant nitrogen uptake. There is currently  
441 one plant resource uptake model, FUN, that quantitatively predicts carbon costs  
442 to acquire nitrogen within a framework for predicting plant nitrogen uptake for  
443 different nitrogen acquisition strategies (Fisher et al. 2010; Brzostek et al. 2014)

444 (Fisher et al. 2010; Brzostek et al. 2014). Iterations of FUN are currently  
445 coupled to two terrestrial biosphere models: the Community Land Model 5.0 and  
446 the Joint UK Land Environment Simulator (Shi et al. 2016; Lawrence et al.  
447 2019; Clark et al. 2011). Recent work suggests that coupling FUN to CLM 5.0  
448 caused a large overprediction of plant nitrogen uptake associated with nitrogen  
449 fixation (Davies-Barnard et al. 2020). Thus, empirical data from manipulative  
450 experiments that explicitly quantify carbon costs to acquire nitrogen in species  
451 capable of associating with nitrogen-fixing bacteria across different environmental  
452 contexts is an important step toward identifying potential biases in models such

453 as FUN.

454 Our findings broadly support the FUN formulation of carbon costs to ac-  
455 quire nitrogen in response to soil nitrogen availability. FUN calculates carbon  
456 costs to acquire nitrogen based on the sum of carbon costs to acquire nitrogen  
457 via nitrogen fixation, mycorrhizal active uptake, non-mycorrhizal active uptake,  
458 and retranslocation (Fisher et al. 2010; Brzostek et al. 2014). Carbon costs to  
459 acquire nitrogen via mycorrhizal or non-mycorrhizal active uptake pathways are  
460 derived as a function of nitrogen availability, root biomass, and two parameterized  
461 values based on nitrogen acquisition strategy (Brzostek et al. 2014). Due to this,  
462 FUN simulates a net decrease in carbon costs to acquire nitrogen with increasing  
463 nitrogen availability for mycorrhizal and non-mycorrhizal active uptake pathways,  
464 assuming constant root biomass. This was a pattern we observed in *G. hirsutum*  
465 regardless of light availability. In contrast, FUN would not simulate a net change  
466 in carbon costs to acquire nitrogen via nitrogen fixation due to nitrogen avail-  
467 ability. This is because carbon costs to acquire nitrogen via nitrogen fixation are  
468 derived from a well-established function of soil temperature, which is independent  
469 of soil nitrogen availability (Houlton et al. 2008; Fisher et al. 2010). We observed  
470 a net reduction in carbon costs to acquire nitrogen in *G. max*, except when in-  
471 dividuals were grown under 0% shade cover (Fig. 2.1). While a net reduction of  
472 carbon costs in response to nitrogen fertilization runs counter to nitrogen fixa-  
473 tion carbon costs simulated by FUN, these patterns were likely because *G. max*  
474 individuals switched their primary mode of nitrogen acquisition from symbiotic  
475 nitrogen fixation to a non-symbiotic active uptake pathway (Fig. 2.4B).

476 It should be noted that the metric used in this study to determine carbon

477 costs to acquire nitrogen has several limitations. Most notably, this metric uses  
478 root carbon biomass as a proxy for estimating the amount of carbon spent on  
479 nitrogen acquisition. While it is true that most carbon allocated belowground  
480 has at least an indirect structural role in acquiring soil resources, it remains un-  
481 clear whether this assumption holds true for species that acquire nitrogen via  
482 symbiotic nitrogen fixation. We also cannot quantify carbon lost through root  
483 exudates or root turnover, which may increase due to factors that increase plant  
484 nitrogen demand (Tingey et al. 2000; Phillips et al. 2011), and can increase the  
485 magnitude of available nitrogen from soil organic matter through priming effects  
486 on soil microbial communities (Uselman et al. 2000; Bengtson et al. 2012). It is  
487 also not clear whether these assumptions hold under all environmental conditions,  
488 such as those that shift belowground carbon allocation toward a different mode of  
489 nitrogen acquisition (Taylor and Menge 2018; Friel and Friesen 2019) or between  
490 species with different acquisition strategies. In this study, increasing soil nitrogen  
491 fertilization increased carbon investment to roots relative to carbon transferred  
492 to root nodules (Fig. 2.4B). By assuming that carbon allocated to root carbon  
493 was proportional to carbon allocated to root nodules across all treatment com-  
494 binations, these observed responses to soil nitrogen fertilization were likely to be  
495 overestimated in *G. max*. We encourage future research to quantify these carbon  
496 fates independently.

497 Researchers conducting pot experiments must carefully choose pot volume  
498 to minimize the likelihood of pot volume-induced growth limitation (Poorter et al.  
499 2012). Poorter et al. (2012) indicate that researchers are likely to avoid growth  
500 limitations associated with pot volume if measurements are collected when the

501 plant biomass:pot volume ratio is less than 1 g L<sup>-1</sup>. In this experiment, all treat-  
502 ment combinations in both species had biomass:pot volume ratios less than 1 g  
503 L<sup>-1</sup> except for *G. max* and *G. hirsutum* that were grown under 0% shade cover  
504 and had received 630 ppm N. Specifically, *G. max* and *G. hirsutum* had average  
505 respective biomass:pot volume ratios of 1.24±0.07 g L<sup>-1</sup> and 1.34±0.13 g L<sup>-1</sup>, when  
506 grown under 0% shade cover and received 630 ppm N (Supplementary Tables S2,  
507 S3; Supplementary Fig. S1). If growth in this treatment combination was limited  
508 by pot volume, then individuals may have had larger carbon costs to acquire ni-  
509 trogen than would be expected if they were grown in larger pots. This pot volume  
510 induced growth limitation could cause a reduction in per-root nitrogen uptake as-  
511 sociated with more densely packed roots, which could reduce the positive effect  
512 of nitrogen fertilization on whole-plant nitrogen biomass relative to root carbon  
513 biomass (Poorter et al. 2012).

514 Growth limitation associated with pot volume provides a possible explana-  
515 tion for the marginally insignificant effect of increasing nitrogen fertilization on *G.*  
516 *max* carbon costs to acquire nitrogen when grown under 0% shade cover (Table  
517 2.3; Fig. 2.1). This is because the regression line describing the relationship be-  
518 tween carbon costs to acquire nitrogen and nitrogen fertilization in *G. max* grown  
519 under 0% shade cover would have flattened if growth limitation had caused larger  
520 than expected carbon costs to acquire nitrogen in the 0% shade cover, 630 ppm  
521 N treatment combination. This may have been exacerbated by the fact that *G.*  
522 *max* likely shifted relative carbon allocation from nitrogen fixation to soil nitrogen  
523 acquisition, which could have increased the negative effect of more densely packed  
524 roots on nitrogen uptake. These patterns could have also occurred in *G. hirsutum*

525 grown under 0% shade cover; however, there was no change in the effect of nitro-  
526 gen fertilization on *G. hirsutum* carbon costs to acquire nitrogen grown under 0%  
527 shade cover relative to other shade cover treatments. Regardless, the possibility  
528 of growth limitation due to pot volume suggests that effects of increasing nitro-  
529 gen fertilization on carbon costs to acquire nitrogen in both species grown under  
530 0% shade cover could have been underestimated. Follow-up studies using a simi-  
531 lar experimental design with a larger pot volume would be necessary in order to  
532 determine whether these patterns were impacted by pot volume-induced growth  
533 limitation.

534 In conclusion, this study provides empirical evidence that carbon costs to  
535 acquire nitrogen are influenced by light availability and soil nitrogen fertilization  
536 in a species capable of acquiring nitrogen via symbiotic nitrogen fixation and a  
537 species not capable of forming such associations. We show that carbon costs to  
538 acquire nitrogen generally increase with increasing light availability and decrease  
539 with increasing nitrogen fertilization. This study provides important empirical  
540 data needed to evaluate the formulation of carbon costs to acquire nitrogen in  
541 terrestrial biosphere models, particularly carbon costs to acquire nitrogen that  
542 are associated with symbiotic nitrogen fixation. Our findings broadly support  
543 the general formulation of these carbon costs in the FUN biogeochemical model  
544 in response to shifts in nitrogen availability. However, there is a need for future  
545 studies to explicitly quantify carbon costs to acquire nitrogen under different en-  
546 vironmental contexts, over longer temporal scales, and using larger selections of  
547 phylogenetically related species. In addition, we suggest that future studies mini-  
548 mize the limitations associated with the metric used here by explicitly measuring

**549** belowground carbon fates independently.

550

### Chapter 3

551     **Soil nitrogen availability modifies leaf nitrogen economies in mature**  
552     **temperate deciduous forests: a direct test of photosynthetic least-cost**  
553     **theory**

554     3.1     Introduction

555             Photosynthesis represents the largest carbon flux between the atmosphere  
556     and land surface (IPCC 2021), and plays a central role in biogeochemical cycling  
557     at multiple spatial and temporal scales (Vitousek and Howarth 1991; LeBauer and  
558     Treseder 2008; Kaiser et al. 2015; Wieder et al. 2015). Therefore, carbon and  
559     energy fluxes simulated by terrestrial biosphere models are sensitive to the formu-  
560     lation of photosynthetic processes (Ziehn et al. 2011; Bonan et al. 2011; Booth  
561     et al. 2012; Smith et al. 2016; Smith et al. 2017) and must be represented using  
562     robust, empirically tested processes (Prentice et al. 2015; Wieder et al. 2019).  
563             Current formulations of photosynthesis vary across terrestrial biosphere models  
564     (Smith and Dukes 2013; Rogers et al. 2017), which causes variation in modeled  
565     ecosystem processes (Knorr 2000; Knorr and Heimann 2001; Bonan et al. 2011;  
566     Friedlingstein et al. 2014) and casts uncertainty on the ability of these models to  
567     accurately predict terrestrial ecosystem responses and feedbacks to global change  
568     (Zaehle et al. 2005; Schaefer et al. 2012; Davies-Barnard et al. 2020).

569             Terrestrial biosphere models commonly represent C<sub>3</sub> photosynthesis through  
570     variants of the Farquhar et al. (1980) biochemical model (Smith and Dukes 2013;  
571     Rogers 2014; Rogers et al. 2017). This well-tested photosynthesis model es-  
572     timates leaf-level carbon assimilation, or photosynthetic capacity, as a function  
573     of the maximum rate of Ribulose-1,5-bisphosphate carboxylase-oxygenase (Ru-

574 bisco) carboxylation ( $V_{cmax}$ ) and the maximum rate of Ribulose-1,5-bisphosphate  
575 (RuBP) regeneration ( $J_{max}$ ) (Farquhar et al. 1980). Many terrestrial biosphere  
576 models predict these model inputs based on plant functional group specific linear  
577 relationships between leaf nutrient content and  $V_{cmax}$  (Smith and Dukes 2013;  
578 Rogers 2014; Rogers et al. 2017) under the tenet that a large fraction of leaf  
579 nutrients, and nitrogen (N) in particular, are partitioned toward building and  
580 maintaining enzymes that support photosynthetic capacity, such as Rubisco (Brix  
581 1971; Gulmon and Chu 1981; Evans 1989; Kattge et al. 2009; Walker et al. 2014).  
582 Terrestrial biosphere models also predict leaf nutrient content from soil nutrient  
583 availability based on the assumption that increasing soil nutrients generally in-  
584 creases leaf nutrients (Firn et al. 2019; Li et al. 2020; Liang et al. 2020) which, in  
585 the case of N, generally corresponds with an increase in photosynthetic processes  
586 (Li et al. 2020; Liang et al. 2020).

587 Recent work calls the generality of relationships between soil nutrient avail-  
588 ability, leaf nutrient content, and photosynthetic capacity into question, suggest-  
589 ing instead that leaf nutrients and photosynthetic capacity are better predicted as  
590 an integrated product of aboveground climate, leaf traits, and soil nutrient avail-  
591 ability, rather than soil nutrient availability alone (Dong et al. 2017; Dong et al.  
592 2020; Dong et al. 2022; Firn et al. 2019; Smith et al. 2019; Peng et al. 2021).  
593 It has been reasoned that this result is because plants allocate added nutrients to  
594 growth and storage rather than alterations in leaf chemistry (Smith et al. 2019),  
595 perhaps as a result of nutrient limitation of primary productivity (LeBauer and  
596 Treseder 2008; Fay et al. 2015). Additionally, recent work suggests that relation-  
597 ships between leaf nutrient content and photosynthesis vary across environments,

598 and that the proportion of leaf nutrient content allocated to photosynthetic tis-  
599 sue varies over space and time with plant acclimation and adaptation responses  
600 to light availability, vapor pressure deficit, soil pH, soil nutrient availability, and  
601 environmental factors that influence leaf mass per area (Pons and Pearcy 1994;  
602 Niinemets and Tenhunen 1997; Evans and Poorter 2001; Hikosaka and Shigeno  
603 2009; Ghimire et al. 2017; Onoda et al. 2017; Luo et al. 2021). The use of linear  
604 relationships between leaf nutrient content and Vcmax to predict photosynthetic  
605 capacity, as commonly used in terrestrial biosphere models (Rogers 2014), is not  
606 capable of detecting such responses.

607 Photosynthetic least-cost theory provides an alternative framework for un-  
608 derstanding relationships between soil nutrient availability, leaf nutrient content,  
609 and photosynthetic capacity (Harrison et al. 2021). Leveraging a two-input mi-  
610 croeconomics approach (Wright et al. 2003), the theory posits that plants accli-  
611 mate to a given environment by optimizing leaf photosynthesis rates at the lowest  
612 summed cost of using nutrients and water (Prentice et al. 2014; Wang et al. 2017;  
613 Smith et al. 2019; Paillassa et al. 2020). Across resource availability gradients,  
614 the theory predicts that optimal photosynthetic rates can be achieved by trading  
615 less efficient use of a resource that is less costly to acquire (or more abundant)  
616 for more efficient use of a resource more costly to acquire (or less abundant). For  
617 example, an increase in soil nutrient availability should reduce the cost of acquir-  
618 ing and using nutrients (Bae et al. 2015; Eastman et al. 2021; Perkowski et al.  
619 2021), which could increase leaf nutrient investments in photosynthetic proteins to  
620 allow similar photosynthetic rates to be achieved with higher nutrient use (lower  
621 nutrient use efficiency) but lower water use (greater water use efficiency). The

622 theory suggests similar tradeoffs in response to increasing soil pH (Paillassa et al.  
623 2020), specifically, that increasing soil pH should reduce the cost of acquiring soil  
624 nutrients due to an increase in plant-available nutrient concentration (Paillassa  
625 et al. 2020; Dong et al. 2022). The theory is also capable of reconciling dynamic  
626 leaf nutrient-photosynthesis relationships at global scales (Luo et al. 2021).

627 Patterns expected from photosynthetic least-cost theory have recently re-  
628 ceived empirical support both in global environmental gradient (Smith et al.  
629 2019; Paillassa et al. 2020; Luo et al. 2021; Querejeta et al. 2022; Wester-  
630 band et al. 2023) and local manipulative invasion (Bialic-Murphy et al. 2021)  
631 studies. However, nutrient addition experiments that directly examine nutrient-  
632 water use tradeoffs expected from the theory are rare (Guerrieri et al. 2011), and  
633 only global gradient studies testing the theory have considered soil pH in their  
634 analyses. As a result, there is a need to use nutrient addition and soil pH manu-  
635 lation experiments to test mechanisms driving responses predicted by the theory.  
636 Such experiments would also be useful to detect whether patterns expected from  
637 theory translate to finer spatial scales.

638 In this study, we measured leaf responses to soil N availability in five decid-  
639 uous tree species growing in the upper canopy of mature closed canopy temperate  
640 forests in the northeastern United States. Soil N availability and pH were manip-  
641 ulated through a N-by-pH field manipulation experiment with treatments applied  
642 since 2011, eight years prior to measurement. Two different soil N treatments were  
643 applied to increase N availability with opposing effects on soil pH. An additional  
644 N-free acidifying treatment was expected to decrease soil pH. We hypothesized  
645 that increased soil N availability would enable plants to increase nutrient uptake

646 and create more photosynthetic enzymes per leaf, allowing similar photosynthetic  
647 rates achieved with lower leaf C<sub>i</sub>:C<sub>a</sub> and increased leaf N content allocated to  
648 photosynthetic leaf tissue. We expected that this response would be driven by a  
649 reduction in the cost of acquiring N, which would cause trees to sacrifice efficient  
650 N use to enable more efficient use of other limiting resources (i.e., water). We  
651 hypothesized similar leaf responses to increasing soil pH.

652 3.2 Methods

653 3.2.1 *Study site description*

654 We conducted this study in summer 2019 at three stands located within  
655 a 20-km radius of Ithaca, NY, USA (42.444 °N, 76.502 °W). All stands contain  
656 mature, closed-canopy forests dominated by deciduous tree species. Stands con-  
657 tained abundant sugar maple (*Acer saccharum* Marshall), American beech (*Fagus*  
658 *grandifolia* Ehrh.), and white ash (*Fraxinus americana* L.), accounting for 43%,  
659 15%, and 17% of the total aboveground biomass across the three stands, respec-  
660 tively, with less frequent red maple (*Acer rubrum* L.; 9% of total aboveground  
661 biomass) and red oak occurrences (*Quercus rubra* L.; 10% of total aboveground  
662 biomass). Soils at each site were broadly classified as a channery silt loam Incep-  
663 tisols using the USDA NRCS Web Soil Survey data product (Soil Survey Staff  
664 2022). Between 2006 and 2020, study sites averaged 972 mm of precipitation per  
665 year and had an average temperature of 7.9 °C per a weather station located near  
666 the Cornell University campus (42.449 °N, 76.449 °W) part of the NOAA NCEI  
667 Global Historical Climatology Network (Menne et al. 2012).

**668** 3.2.2 *Experimental design*

**669** Four 40 m x 40 m plots were set up at each site in 2009, each with an  
**670** additional 10 m buffer along plot perimeters (60 m x 60 m total). The plots  
**671** were set up as a nitrogen-by-pH field manipulation experiment, with one each of  
**672** four treatments at each site. Two nitrogen treatments were applied, both at 50  
**673** kg N ha<sup>-1</sup> yr<sup>-1</sup>, as either sodium nitrate (NaNO<sub>3</sub>) to raise soil pH, or ammonium  
**674** sulfate ((NH<sub>4</sub>)<sub>2</sub>SO<sub>4</sub>) to acidify; an elemental sulfur treatment was selected to acid-  
**675** ify without N, applied at the same rate of S addition (57 kg S ha<sup>-1</sup> yr<sup>-1</sup>); and  
**676** control plots received no additions. All amendments were added in pelletized form  
**677** using hand-held fertilizer spreaders to both the main plots and buffers. Amend-  
**678** ments were divided into three equal doses distributed across the growing season  
**679** from 2011-2017 and added as a single dose from 2018 onward. During 2019, plots  
**680** were fertilized during the week of May 20.

**681** 3.2.3 *Leaf gas exchange and trait measurements*

**682** We sampled one leaf each from 6 to 10 individuals per plot between June  
**683** 25 and July 12, 2019 for gas exchange measurements (Table S1). Leaves were  
**684** collected from deciduous broadleaf trees represented across all sites and plots and  
**685** were replicated in efforts to mimic the species abundance of each plot at each  
**686** site. We also attempted to collect leaves from the upper canopy to reduce differ-  
**687** ential shading effects on leaf physiology. Leaves were accessed by pulling down  
**688** small branches using an arborist's slingshot and weighted beanbag attached to a  
**689** throwline. Branches were immediately recut under deionized water and remained  
**690** submerged to reduce stomatal closure and avoid xylem embolism (as in Smith &

691 Dukes, 2018) until gas exchange data were collected.

692 Randomly selected leaves with little to no visible external damage were  
693 attached to a Li-COR LI-6800 (Li-COR Bioscience, Lincoln, Nebraska, USA)  
694 portable photosynthesis machine to measure net photosynthesis ( $A_{\text{net}}$ ;  $\mu\text{mol m}^{-2} \text{s}^{-1}$ ),  
695 stomatal conductance ( $g_{\text{sw}}$ ;  $\text{mol m}^{-2} \text{s}^{-1}$ ), and intercellular  $\text{CO}_2$  concentration  
696 ( $C_i$ ;  $\mu\text{mol mol}^{-1}$ ) at different reference  $\text{CO}_2$  concentrations ( $C_a$ ;  $\mu\text{mol mol}^{-1}$ )  
697 concentrations (i.e., an  $A_{\text{net}}/C_i$  curve) under saturating light conditions (2,000  
698  $\mu\text{mol m}^{-2} \text{s}^{-1}$ ). Reference  $\text{CO}_2$  concentrations followed the sequence: 400, 300,  
699 200, 100, 50, 400, 400, 600, 800, 1000, 1200, 1500, and 2000  $\mu\text{mol mol}^{-1} \text{CO}_2$ . Leaf  
700 temperatures were not controlled in the cuvette and ranged from 21.8 °C to 31.7  
701 °C (mean±SD:  $27.2 \pm 2.2$  °C). A linear and second order log-polynomial nonlinear  
702 regression suggested no effect of temperature on stomatal conductance measured  
703 at 400  $\mu\text{mol mol}^{-1} \text{CO}_2$  or net photosynthesis measured at  $\mu\text{mol mol}^{-1} \text{CO}_2$  (Ta-  
704 ble S2-3; Fig. S1). All  $A_{\text{net}}/C_i$  curves were generated within one hour of branch  
705 severance.

706 Leaf morphological and chemical traits were collected on the same leaf used  
707 to generate each  $A_{\text{net}}/C_i$  curve. Images of each leaf were taken using a flat-bed  
708 scanner to determine fresh leaf area using the ‘LeafArea’ R package (Katabuchi  
709 2015), which automates leaf area calculations using ImageJ software (Schneider  
710 et al. 2012). Each leaf was dried at 65°C for at least 48 hours, weighed, and  
711 ground using a Retsch MM200 ball mill grinder (Verder Scientific, Inc., Newtown,  
712 PA, USA) until homogenized. Leaf mass per area ( $M_{\text{area}}$ ,  $\text{g m}^{-2}$ ) was calculated  
713 as the ratio of dry leaf biomass to fresh leaf area. Using a subsample of ground and  
714 homogenized leaf biomass, leaf N content ( $N_{\text{mass}}$ ;  $\text{gN g}^{-1}$ ) and leaf  $\delta^{13}\text{C}$  (‰, rela-

715 tive to VPDB) were measured at the Cornell Stable Isotope Lab with an elemental  
 716 analyzer (NC 2500, CE Instruments, Wigan, UK) interfaced to an isotope ratio  
 717 mass spectrometer (Delta V Isotope Ratio Mass Spectrometer, ThermoFisher Sci-  
 718 entific, Waltham, MA, USA). Leaf N content per unit leaf area ( $N_{\text{area}}$ ; gN m<sup>-2</sup>)  
 719 was calculated by multiplying  $N_{\text{mass}}$  by  $M_{\text{area}}$ .

720 We used leaf  $\delta^{13}\text{C}$  values to estimate  $\chi$  (unitless), which is an isotope-  
 721 derived estimate of the leaf  $C_i:C_a$  ratio. While intercellular and atmospheric CO<sub>2</sub>  
 722 concentrations were directly measured during each  $A_{\text{net}}/C_i$  curve, deriving  $\chi$  from  
 723  $\delta^{13}\text{C}$  provides a more integrative estimate of the  $C_i:C_a$  over an individual leaf's  
 724 lifespan. We derived  $\chi$  following the approach of Farquhar et al. (1989) described  
 725 in Cernusak et al. (2013):

$$\chi = \frac{\Delta^{13}C - a}{b - a} \quad (3.1)$$

726 where  $\Delta^{13}\text{C}$  represents the relative difference between leaf  $\delta^{13}\text{C}$  (‰) and air  $\delta^{13}\text{C}$   
 727 (‰), and is calculated from the following equation:

$$\Delta^{13}C = \frac{\delta^{13}C_{\text{air}} - \delta^{13}C_{\text{leaf}}}{1 + \delta^{13}C_{\text{leaf}}} \quad (3.2)$$

728 where  $\delta^{13}C_{\text{air}}$  is assumed to be -8‰ (Keeling et al. 1979; Farquhar et al. 1989), a  
 729 represents the fractionation between <sup>12</sup>C and <sup>13</sup>C due to diffusion in air, assumed  
 730 to be 4.4‰, and b represents the fractionation caused by Rubisco carboxylation,  
 731 assumed to be 27‰ (Farquhar et al. 1989).

**732** 3.2.4  $A_{net}/C_i$  curve-fitting and parameter estimation

**733** We fit  $A_{net}/C_i$  curves of each individual using the ‘fitaci’ function in the  
**734** ‘plantecophys’ R package (Duursma 2015). This function estimates the maximum  
**735** rate of Rubisco carboxylation  $V_{cmax}$ ;  $\mu\text{mol m}^{-2} \text{s}^{-1}$ ) and maximum rate of electron  
**736** transport for RuBP regeneration ( $J_{max}$ ;  $\mu\text{mol m}^{-2} \text{s}^{-1}$ ) based on the Farquhar,  
**737** von Caemmerer, and Berry biochemical model of C<sub>3</sub> photosynthesis (Farquhar  
**738** et al. 1980). For each curve fit, we included triose phosphate utilization (TPU)  
**739** limitation to avoid underestimating  $J_{max}$  (Gregory et al. 2021). Curves were  
**740** visually examined to confirm the likely presence of TPU limitation.

**741** We determined Michaelis-Menten coefficients for Rubisco affinity to CO<sub>2</sub>  
**742** ( $K_c$ ;  $\mu\text{mol mol}^{-1}$ ) and O<sub>2</sub> ( $K_o$ ;  $\mu\text{mol mol}^{-1}$ ), and the CO<sub>2</sub> compensation point  
**743** ( $\Gamma^*$ ;  $\mu\text{mol mol}^{-1}$ ) using leaf temperature and equations described in Medlyn et al.  
**744** (2002) and derived in Bernacchi et al. (2001). Specifically,  $K_c$  and  $K_o$  were  
**745** calculated as:

$$K_c = 404.9 * \exp^{\frac{79430(T_k - 298)}{298RT_k}} \quad (3.3)$$

**746** and

$$K_o = 278.4 * \exp^{\frac{36380(T_k - 298)}{298RT_k}} \quad (3.4)$$

**747** while  $\Gamma^*$  was calculated as:

$$\Gamma^* = 42.75 * \exp^{\frac{37830(T_k - 298)}{298RT_k}} \quad (3.5)$$

**748** In all three equations,  $T_k$  is the leaf temperature (in Kelvin) during each  $A_{\text{net}}/C_i$

**749** curve and R is the universal gas constant ( $8.314 \text{ J mol}^{-1} \text{ K}^{-1}$ ).

**750** We standardized  $V_{\text{cmax}}$  and  $J_{\text{max}}$  estimates to  $25^\circ\text{C}$  using a modified Ar-

**751** rhenius equation (Kattge and Knorr 2007):

$$k_{25} = \frac{k_{\text{obs}}}{e^{\frac{H_a(T_{\text{obs}} - T_{\text{ref}})}{T_{\text{ref}}RT_{\text{obs}}}} * \frac{1+e^{\frac{T_{\text{ref}}\Delta S - H_d}{T_{\text{obs}}}}}{1+e^{\frac{T_{\text{obs}}\Delta S - H_d}{T_{\text{obs}}}}}} \quad (3.6)$$

**752**  $k_{25}$  represents the standardized  $V_{\text{cmax}}$  or  $J_{\text{max}}$  rate at  $25^\circ\text{C}$ ,  $k_{\text{obs}}$  represents

**753** the  $V_{\text{cmax}}$  or  $J_{\text{max}}$  estimate at the average leaf temperature measured inside the

**754** cuvette during the  $A_{\text{net}}/C_i$  curve.  $H_a$  is the activation energy of  $V_{\text{cmax}}$  ( $71,513$

**755**  $\text{J mol}^{-1}$ ) Kattge and Knorr (2007) or  $J_{\text{max}}$  ( $49,884 \text{ J mol}^{-1}$ ) (Kattge and Knorr

**756** 2007).  $H_d$  represents the deactivation energy of both  $V_{\text{cmax}}$  and  $J_{\text{max}}$  ( $200,000 \text{ J}$

**757**  $\text{mol}^{-1}$ ) (Medlyn et al. 2002), and R represents the universal gas constant ( $8.314$

**758**  $\text{J mol}^{-1} \text{ K}^{-1}$ ).  $T_{\text{ref}}$  represents the standardized temperature of  $298.15 \text{ K}$  ( $25^\circ\text{C}$ )

**759** and  $T_{\text{obs}}$  represents the mean leaf temperature (in K) during each  $A_{\text{net}}/C_i$  curve.

**760**  $\Delta S$  is an entropy term that (Kattge and Knorr 2007) derived as a linear relation-

**761** ship with average growing season temperature ( $T_g$ ;  $^\circ\text{C}$ ), where:

$$\Delta S_{v_{\text{cmax}}} = -1.07 T_g + 668.39 \quad (3.7)$$

**762** and

$$\Delta S_{j_{\text{max}}} = -0.75 T_g + 659.70 \quad (3.8)$$

**763** We estimated  $T_g$  in Equations 3.7 and 3.8 based on mean daily (24-hour) air  
**764** temperature of the 30 days leading up to the day of each sample collection using  
**765** the same weather station reported in the site description. We then used  $V_{cmax25}$   
**766** and  $J_{max25}$  estimates to calculate the ratio of  $J_{max25}$  to  $V_{cmax25}$  ( $J_{max25}:V_{cmax25}$ ;  
**767** unitless).

**768** 3.2.5 *Proportion of leaf nitrogen allocated to photosynthesis and structure*

**769** We used equations from Niinemets and Tenhunen (1997) to estimate the  
**770** proportion of leaf N content allocated to Rubisco and bioenergetics. The propor-  
**771** tion of leaf N allocated to Rubisco ( $\rho_{rub}$ ; gN gN<sup>-1</sup>) was calculated as a function  
**772** of  $V_{cmax25}$  and  $N_{area}$ :

$$\rho_{rubisco} = \frac{V_{cmax25}N_r}{V_{cr}N_{area}} \quad (3.9)$$

**773** where  $N_r$  is the amount of nitrogen in Rubisco, set to 0.16 gN (gN in Rubisco)<sup>-1</sup>  
**774** and  $V_{cr}$  is the maximum rate of RuBP carboxylation per unit Rubisco protein,  
**775** set to 20.5 μmol CO<sub>2</sub> (g Rubisco)<sup>-1</sup>. The proportion of leaf nitrogen allocated to  
**776** bioenergetics ( $\rho_{bioe}$ ; gN gN<sup>-1</sup>) was similarly calculated as a function of  $J_{max25}$  and  
**777**  $N_{area}$ :

$$\rho_{bioe} = \frac{J_{max25}N_b}{J_{mc}N_{area}} \quad (3.10)$$

**778** where  $N_b$  is the amount of nitrogen in cytochrome f, set to 0.12407 gN (μmol  
**779** cytochrome f)<sup>-1</sup> assuming a constant 1: 1: 1.2 cytochrome f: ferredoxin NADP  
**780** reductase: coupling factor molar ratio (Evans and Seemann 1989; Niinemets and

781 Tenhunen 1997), and  $J_{mc}$  is the capacity of electron transport per cytochrome f,  
782 set to  $156 \mu\text{mol electron} (\mu\text{mol cytochrome f})^{-1}\text{s}^{-1}$ .

783 We estimated the proportion of leaf N content allocated to photosynthetic  
784 tissue ( $\rho_{photo}$ ;  $\text{gN gN}^{-1}$ ) as the sum of  $\rho_{rub}$  and  $\rho_{bioe}$ . This calculation is an un-  
785 derestimate of the proportion of leaf N allocated to photosynthetic tissue because  
786 it does not include N allocated to light harvesting proteins. This leaf N pool was  
787 not included because we did not perform chlorophyll extractions on focal leaves.  
788 However, the proportion of leaf N content allocated to light harvesting proteins  
789 tends to be small relative to  $\rho_{rub}$  and  $\rho_{bioe}$ , and may scale with changes in  $\rho_{rub}$   
790 and  $\rho_{bioe}$  (Niinemets and Tenhunen 1997).

791 Finally, we estimated the proportion of leaf N content allocated to struc-  
792 tural tissue ( $\rho_{str}$ ;  $\text{gN gN}^{-1}$ ) using an empirical equation from Onoda et al. (2017):

$$N_{cw} = 0.000355 * M_{area}^{1.39} \quad (3.11)$$

793 where  $N_{cw}$  is the leaf N content allocated to cell walls ( $\text{gN m}^{-2}$ ).  $\rho_{str}$  was estimated  
794 by dividing  $N_{cw}$  by  $N_{area}$ .

795 3.2.6 *Tradeoffs between nitrogen and water use*

796 Photosynthetic nitrogen use efficiency (PNUE;  $\mu\text{mol CO}_2 \text{ mol}^{-1} \text{ N s}^{-1}$ )  
797 was calculated by dividing  $A_{net}$  by  $N_{area}$ , first converting  $N_{area}$  to  $\text{mol N m}^{-2}$   
798 using the molar mass of N ( $14 \text{ g mol}^{-1}$ ). We used  $\chi$  as an indicator of water  
799 use efficiency, which exploratory analyses suggest had similar responses to soil N  
800 availability and pH as intrinsic water use efficiency measured from gas exchange

801 ( $A_{\text{net}}/g_s$ ). Tradeoffs between nitrogen and water use were determined by cal-  
802 culating the ratio of  $N_{\text{area}}$  to  $\chi$  ( $N_{\text{area}}:\chi$ ; g N m<sup>-2</sup>) and  $V_{\text{cmax25}}$  to  $\chi$  ( $V_{\text{cmax25}}:\chi$ ;  
803  $\mu\text{mol m}^{-2} \text{s}^{-1}$ ). This approach is similar to tradeoff calculations in which nitrogen-  
804 water use tradeoffs are measured as the ratio of  $N_{\text{area}}$  or  $V_{\text{cmax25}}$  to  $g_s$  (Paillassa  
805 et al. 2020; Bialic-Murphy et al. 2021). In this study, we quantify these re-  
806 lationships using  $\chi$  in lieu of  $g_s$  because  $g_s$  rapidly changes with environmental  
807 conditions and therefore may have been altered by recent tree branch severance  
808 and/or placement in the cuvette.

809 3.2.7 *Soil nitrogen availability and pH*

810 To characterize soil N availability at the time of our leaf gas exchange  
811 measurements, we used mixed bed resin bags to quantify mobile ammonium-N  
812 and nitrate-N concentrations in each plot. Lycra mesh bags were filled with 5 g  
813 of Dowex® Marathon MR-3 hydrogen and hydroxide form resin (MilliporeSigma,  
814 Burlington, MA USA) and sealed with a zip tie. Each bag was activated by  
815 soaking in 0.5 M HCl for 20 minutes, then in 2 M NaCl until pH of the saline  
816 solution stabilized, as described in Allison et al. (2008). Five resin bags were  
817 inserted about 10 cm below the soil surface at each plot on June 25, 2019: one  
818 near each of the four plot corners and one near the plot center. All resin bags  
819 were collected 24 days later on July 19, 2019 and were frozen until extracted.

820 Prior to anion and cation extraction, each resin bag was rinsed with ul-  
821 trapure water (MilliQ IQ 7000; Millipore Sigma, Burlington, MA) to remove any  
822 surface soil residues. Anions and cations were extracted from surface-cleaned resin  
823 bags by individually soaking and shaking each bag in 100 mL of a 0.1 M HCl/2.0

824 M NaCl matrix for one hour. Using a microplate reader (Biotek Synergy H1;  
825 Biotek Instruments, Winooski, VT USA), nitrate-N concentrations were quanti-  
826 fied spectrophotometrically at 540 nm with the end product of a single reagent  
827 vanadium (III) chloride reaction (Doane and Horwáth 2003), and ammonium-N  
828 concentrations quantified at 650 nm with the end product of a modified phenol-  
829 hypochlorite reaction (Weatherburn 1967; Rhine et al. 1998). Both the single  
830 reagent vanadium (III) chloride and modified phenol-hypochlorite methodologies  
831 have been well established for determining nitrate-N and ammonium-N concen-  
832 trations in resin bag extracts (Arnone 1997; Allison et al. 2008). We used a  
833 series of negative and positive controls throughout each well plate to verify the  
834 accuracy and precision of our measurements, assaying each resin bag extract and  
835 control in triplicate. Soil N availability was estimated as the sum of the nitrate-N  
836 and ammonium-N concentration in each resin bag, normalized per g of resin and  
837 duration in the field ( $\mu\text{g N g}^{-1} \text{ resin d}^{-1}$ ), then subsequently averaged across all  
838 resin bags in a plot for a plot-level mean.

839 Soil pH was measured on 0-10 cm mineral soil samples collected prior to  
840 fertilization in 2019. Near each of the four plot corners, three 5.5 cm diameter soil  
841 cores were collected after first removing the forest floor where present. Each set  
842 of three cores was placed in a plastic bag, and later composited by hand mixing  
843 and sieved to 4mm. Soil pH was determined for a 1:2 soil:water slurry (10 g field-  
844 moist soil to 20 mL DI water) of each sample using an Accumet AB15 pH meter  
845 with flushable junction probe (Fisher Scientific; Hampton, NH, USA), and was  
846 estimated at the plot level as the mean soil pH within each plot.

**847** 3.2.8 *Statistical analyses*

**848** We built two separate series of linear mixed-effects models to explore effects  
**849** of soil N availability, soil pH, species, and leaf N content on leaf physiological  
**850** traits. In the first series of linear mixed-effects models, we explored the effect  
**851** of soil N availability, soil pH, and species on leaf N content, leaf photosynthesis,  
**852** stomatal conductance, and nitrogen-water use tradeoffs. Models included plot-  
**853** level soil N availability and plot-level soil pH as continuous fixed effects, species  
**854** as a categorical fixed effect, and site as a categorical random intercept term.  
**855** Interaction terms between fixed effects were not included due to the small number  
**856** of experimental plots. We built a series of separate models with this independent  
**857** variable structure to quantify individual effects of soil N availability, soil pH,  
**858** and species on  $N_{\text{area}}$ ,  $M_{\text{area}}$ ,  $N_{\text{mass}}$ ,  $A_{\text{net}}$ ,  $V_{\text{cmax25}}$ ,  $J_{\text{max25}}$ ,  $J_{\text{max25}}:V_{\text{cmax25}}$ ,  $\rho_{\text{rubisco}}$ ,  
**859**  $\rho_{\text{bioenergetics}}$ ,  $\rho_{\text{photo}}$ ,  $\rho_{\text{structure}}$ ,  $\chi$ , PNUE,  $N_{\text{area}}:\chi$ , and  $V_{\text{cmax25}}:\chi$ .

**860** A second series of linear mixed-effects models were built to investigate  
**861** relationships between leaf N content and photosynthetic parameters. Statistical  
**862** models included  $N_{\text{area}}$  as a single continuous fixed effect with species and site des-  
**863** ignated as individual random intercept terms. We used this independent variable  
**864** structure to quantify individual effects of leaf N content on  $A_{\text{net}}$ ,  $V_{\text{cmax25}}$ ,  $J_{\text{max25}}$ ,  
**865**  $J_{\text{max25}}:V_{\text{cmax25}}$ , and  $\chi$ .

**866** For all linear mixed-effects models, we used Shapiro-Wilk tests of normal-  
**867** ity to determine whether linear mixed-effects models satisfied residual normality  
**868** assumptions. If residual normality assumptions were not met, then models were  
**869** fit using dependent variables that were natural log transformed. If residual nor-  
**870** mality assumptions were still not met (Shapiro-Wilk:  $p < 0.05$ ), then models were

871 fit using dependent variables that were square root transformed. All residual nor-  
872 mality assumptions for both sets of models that did not originally satisfy residual  
873 normality assumptions were met with either a natural log or square root data  
874 transformation (Shapiro-Wilk:  $p > 0.05$  in all cases).

875 In the first series of models, models for  $N_{\text{area}}$ ,  $M_{\text{area}}$ ,  $N_{\text{mass}}$ ,  $V_{\text{cmax25}}$ ,  $J_{\text{max25}}$ ,  
876  $\chi$ ,  $N_{\text{area}}:\chi$ , and  $V_{\text{cmax25}}:\chi$ ,  $\rho_{\text{rubisco}}$ ,  $\rho_{\text{bioenergetics}}$ ,  $\rho_{\text{photo}}$ ,  $\rho_{\text{structure}}$  satisfied residual  
877 normality assumptions without data transformations (Shapiro-Wilk:  $p > 0.05$  in  
878 all cases). The model for  $J_{\text{max25}}:V_{\text{cmax25}}$  satisfied residual normality assumptions  
879 with a natural log data transformation, while models for  $A_{\text{net}}$  and PNUE each  
880 satisfied residual normality assumptions with square root data transformations.  
881 In the second series of models, models for  $V_{\text{cmax25}}$ ,  $J_{\text{max25}}$ ,  $\chi$ , and  $V_{\text{cmax25}}:\chi$  satisfied  
882 residual normality assumptions without data transformations (Shapiro-Wilk:  $p$   
883  $> 0.05$  in all cases). The model for  $J_{\text{max25}}:V_{\text{cmax25}}$  required a natural log data  
884 transformation and the model for  $A_{\text{net}}$  required a square root data transformation  
885 (Shapiro-Wilk:  $p > 0.05$  in both cases).

886 In all models, we used the ‘lmer’ function in the ‘lme4’ R package (Bates  
887 et al. 2015) to fit each model and the ‘Anova’ function in the ‘car’ R package (Fox  
888 and Weisberg 2019) to calculate Type II Wald’s  $\chi^2$  and determine the significance  
889 level ( $\alpha = 0.05$ ) of each fixed effect coefficient. Finally, we used the ‘emmeans’  
890 R package (Lenth, 2019) to conduct post-hoc comparisons using Tukey’s tests,  
891 where degrees of freedom were approximated using the Kenward-Roger approach  
892 (Kenward and Roger 1997). All analyses and plots were conducted in R version  
893 4.1.1 (R Core Team 2021)). All figure regression lines and associated 95% confi-  
894 dence interval error bars were plotted using predictions generated across the soil

**895** nitrogen availability gradient using the ‘emmeans’ R package (Lenth 2019).

**896** 3.3 Results

**897** 3.3.1 *Leaf N content*

**898** Increasing soil N availability generally increased  $N_{\text{area}}$  (Table 3.1; Fig. 3.1a). This pattern was driven by an increase in  $N_{\text{mass}}$  (Table 3.1; Fig. 3.1c) and a marginal increase in  $M_{\text{area}}$  (Table 3.1; Fig. 3.1e) with increasing soil N availability. There was no effect of soil pH on  $N_{\text{area}}$ ,  $N_{\text{mass}}$ , or  $M_{\text{area}}$  (Table 3.1); however, we did observe strong differences in  $N_{\text{area}}$  (Fig. 3.1b),  $N_{\text{mass}}$  (Fig. 3.1d), and  $M_{\text{area}}$  (Fig. 3.1e) between species (Table 3.1).

**Table 3.1.** Effects of soil N availability, soil pH, and species on leaf N content per unit leaf area ( $N_{\text{area}}$ ), leaf N content per unit leaf mass ( $N_{\text{mass}}$ ), and leaf mass per unit leaf area ( $M_{\text{area}}$ )

	df	$N_{\text{area}}$			$N_{\text{mass}}$			$M_{\text{area}}$		
		Coefficient	$\chi^2$	p	Coefficient	$\chi^2$	p	Coefficient	$\chi^2$	p
Intercept	-	9.03E-01	-	-	1.68E+00	-	-	4.60E+01	-	-
Soil N	1	1.68E-02	11.990	<b>0.001</b>	1.25E-02	6.902	<b>0.009</b>	4.87E-01	4.143	<b>0.042</b>
Soil pH	1	9.28E-02	0.836	0.361	8.08E-02	0.663	0.415	4.05E+00	0.653	0.419
Species	4	-	72.128	<b>&lt;0.001</b>	-	35.074	<b>&lt;0.001</b>	-	29.869	<b>&lt;0.001</b>

\*Significance determined using Type II Wald  $\chi^2$  tests ( $\alpha = 0.05$ ). P-values  $< 0.05$  are in bold.

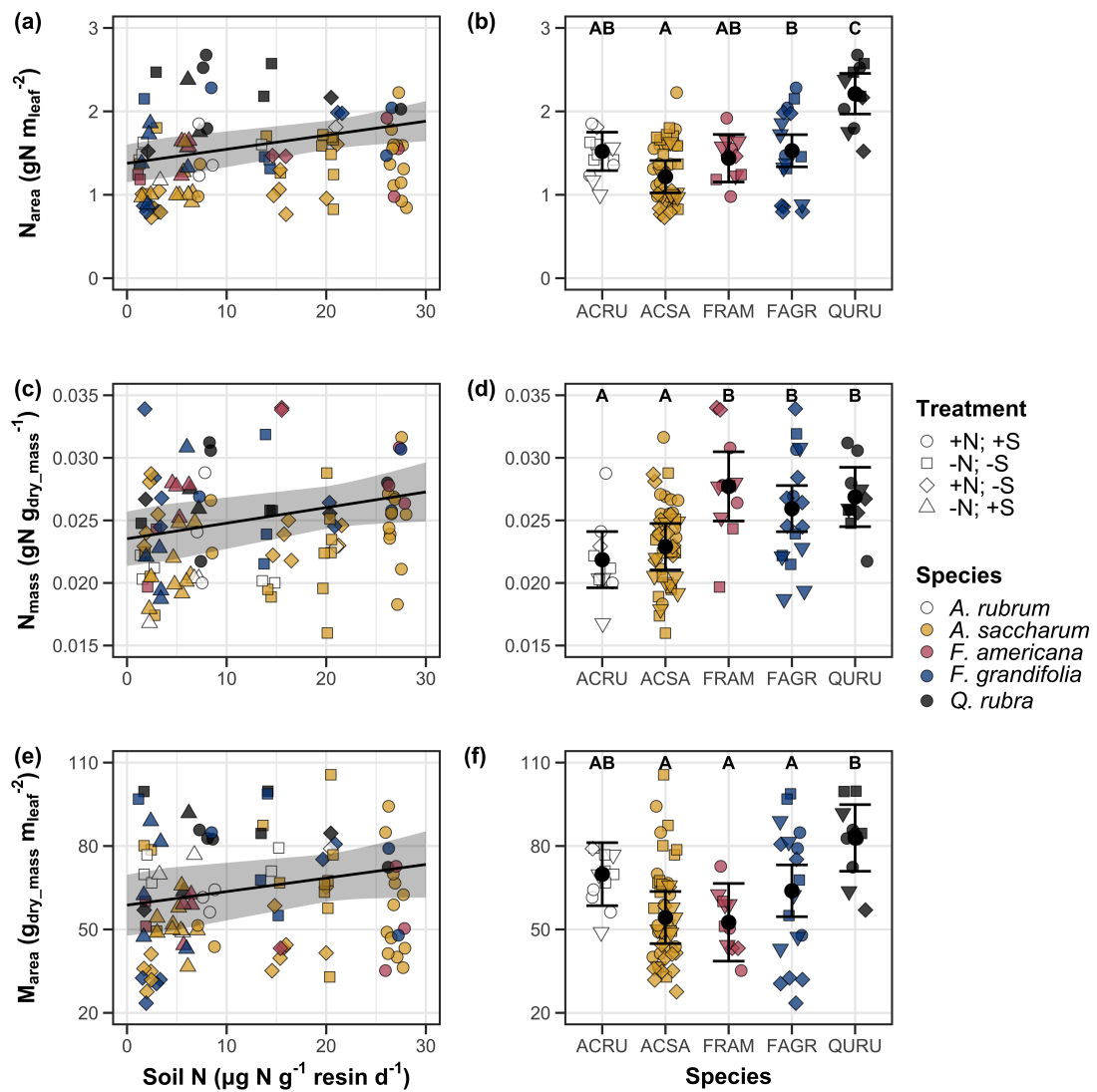


**Figure 3.1.** Effects of soil N availability and species on leaf N content per unit leaf area (a-b), leaf nitrogen content per unit leaf biomass (c-d), and leaf mass per unit leaf area (e-f). Soil N availability is represented on the x-axis in the left column of panels, while species is represented on the x-axis in the right column of panels. Tree species are represented as colored points and treatment plots are represented as shaped points, jittered for visibility. Species are abbreviated in the right column of panels through their assigned NRCS PLANTS Database symbol (USDA NRCS 2022), grouped along the x-axis per common mycorrhizal association, where the first three species commonly associate with arbuscular mycorrhizae (ACRU, ASCA, FAGR) and the second two species with ectomycorrhizae (FAGR, QURU). Trendlines are only included when the regression slope is statistically different from zero ( $p < 0.05$ ).

**904** 3.3.2 *Net photosynthesis and leaf biochemistry*

**905** Increasing soil N availability generally had no effect on  $A_{\text{net}}$ ,  $V_{\text{cmax25}}$ ,  $J_{\text{max25}}$ ,  
**906** or  $J_{\text{max25}}:V_{\text{cmax25}}$  (Table 3.2, Figs. 3.2a, 3.2d, 3.2g). We also observed strong  
**907** species effects on all measured leaf photosynthetic traits (Table 3.2; Figs. 3.2b,  
**908** 3.2e, 3.2h). Increasing soil pH had a marginal negative effect on  $A_{\text{net}}$ , but had no  
**909** effect on  $V_{\text{cmax25}}$ ,  $J_{\text{max25}}$ , or  $J_{\text{max25}}:V_{\text{cmax25}}$  (Table 3.2). There was a weak positive  
**910** effect of increasing  $N_{\text{area}}$  on  $A_{\text{net}}$  (Fig. 3.2c), but quite strong positive effects of  
**911** increasing  $N_{\text{area}}$  on  $V_{\text{cmax25}}$  and  $J_{\text{max25}}$  (Table 3.2; Fig. 3.2f and 3.2i).

**Table 3.2.** Effects of soil N availability, soil pH, species, and  $N_{\text{area}}$  on leaf biochemistry

	$A_{\text{net}}$			$V_{\text{cmax25}}$			$J_{\text{max25}}$			
	df	Coefficient	$\chi^2$	p	Coefficient	$\chi^2$	p	Coefficient	$\chi^2$	p
(Intercept)	-	3.29E+00 <sup>b</sup>	-	-	6.38E+01	-	-	1.12E+02	-	-
Soil N	1	-1.23E-03 <sup>b</sup>	1.798	0.180	-3.84E-01	1.745	0.187	-6.70E-01	2.172	0.141
Soil pH	1	-3.09E-01 <sup>b</sup>	3.312	0.069	-4.91E+00	0.655	0.418	-8.18E+00	0.742	0.389
Species	4	-	11.838	<b>0.019</b>	-	31.748	<0.001	-	27.291	<0.001
( $N_{\text{area}}$ int.)	-	6.59E-01 <sup>b</sup>	-	-	1.45E-01	-	-	2.86E+01	-	-
$N_{\text{area}}$	4	3.13E-01 <sup>b</sup>	4.790	<b>0.029</b>	2.43E+01	22.616	<0.001	4.04E+01	28.259	<0.001

	$J_{\text{max25}}:V_{\text{cmax25}}$			
	df	Coefficient	$\chi^2$	p
(Intercept)	-	6.59E-01 <sup>a</sup>	-	-
Soil N	1	7.04E-04 <sup>a</sup>	0.088	0.767
Soil pH	1	-7.84E-03 <sup>a</sup>	0.025	0.874
Species	4	-	12.745	<b>0.013</b>
( $N_{\text{area}}$ int.)	-	6.69E-01 <sup>a</sup>	-	-
$N_{\text{area}}$	4	-4.69E-02 <sup>a</sup>	1.142	0.285

\*Significance determined using Type II Wald  $\chi^2$  tests ( $\alpha = 0.05$ ).  $P$ -values  $< 0.05$  are in bold, while  $p$ -values between 0.05 and 0.1 are italicized. Superscript letters indicate model coefficients fit to natural-log (<sup>a</sup>) or square-root (<sup>b</sup>) transformed data. Relationships between  $N_{\text{area}}$  and each response variable were fit using the second series of bivariate mixed-effects models, so model coefficients and results are independent from model coefficients and results reported for relationships between soil N, soil pH, and species for each response variable. Key:  $A_{\text{net}}$  – light saturated net photosynthesis rate;  $V_{\text{cmax25}}$  – maximum rate of Rubisco carboxylation at 25°C;  $J_{\text{max25}}$  – maximum rate of electron transport for RuBP regeneration at 25°C,  $J_{\text{max25}}:V_{\text{cmax25}}$  – the ratio of  $J_{\text{max25}}$  to  $V_{\text{cmax25}}$ .

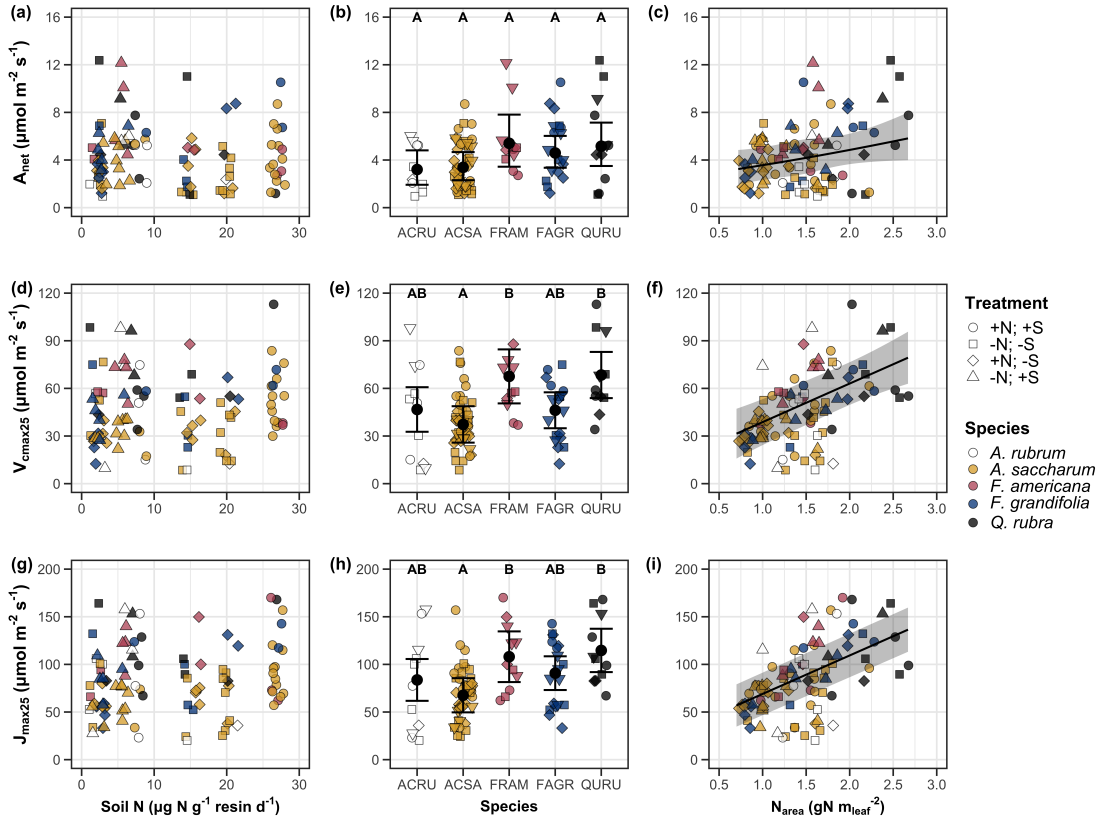


**Figure 3.2.** Effects of soil N availability (left column of panels), species (middle column of panels), and leaf N content per unit leaf area (right column of panels) on net photosynthesis (a-c), maximum Rubisco carboxylation rate (d-f), and maximum RuBP regeneration rate (g-i). Soil N availability is represented on the x-axis in the left column of panels, species is represented on the x-axis in the middle column of panels, and leaf N content per unit leaf area is represented continuously on the x-axis in the right column of panels. Species abbreviations and position along the x-axis in the middle column of panels, colored points, shapes, and trendlines are as explained in Figure 3.1.

**912** 3.3.3 *Leaf N allocation*

**913** Neither soil N availability nor soil pH affected the proportion of leaf N  
**914** allocated to Rubisco or bioenergetics (Table 3.3; Fig. 3.3a, Fig. 3.3c), nor was  
**915** there any subsequent effect on the proportion of leaf N allocated to photosynthesis  
**916** (Table 3.3; Fig. 3.3f). We also found no effect of soil N availability or soil pH on  
**917** the proportion of leaf N allocated to structure (Table 3.3; Fig 3.3g). Species varied  
**918** in the proportion of leaf N allocated to Rubisco, photosynthesis, and structure (Fig  
**919** 3.3b, Fig. 3.3d, Fig 3.3h), with no detectable species effect on the proportion of  
**920** leaf N allocated to bioenergetics (Table 3.3).

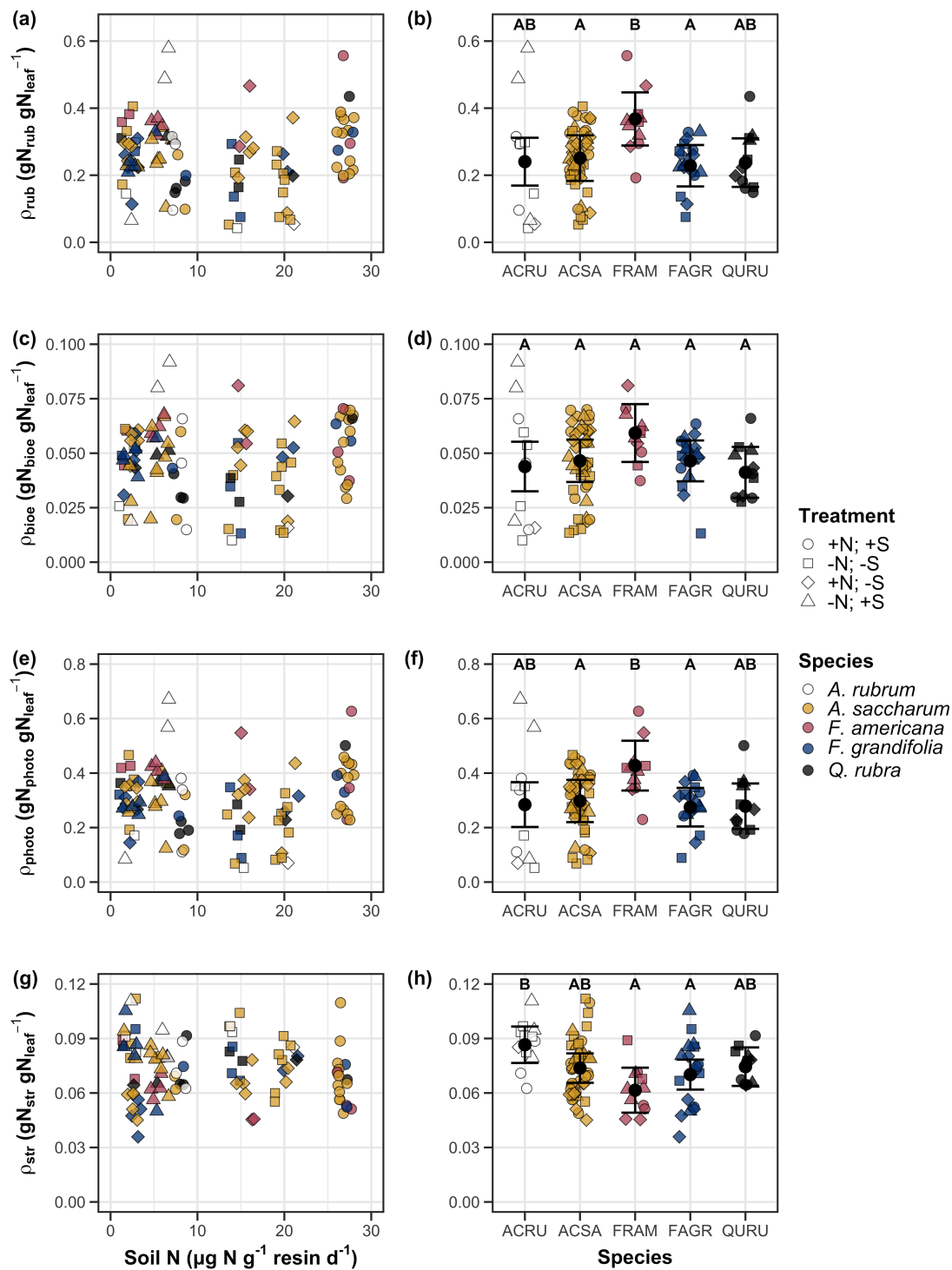
**Table 3.3.** Effects of soil N availability, soil pH, and species on the proportion of leaf nitrogen content allocated to photosynthesis, Rubisco, bioenergetics, and structure

	$\rho_{\text{photo}}$			$\rho_{\text{rub}}$			$\rho_{\text{bioe}}$			
	df	Coefficient	$\chi^2$	p	Coefficient	$\chi^2$	p	Coefficient	$\chi^2$	p
Intercept	-	4.93E-01	-	-	4.17E-01	-	-	7.64E-02	-	-
Soil N	1	-1.23E-03	0.521	0.470	-1.04E-03	0.501	0.479	-1.77E-04	0.557	0.455
Soil pH	1	-4.37E-02	1.581	0.209	-3.70E-02	1.511	0.219	-6.84E-03	1.941	0.164
Species	4	-	13.106	<b>0.011</b>	-	14.152	<b>0.007</b>	-	7.300	0.121

	$\rho_{\text{str}}$			
	df	Coefficient	$\chi^2$	p
Intercept	-	9.77E-02	-	-
Soil N	1	-2.29E-04	1.165	0.280
Soil pH	1	-1.87E-03	0.179	0.672
Species	4	-	16.428	<b>0.002</b>

\*Significance determined using Type II Wald  $\chi^2$  tests ( $\alpha = 0.05$ ). P-values  $< 0.05$  are in bold. Key:  $\rho_{\text{photo}}$  - proportion of leaf nitrogen content allocated to photosynthesis;  $\rho_{\text{rub}}$  - proportion of leaf nitrogen content allocated to Rubisco;  $\rho_{\text{bioe}}$  - proportion of leaf nitrogen content allocated to bioenergetics;  $\rho_{\text{str}}$  - proportion of leaf nitrogen content allocated to structure.



**Figure 3.3.** Effects of soil nitrogen availability and species on the proportion of leaf nitrogen content allocated to Rubisco (a-b), bioenergetics (c-d), photosynthesis (e-f), and structure (g-h)

**921** 3.3.4 *Tradeoffs between nitrogen and water use*

**922** Although soil N availability did not affect  $\chi$  (Table 3.4; Fig. 3.4a), increasing  
**923** soil N availability decreased PNUE (Table 3.4; Fig. 3.4d) and increased the  
**924** ratio of  $N_{\text{area}}:\chi$  (Table 3.4; Fig. 3.4f). Specifically, this response yielded a 26%  
**925** reduction in PNUE and 37% stimulation in  $N_{\text{area}}:\chi$  across the soil nitrogen avail-  
**926** ability gradient. There was no apparent effect of soil N availability on  $V_{\text{cmax25}}:\chi$   
**927** (Table 3.4; Fig. 3.4h). Increasing soil pH had a weak marginal negative effect  
**928** on PNUE, but did not influence  $\chi$ ,  $N_{\text{area}}:\chi$ , or  $V_{\text{cmax25}}:\chi$  (Table 3.4). We also  
**929** observed differences in  $\chi$  (Fig. 3.4b), PNUE (Fig. 3.4e),  $N_{\text{area}}:\chi$  (Fig. 3.4g), and  
**930**  $V_{\text{cmax25}}:\chi$  (Fig. 3.4i) between species (Table 3.4). Finally, increasing  $N_{\text{area}}$  had a  
**931** strong negative effect on  $\chi$  (Table 3.4; Fig. 3.4c) and a strong positive effect on  
**932**  $V_{\text{cmax25}}:\chi$  (Table 3.4; Fig. 3.4j).

**Table 3.4.** Effects of soil N availability, soil pH, species, and  $N_{\text{area}}$  on tradeoffs between nitrogen and water use

	$\chi$			PNUE			$N_{\text{area}}:\chi$			
	df	Coefficient	$\chi^2$	p	Coefficient	$\chi^2$	p	Coefficient	$\chi^2$	p
(Intercept)	-	8.12E-01	-	-	9.57E+00	-	-	9.19E-01	-	-
Soil N	1	-1.14E-03	1.698	0.193	-6.63E-02	6.396	<b>0.011</b>	2.60E-02	9.533	<b>0.002</b>
Soil pH	1	-1.91E-02	1.087	0.297	-9.25E-01	2.843	<i>0.092</i>	2.03E-01	1.321	0.250
Species	4	-	18.843	<b>0.001</b>	-	13.454	<b>0.009</b>	-	52.983	<b>&lt;0.001</b>
( $N_{\text{area}}$ int.)	-	8.93E-01	-	-	-	-	-	-	-	-
$N_{\text{area}}$	1	-1.11E-01	80.606	<b>&lt;0.001</b>	-	-	-	-	-	-

	$V_{\text{cmax}25}:\chi$			
	df	Coefficient	$\chi^2$	p
(Intercept)	-	7.20E+01	-	-
Soil N	1	3.99E-01	0.963	0.326
Soil pH	1	-3.12E+00	0.138	0.711
Species	4	-	31.450	<b>&lt;0.001</b>
( $N_{\text{area}}$ int.)	-	1.18E+01	-	-
$N_{\text{area}}$	4	3.87E+01	32.797	<b>&lt;0.001</b>

\*Significance determined using Type II Wald  $\chi^2$  tests ( $\alpha = 0.05$ ).  $P$ -values  $< 0.05$  are in bold, while  $p$ -values between 0.05 and 0.1 are italicized. Superscript letters indicate model coefficients fit to natural-log <sup>(a)</sup> or square-root <sup>(b)</sup> transformed data. Relationships between  $N_{\text{area}}$  and each response variable were fit using the second series of bivariate mixed-effects models, so model coefficients and results are independent from model coefficients and results reported for relationships between soil N, soil pH, and species for each response variable. Key:  $\chi$  - isotope-derived estimate of the  $C_i:C_a$ ; PNUE - photosynthetic N use efficiency, ratio of net photosynthesis to leaf N content per unit leaf area;  $N_{\text{area}}:\chi$  - ratio of  $N_{\text{area}}$  to  $\chi$ ;  $V_{\text{cmax}25}:\chi$  - ratio of  $V_{\text{cmax}25}$  to  $\chi$ .

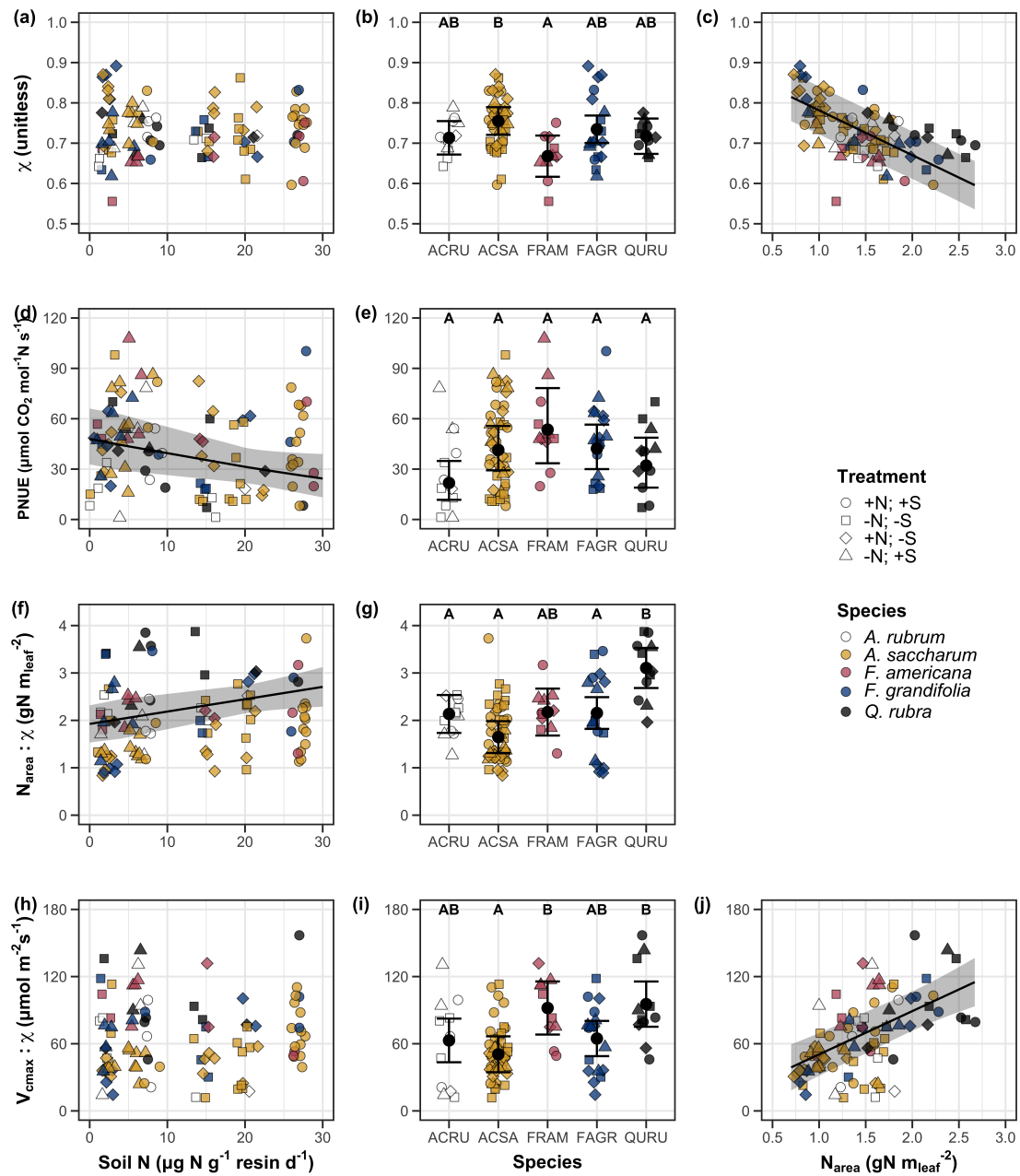


**Figure 3.4.** Effects of soil nitrogen availability and species on the proportion of leaf nitrogen content allocated to Rubisco (a-b), bioenergetics (c-d), photosynthesis (Rubisco + bioenergetics; e-f), and structure (g-h). Soil nitrogen availability is represented on the x-axis in the left column of panels and species are represented on the x-axis in the right column of panels. Species abbreviations and position along the x-axis in the middle column of panels, colored points, shapes, trendlines, error bars, and compact lettering are as explained in Figure 3.1.

**933** 3.4 Discussion

**934** Photosynthetic least-cost theory provides an explanation for understand-  
**935** ing relationships between soil nutrient availability, leaf nutrient allocation, and  
**936** photosynthetic capacity. The theory suggests that plants acclimate to a given  
**937** environment by optimizing leaf photosynthesis rates at the lowest summed cost  
**938** of using nutrients and water Prentice et al. (2014), Wang et al. (2017), Smith  
**939** et al. (2019), Paillassa et al. (2020). The theory predicts that an increase in  
**940** soil nutrient availability should allow similar photosynthesis rates to be achieved  
**941** with increased leaf nutrient content and photosynthetic capacity (i.e.,  $V_{cmax25}$  and  
**942**  $J_{max25}$ ) at lower leaf  $C_i:C_a$  ( $\chi$ ), resulting in an increase in water use efficiency,  
**943** decrease in nutrient use efficiency, and increase in both leaf nutrient content and  
**944** photosynthetic capacity per unit  $\chi$ . The theory predicts similar leaf responses to  
**945** increasing soil pH under acidic conditions, presumably due to generally faster nu-  
**946** trient cycle dynamics and consequent reductions in the cost of acquiring nutrients  
**947** relative to water with increasing soil pH (Wang et al. 2017; Paillassa et al. 2020;  
**948** Dong et al. 2020).

**949** Supporting the theory, we showed that increasing soil N availability was  
**950** associated with increased leaf N content (Fig 3.1a, 3.1c), a pattern that reduced  
**951** photosynthetic N use efficiency (Fig 3.4d) and increased leaf N content per unit  
**952**  $\chi$  (Fig 3.4f). Increasing soil N coincided with slight, but non-significant decreases  
**953** in  $\chi$  and increases in  $V_{cmax25}$  and  $J_{max25}$  ( $p < 0.2$ , Table 3.2). The positive trend  
**954** between soil N availability and photosynthetic capacity was supported by the con-  
**955** current strong increase in leaf N content with increasing soil N availability, which  
**956** resulted in no change in the proportion of leaf N content allocated to photosynthe-

957 sis across the soil N availability gradient. Additionally, leaf N content exhibited a  
958 strong negative correlation with  $\chi$ , indicative of strong nitrogen-water use trade-  
959 offs at the leaf level. Responses tended to vary more due to soil N availability  
960 than soil pH. Overall, these findings are consistent with the nutrient-water use  
961 tradeoffs predicted from theory.

962 3.4.1 *Soil nitrogen availability modifies tradeoffs between nitrogen and water use*

963 In support of expected least-cost outcomes and past environmental gradient  
964 studies (Dong et al. 2017; Paillassa et al. 2020), we found that increasing soil N  
965 availability was associated with increased leaf N content. Soil N availability had  
966 smaller impacts on measures of net photosynthesis and  $\chi$ , which led to reductions  
967 in PNUE and increases in leaf N content per unit  $\chi$ , as expected from theory.  
968 Photosynthetic least-cost theory suggests that reductions in PNUE should be  
969 driven by an increase in the proportion of leaf N allocated to photosynthetic tissue,  
970 a pattern that should allow plants to achieve optimal photosynthetic rates with  
971 greater photosynthetic capacity to make better use of available light. Contrasting  
972 theory predictions, we found no effect of soil N availability on photosynthetic  
973 capacity. However, photosynthetic capacity did tend to increase with increasing  
974 soil N availability ( $p < 0.20$ ; Table 3.2) resulting in no effect of soil N availability on  
975 the relative fraction of leaf N allocated to photosynthesis, Rubisco, or bioenergetics  
976 (Fig. 3.3). These lines of evidence support the idea that trees use additional N  
977 to support increased leaf N allocation toward photosynthetic tissue and enhance  
978 photosynthetic capacity (Wright et al. 2003).

979 Soil N availability had a stronger effect on leaf N than photosynthetic ca-

980 pacity. This pattern suggests that additional plant N uptake due to increased  
981 soil N availability was also being used to support non-photosynthetic N pools,  
982 possibly to structural tissue or stress-induced amino acid and polyamine synthe-  
983 sis (Minocha et al. 2000; Onoda et al. 2004; Bubier et al. 2011). While we  
984 found no change in the proportion of leaf N allocated to leaf structural tissue, the  
985 overall stimulation in leaf N content with increasing soil N availability suggests an  
986 increase in the net amount of N invested in leaf structural tissue along the N avail-  
987 ability gradient. Importantly, leaf N allocated to structure was calculated using  
988 an empirical relationship between  $M_{\text{area}}$  and the amount of leaf N allocated to cell  
989 walls (Onoda et al. 2017). As the generality of relationships between  $M_{\text{area}}$  and  
990 the amount of leaf N allocated to cell walls has been called into question (Harrison  
991 et al. 2009), future work should consider explicitly measuring N allocation to cell  
992 wall tissue and stress-induced amino acid synthesis to confirm these patterns.

993 In opposition to patterns expected from least cost theory, increasing soil  
994 N availability had no apparent effect on  $\chi$  (Fig. 3.4a). Interestingly, despite  
995 the null effect of soil N availability on  $\chi$ , we observed a strong negative effect of  
996 increasing  $N_{\text{area}}$  on  $\chi$  (Fig. 3.4c), consistent with the nitrogen-water use tradeoffs  
997 expected from theory. The null response of  $\chi$  to increasing soil N availability may  
998 have been due to a lack of water limitation in the system, given that the area  
999 received approximately 20% more precipitation (1167 mm) during the 12-month  
1000 period leading up to our measurement period than normally expected (972 mm).  
1001 However, droughts can and do occur in temperate forests of the northeastern  
1002 United States (Sweet et al. 2017), so the observed increase in leaf N content  
1003 with increasing soil N availability could be a strategy that allows trees to hedge

**1004** bets against drier than normal growing seasons (Onoda et al. 2004; Onoda et al.  
**1005** 2017; Hallik et al. 2009). As was suggested in Paillassa et al. (2020), and more  
**1006** recently by Querejeta et al. (2022), negative effects of soil N availability on  $\chi$  may  
**1007** increase with increasing aridity. This strategy would be especially advantageous if  
**1008** it allows individuals growing in arid regions to maintain carbon assimilation rates  
**1009** with reduced water loss. Future work should attempt to quantify interactive roles  
**1010** of climate and soil nitrogen availability on nitrogen-water use tradeoffs, which  
**1011** could be done by leveraging coordinated and multi-factor nutrient (Borer et al.  
**1012** 2014) and water (Knapp et al. 2017) manipulation experiments across broad  
**1013** climatic gradients.

**1014** 3.4.2 *Soil pH did not modify tradeoffs between nitrogen and water usage*

**1015** While the primary purpose of this study was to examine the role of soil N  
**1016** availability on nitrogen-water use tradeoffs, our experimental design manipulated  
**1017** both soil N and pH, providing an opportunity to isolate the roles of these variables.  
**1018** Previous correlational studies along environmental gradients identified soil pH as  
**1019** a particularly important factor that can modify tradeoffs between nutrient and  
**1020** water use (Smith et al. 2019; Paillassa et al. 2020; Westerband et al. 2023)  
**1021** and the proportion of leaf nitrogen allocated to photosynthesis (Luo et al. 2021).  
**1022** Such studies implied that these patterns may be driven by reductions in the cost of  
**1023** acquiring nutrients relative to water with increasing pH, which may be exacerbated  
**1024** in acidic soils.

**1025** Consistent with theory (Wright et al. 2003; Prentice et al. 2014), our  
**1026** results indicate that increasing soil pH was negatively associated with PNUE.

1027 However, there was no effect of soil pH on leaf N content,  $\chi$ , or leaf N content per  
1028 unit  $\chi$ , most likely because the experimental N additions increased soil N sup-  
1029 ply while both increasing (sodium nitrate) and decreasing (ammonium sulfate)  
1030 soil pH. These results suggest that soil pH did not play a major role in modify-  
1031 ing expected photosynthetic least-cost theory patterns, contrasting findings from  
1032 Paillassa et al. (2020) and other gradient studies that note positive effects of in-  
1033 creasing soil pH on leaf N content, Rubisco carboxylation, and  $\chi$  (Viet et al. 2013;  
1034 Cornwell et al. 2018; Luo et al. 2021). Instead, null responses to soil pH show  
1035 that leaf photosynthetic parameters depend more on soil N availability than pH  
1036 per se, and that inferences from gradient studies might be confounding covariation  
1037 between N availability and soil acidity.

1038 3.4.3 *Species identity explains a large amount of variation in leaf and whole*  
1039 *plant traits*

1040 Species generally explained a larger amount of variation in measured leaf  
1041 traits than soil N availability or soil pH. Interspecies variation is an important  
1042 factor to consider when deducing mechanisms that drive photosynthetic least-  
1043 cost theory, particularly for species that form distinct mycorrhizal associations or  
1044 have different photosynthetic pathways, growth forms, or leaf habit (Espelta et al.  
1045 2005; Adams et al. 2016; Bialic-Murphy et al. 2021; Scott and Smith 2022). The  
1046 need to consider species may also be important when comparing nutrient-water  
1047 use tradeoffs in early and late successional species, or in species with different  
1048 resource economic strategies (Abrams and Mostoller 1995; Ellsworth and Reich  
1049 1996; Wright et al. 2004; Reich 2014; Onoda et al. 2017; Ziegler et al. 2020).

1050        A strength of the study design and sampling effort is that it controls for  
1051 many species differences that should modify nitrogen-water use tradeoffs expected  
1052 from theory. All tree species measured in this study shared the leaf habit of decid-  
1053 uous broadleaves, were growing in forests of similar successional stage, but differed  
1054 in mycorrhizal association and consequent resource economic strategies. As stands  
1055 tended to be dominated by trees that associate with arbuscular mycorrhizae (*Frax-*  
1056 *inus* and both *Acer* species made up 70% of total aboveground biomass across  
1057 stands), ecosystem biogeochemical cycle dynamics may be more closely aligned  
1058 to the inorganic nutrient economy proposed in Phillips et al. (2013), which may  
1059 promote stronger nitrogen-water use tradeoffs in tree species that associate with  
1060 arbuscular mycorrhizae. This result was not observed here, as photosynthetic  
1061 properties varied as much within as across the two mycorrhizal associations rep-  
1062 resented. Given the high variability in measured photosynthetic traits within  
1063 and across species, effects of mycorrhizal association likely require more intensive  
1064 sampling efforts to detect than were possible here.

1065 3.4.4 *Implications for photosynthetic least-cost theory model development*

1066        In the field, soil nutrient availability is heterogeneous across time and space  
1067 (Table S4). Unaccounted within-plot heterogeneity may have contributed to the  
1068 low amount of variation explained by soil N availability in our statistical mod-  
1069 els, as resin bags are a coarse surrogate for soil N availability. Despite this, we  
1070 still observed evidence for nutrient-water use tradeoffs, suggesting that observed  
1071 responses reported here may be an underestimate toward the net effect of soil  
1072 N availability on these tradeoffs. While we urge caution in the interpretation of

**1073** these results, they do provide a promising baseline for future studies investigating  
**1074** patterns expected from photosynthetic least-cost theory at finer spatiotemporal  
**1075** resolutions.

**1076** The general stronger relationship between leaf N content and photosynthetic parameters versus between leaf N content and soil N availability suggests  
**1077** that leaf N content is more directly tied to photosynthesis than soil N availability.  
**1078** While this could be due to the high spatiotemporal heterogeneity of soil N availability,  
**1079** principles from photosynthetic least-cost theory suggest that leaf N content is the downstream product of leaf nutrient demand to build and maintain  
**1080** photosynthetic machinery, which is set by aboveground environmental conditions  
**1081** such as light availability, CO<sub>2</sub>, temperature, or vapor pressure deficit (Smith  
**1082** et al. 2019; Paillassa et al. 2020; Peng et al. 2021; Westerband et al. 2023). The  
**1083** stronger relationship between leaf N and photosynthetic parameters paired with  
**1084** the strong negative relationship between leaf N and  $\chi$  could indicate a relatively  
**1085** stronger effect of climate on leaf N-photosynthesis relationships than soil resource  
**1086** availability. However, the short distance between plots and across sites limited  
**1087** our ability to test this mechanism.

**1090** Variation in soil pH affected least cost responses less than variations in  
**1091** soil N availability, in part because experimental treatments directly increased soil  
**1092** N and affected soil pH in opposite directions. While soil pH has been shown  
**1093** to drive nitrogen-water tradeoffs in global gradient analyses (Viet et al. 2013;  
**1094** Paillassa et al. 2020), these responses may be due to covariations between soil pH  
**1095** and nutrient cycling rather than a role of pH per se. The direct manipulations  
**1096** of soil pH and soil N availability in this study allowed us to partly disentangle

**1097** these factors and show that variation in N availability matters more for least-cost  
**1098** tradeoffs than pH alone.

**1099** 3.4.5 *Conclusions*

**1100** Increasing soil N availability generally increased leaf N content (both area-  
**1101** and mass-based), but did not significantly influence  $\chi$ . This shift in leaf N led  
**1102** to a reduction in PNUE, and an increase in leaf N per unit  $\chi$  with increasing  
**1103** soil N availability. Despite null effects of soil N availability on  $\chi$ , we observed a  
**1104** strong negative relationship between leaf N content and  $\chi$ . These results provide  
**1105** empirical support for the nutrient-water use tradeoffs expected from photosyn-  
**1106** thetic least-cost theory in response to soil nutrient availability, but suggest that  
**1107** all tenets of the theory may not hold in every environment. These results exper-  
**1108** imentially test previous work suggesting that leaf water-nitrogen economies vary  
**1109** across gradients of soil nutrient availability and pH, and show that variations in  
**1110** nutrient availability matter more for determining variation in leaf photosynthetic  
**1111** traits than soil pH.

1112

## Chapter 4

1113 The relative cost of resource use for photosynthesis drives variance in  
1114 leaf nitrogen content across climate and soil resource availability  
1115 gradients

1116 4.1 Introduction

1117 Terrestrial biosphere models, which comprise the land surface component of  
1118 Earth system models, are sensitive to the formulation of photosynthetic processes  
1119 (Knorr 2000; Ziehn et al. 2011; Booth et al. 2012). This is because photosynthe-  
1120 sis is the largest carbon flux between the atmosphere and terrestrial biosphere,  
1121 and is constrained by ecosystem carbon and nutrient cycles (Hungate et al. 2003;  
1122 LeBauer and Treseder 2008; IPCC 2021; Fay et al. 2015). Many terrestrial bio-  
1123 sphere models formulate photosynthesis by parameterizing photosynthetic capac-  
1124 ity within plant functional groups through empirical linear relationships between  
1125 area-based leaf nitrogen content ( $N_{\text{area}}$ ) and the maximum carboxylation rate  
1126 of Ribulose-1,5-bisphosphate carboxylase/oxygenase (Kattge et al. 2009; Rogers  
1127 2014; Rogers et al. 2017). Models are also beginning to include connected carbon-  
1128 nitrogen cycles (Wieder et al. 2015; Shi et al. 2016; Davies-Barnard et al. 2020;  
1129 Braghieri et al. 2022), which allows leaf photosynthesis to be predicted directly  
1130 through changes in  $N_{\text{area}}$  and indirectly through changes in soil nitrogen avail-  
1131 ability (e.g., LPJ-GUESS, Smith et al., 2014; CLM5.0, Lawrence et al., 2019).  
1132 Despite recent model developments, open questions remain regarding the gen-  
1133 erality of ecological relationships between soil nitrogen availability, leaf nitrogen  
1134 content, and leaf photosynthesis across edaphic and climatic gradients.  
1135 Empirical support for positive relationships between soil nitrogen avail-

ability and  $N_{\text{area}}$  is abundant (Firn et al. 2019; Liang et al. 2020), and is a result often attributed to the high nitrogen cost of building and maintaining Rubisco (Evans 1989; Evans and Seemann 1989; Onoda et al. 2004; Onoda et al. 2017; Dong et al. 2020). Such patterns imply that positive relationships between soil nitrogen availability and  $N_{\text{area}}$  should cause an increase in leaf photosynthesis and photosynthetic capacity by increasing the maximum rate of Rubisco carboxylation through increased investments to Rubisco construction and maintenance. This integrated  $N_{\text{area}}$ -photosynthesis response to soil nitrogen availability has been observed both in manipulative experiments and across environmental gradients (Field and Mooney 1986; Evans 1989; Walker et al. 2014; Li et al. 2020), and is thought to be driven by ecosystem nitrogen limitation, which limits its primary productivity globally (LeBauer and Treseder 2008; Fay et al. 2015). However, this response is not consistently observed, as recent studies note variable  $N_{\text{area}}$ -photosynthesis relationships across soil nitrogen availability gradients (Liang et al. 2020; Luo et al. 2021) and that aboveground growing conditions (e.g., light availability, temperature, vapor pressure deficit) or species identity traits (e.g., photosynthetic pathway, nitrogen acquisition strategy) may be more important for explaining variance in  $N_{\text{area}}$  and photosynthetic capacity across time and space (Adams et al. 2016; Dong et al. 2017; Dong et al. 2020; Dong et al. 2022; Smith et al. 2019; Peng et al. 2021; Westerband et al. 2023).

**1156** 4.2 Methods

**1157** 4.2.1 textit{Site descriptions and sampling methodology}

**1158** We collected leaf and soil samples from 24 open grassland sites across cen-  
**1159** tral and eastern Texas in summer 2020 and summer 2021 (Fig. 4.1). Twelve  
**1160** sites were visited between June and July 2020 and 14 sites (11 unique from 2020)  
**1161** were visited between May and June 2021 (Table 1). We explicitly chose sites  
**1162** that maximized variability in precipitation and edaphic variability between sites  
**1163** while minimizing temperature variability across the environmental gradient (Ta-  
**1164** ble 1). No site with personally communicated or anecdotal evidence of grazing  
**1165** or disturbance (e.g., mowing, feral hog activity, etc.) were used. We collected  
**1166** leaf material from three individuals each of the five most abundant species at ran-  
**1167** dom locations at each site, only selecting species that were broadly classified as  
**1168** graminoid, forb/herb, shrub, or subshrub growth habits per the USDA PLANTS  
**1169** database (USDA NRCS 2022). All collected leaves were fully expanded with no  
**1170** visible herbivory or other external damage and also free from shading by nearby  
**1171** shrubs or trees. Five soil samples were collected from 0-15cm below the soil sur-  
**1172** face at each site near the leaf collection sample locations. Soil samples were later  
**1173** mixed together by hand to create one composite soil sample per site.

**1174** 4.2.2 *Leaf trait measurements*

**1175** Images of each leaf were taken immediately following each site visit using  
**1176** a flat-bed scanner. Fresh leaf area was determined from each image using the  
**1177** 'LeafArea' R package (Katabuchi 2015), which automates leaf area calculations  
**1178** using ImageJ software (Schneider et al. 2012). Each leaf was dried at 65°C for at

**1179** least 48 hours to a constant mass, weighed, and manually ground in a mortar and  
**1180** pestle until homogenized. Leaf mass per area ( $M_{\text{area}}$ ; g m<sup>-2</sup>) was calculated as the  
**1181** ratio of dry leaf biomass to fresh leaf area. Subsamples of dried and homogenized  
**1182** leaf tissue were used to measure leaf nitrogen content ( $N_{\text{mass}}$ ; gN g<sup>-1</sup>) through el-  
**1183** emental combustion analysis (Costech-4010, Costech Instruments, Valencia, CA).  
**1184** Leaf nitrogen content per unit leaf area ( $N_{\text{area}}$ ; gN m<sup>-2</sup>) was then calculated as  
**1185** the product of  $N_{\text{mass}}$  and  $M_{\text{area}}$ .

**1186** Subsamples of dried and homogenized leaf tissue were sent to the University  
**1187** of California-Davis Stable Isotope Facility to determine leaf  $\delta^{13}\text{C}$ . Leaf  $\delta^{13}\text{C}$  values  
**1188** were determined using an elemental analyzer (PDZ Europa ANCA-GSL; Sercon  
**1189** Ltd., Chestshire, UK) interfaced to an isotope ratio mass spectrometer (PDZ  
**1190** Europa 20-20 Isotope Ratio Mass Spectrometer, Sercon Ltd., Chestshire, UK).  
**1191** We used leaf  $\delta^{13}\text{C}$  values (‰; relative to Vienna Pee Dee Belemnite international  
**1192** reference standard) to estimate the ratio of intercellular ( $C_i$ ) to extracellular ( $C_a$ )  
**1193** CO<sub>2</sub> ratio (leaf  $C_i:C_a$ ,  $\chi$ ; unitless) following the approach of Farquhar et al. (1989)  
**1194** described in Cernusak et al. (2013). We derived  $\chi$  as:

$$\chi = \frac{C_i}{C_a} = \frac{\Delta^{13}\text{C} - a}{b - a} \quad (4.1)$$

**1195** where  $\Delta^{13}\text{C}$  represents the relative difference between leaf  $\delta^{13}\text{C}$  (‰) and air  $\delta^{13}\text{C}$   
**1196** (‰), and is calculated as:

$$\Delta^{13}\text{C} = \frac{\delta^{13}\text{C}_{\text{air}} - \delta^{13}\text{C}_{\text{leaf}}}{1 + \delta^{13}\text{C}_{\text{leaf}}} \quad (4.2)$$

**1197**  $\delta^{13}\text{C}_{\text{air}}$ , traditionally assumed to be -8‰ (Keeling et al. 1979; Farquhar et al.

**1198** 1989), was calculated as a function of calendar year  $t$  using an empirical equation  
**1199** derived in Feng (1999):

$$\delta^{13}C_{air} = -6.429 - 0.006e^{0.0217(t-1740)} \quad (4.3)$$

**1200** This calculation resulted in  $\delta^{13}C_{air}$  values for 2020 and 2021 as -9.04 and -9.09,  
**1201** respectively. a represents the fractionation between  $^{12}\text{C}$  and  $^{13}\text{C}$  due to diffusion  
**1202** in air, assumed to be 4.4‰, and b represents the fractionation caused by Rubisco  
**1203** carboxylation, assumed to be 27‰ (Farquhar et al. 1989). For  $C_4$  species, b in  
**1204** Eqn. 4.1 was set to 6.3‰, and was derived from:

$$b = c + (d \cdot \phi) \quad (4.4)$$

**1205** Where c was set to -5.7‰ and d was set to 30‰ (Farquhar et al. 1989).  $\phi$ , which  
**1206** is the bundle sheath leakiness term, was set to 0.4. All  $\chi$  values less than 0.2 and  
**1207** greater than 1.0 were assumed to be incorrect and removed.

**1208** We derived the unit cost of resource use ( $\beta$ ) using leaf  $\chi$  and site climate  
**1209** data with equations first described in Prentice et al. (2014) and simplified in  
**1210** Lavergne et al. (2020):

$$\beta = 1.6\eta^*D \frac{\chi - (\frac{\Gamma^*}{C_a})^2}{(1 - \chi)^2(K_m + \Gamma^*)} \quad (4.5)$$

**1211** where  $\eta^*$  is the viscosity of water relative to 25°C, calculated using elevation and  
**1212** mean air temperature of the seven days leading up to each site visit following  
**1213** equations in Huber et al. (2009). D represents vapor pressure deficit (Pa), set

**1214** to the mean vapor pressure deficit of the seven days leading up to each site visit,  
**1215**  $C_a$  represents atmospheric CO<sub>2</sub> concentration, arbitrarily set to 420  $\mu\text{mol mol}^{-1}$   
**1216** CO<sup>2</sup>.  $K_m$  (Pa) is the Michaelis-Menten coefficient for Rubisco affinity to CO<sub>2</sub> and  
**1217** O<sub>2</sub>, calculated as:

$$K_m = K_c \cdot \left(1 + \frac{O_i}{K_o}\right) \quad (4.6)$$

**1218** where  $K_c$  (Pa) and  $K_o$  (Pa) are the Michaelis-Menten coefficients for Rubisco  
**1219** affinity to CO<sub>2</sub> and O<sub>2</sub>, respectively, and  $O_i$  is the intercellular O<sub>2</sub> concentration.  
**1220**  $\Gamma^*$  (Pa) is the CO<sub>2</sub> compensation point in the absence of dark respiration.  $K_c$ ,  $K_o$ ,  
**1221** and  $\Gamma^*$  were determined using equations described in Medlyn et al. (2002) and  
**1222** derived in Bernacchi et al. (2001), invoking an elevation correction for atmospheric  
**1223** pressure as explained in Stocker et al. (2020).

**1224**

placeholder for Table 1

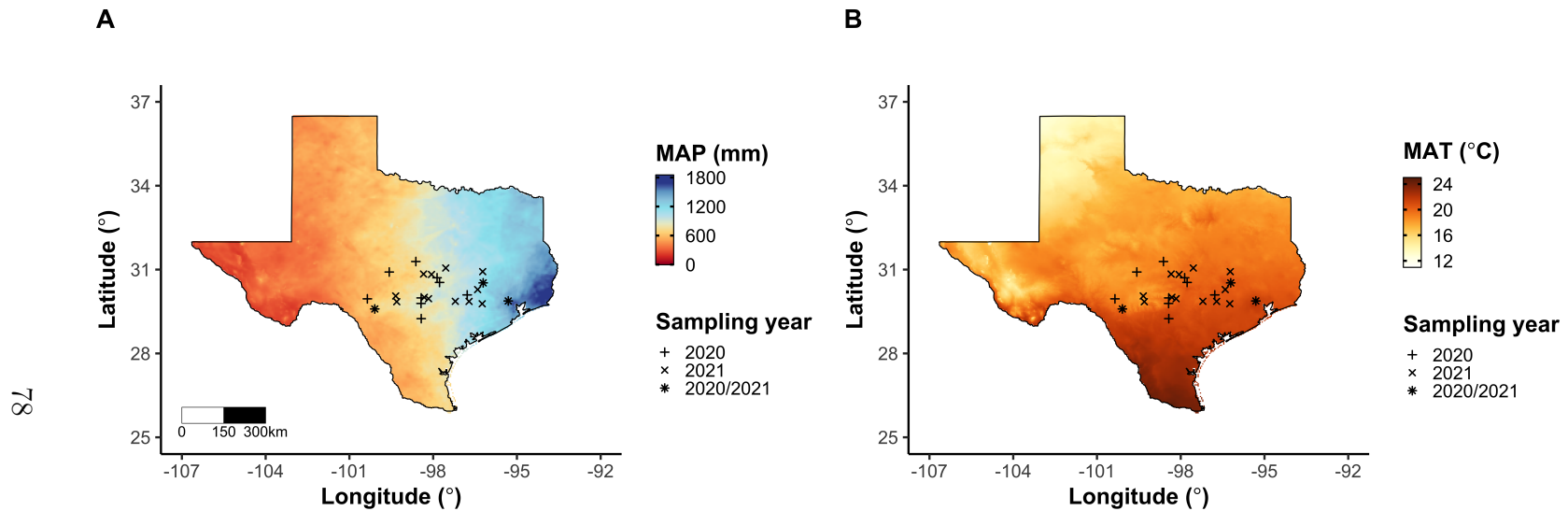


**Figure 4.1.** Maps that detail site locations along 2006-2020 mean annual precipitation (panel A) and mean annual temperature (panel B) gradients in Texas, USA. Precipitation and temperature data were plotted at a 4-km grid resolution and are masked to include only grid cells that occur in the Texas state boundary in the United States. In both panels, open circles refer to sites visited in 2020, open triangles to sites visited in 2021, and closed circles to sites visited in 2020 and 2021. The scale bar in panel A also applies to panel B.

**1225** 4.2.3 *Site climate data*

**1226** We used the Parameter-elevation Regressions on Independent Slopes Model  
**1227** (PRISM) (Daly et al. 2008) climate product to access gridded daily temperature  
**1228** and precipitation data for the coterminous United States at a 4-km grid resolution  
**1229** between January 1, 2006 and July 31, 2021 (PRISM Climate Group, Oregon State  
**1230** University, <https://prism.oregonstate.edu>, data created 4 Feb 2014, accessed 24  
**1231** Mar 2022). Daily mean air temperature, mean VPD, and total precipitation  
**1232** data were extracted from the grid cell that contained the latitude and longitude  
**1233** of each property using the ‘extract’ function in the ‘terra’ R package (Hijmans  
**1234** 2022). PRISM data were used in lieu of local weather station data because several  
**1235** rural sites did not have a local weather station present within a 20-km radius of  
**1236** the site. Daily site climate data were used to estimate mean annual precipitation  
**1237** and mean annual temperature for each site between 2006 and 2020 (Table 1). We  
**1238** then calculated total precipitation and mean daily VPD for the prior 1, 2, 3, 4, 5,  
**1239** 6, 7, 8, 9, 10, 15, 20, 25, 30, 60, and 90 days leading up to each site visit.

**1240** 4.2.4 *Site edaphic characteristics*

**1241** Subsamples of composited soil samples were sent to the Texas A & M  
**1242** Soil, Water and Forage Laboratory to quantify soil nitrate concentration (NO<sub>3</sub>-N;  
**1243** ppm). Soil NO<sub>3</sub>-N was determined by extracting composite soil samples in 1 M  
**1244** KCl, measuring absorbance values of extracts at 520 nm using the end product of  
**1245** a NO<sub>3</sub>-N to NO<sub>2</sub>-N cadmium reduction reaction (Kachurina et al. 2000). Soil tex-  
**1246** ture data from 0-15cm below the soil surface were accessed using the SoilGrids2.0  
**1247** data product (Poggio et al. 2021) through the ‘fetchSoilGrids’ function in the

**1248** ‘soilDB’ R package (Beaudette et al. 2022). We used SoilGrids2.0 to access soil  
**1249** texture data in lieu of analyses using the collected composite soil sample due to  
**1250** a lack of soil material from some sites after sending samples for soil NO<sub>3</sub>-N.

**1251** Soil moisture was not measured in the field, but was estimated using  
**1252** the ‘Simple Process-Led Algorithms for Simulating Habitats’ model (‘SPLASH’)  
**1253** (Davis et al. 2017). This model, derived from the STASH model (Cramer and  
**1254** Prentice 1988), spins up a bucket model using Priestley-Taylor equations (Priest-  
**1255** ley and Taylor 1972) to calculate daily soil moisture ( $W_n$ ; mm) as a function  
**1256** of the previous day’s soil moisture ( $W_{n-1}$ ; mm), daily precipitation ( $P_n$ ; mm),  
**1257** condensation ( $C_n$ ; mm), actual evapotranspiration ( $E_n^a$ ; mm), and runoff (RO;  
**1258** mm):

$$W_n = W_{n-1} + P_n + C_n - E_n^a - RO \quad (4.7)$$

**1259** Models were spun up by equilibrating the previous day’s soil moisture using  
**1260** successive model iterations with daily mean air temperature, daily precipitation  
**1261** total, the number of daily sunlight hours, and latitude as model inputs (Davis et al.  
**1262** 2017). Daily sunlight hours were estimated for each day at each site using the  
**1263** ‘getSunlightTimes’ function in the ‘suncalc’ R package, which estimated sunrise  
**1264** and sunset times of each property using date and site coordinates (Thieurmel and  
**1265** Elmarhraoui 2019). Water holding capacity (mm), or bucket size, was estimated  
**1266** as a function of soil texture using pedotransfer equations explained in Saxton and  
**1267** Rawls (2006), as done in Stocker et al. (2020) and Bloomfield et al. (2022). A  
**1268** summary of these equations is included in the Supplemental Information.

1269 Daily soil moisture outputs from the SPLASH model for each site were  
1270 used to calculate mean daily soil moisture for the prior 1, 2, 3, 4, 5, 6, 7, 8, 9,  
1271 10, 15, 20, 25, 30, 60, and 90 days leading up to each site visit. Mean daily  
1272 soil moisture values were then expressed as a fraction of water holding capacity  
1273 to normalize across sites with different bucket depths, as done in Stocker et al.  
1274 (2018).

1275 4.2.5 *Plant functional group assignments*

1276 Plant functional group was assigned to each species and used as the pri-  
1277 mary descriptor of species identity. Specifically, we assigned plant functional  
1278 groups based on photosynthetic pathway ( $C_3$ ,  $C_4$ ) and ability to form associations  
1279 with symbiotic nitrogen-fixing bacteria. The ability to form associations with  
1280 symbiotic nitrogen-fixing bacteria was assigned based on whether species were in  
1281 the *Fabaceae* family, and photosynthetic pathway of each species was determined  
1282 from past literature and confirmed through leaf  $\delta^{13}\text{C}$  values. We chose these plant  
1283 functional groups based on *a priori* hypotheses regarding the functional role of  
1284 nitrogen fixation and photosynthetic pathway on the sensitivity of plant nitrogen  
1285 uptake and leaf nitrogen allocation to soil nutrient availability and aboveground  
1286 growing conditions. These plant functional group classifications resulted in three  
1287 distinct plant functional groups within our dataset:  $C_3$  legumes ( $n = 53$ ),  $C_3$   
1288 non-legumes ( $n = 350$ ), and  $C_4$  non-legumes ( $n = 117$ ).

**1289** 4.2.6 *Data analysis*

**1290** All analyses and plotting were conducted in R version 4.1.1 (R Core Team  
**1291** 2021). We constructed a series of separate linear mixed-effects models to inves-  
**1292** tigate environmental drivers of  $\beta$ ,  $\chi$ ,  $N_{\text{area}}$ ,  $N_{\text{mass}}$ , and  $M_{\text{area}}$ , followed by a path  
**1293** analysis using a piecewise structural equation model to investigate direct and  
**1294** indirect effects of climate and soil resource availability on  $N_{\text{area}}$ .

**1295** To explore environmental drivers of  $\beta$ , we built a linear mixed-effects model  
**1296** that included soil moisture, soil nitrogen availability, and plant functional group  
**1297** as fixed effect coefficients. Species were designated as a random intercept term.  
**1298** Interaction coefficients between all possible combinations of the three fixed effect  
**1299** coefficients were also included.  $\beta$  was natural log transformed to linearize data.  
**1300** We used an information-theoretic model selection approach to determine whether  
**1301** 90-, 60-, 30-, 20-, 15-, 10-, 9-, 8-, 7-, 6-, 5-, 4-, 3-, 2-, or 1-day mean daily  
**1302** soil moisture conferred the best model fit for  $\beta$ . To do this, we constructed 16  
**1303** separate linear mixed-effects models where log-transformed  $\beta$  was included as the  
**1304** response variable and each soil moisture timestep was separately included as a  
**1305** single continuous fixed effect. Species were included as a random intercept term  
**1306** for all models. We used corrected Akaike Information Criterion (AICc) to select  
**1307** the soil moisture timescale that conferred the best model fit, indicated by the  
**1308** model with the lowest AICc score (Table S2; Fig. S2).

**1309** To explore environmental drivers of  $\chi$ , we constructed a second linear mixed  
**1310** effects model that included VPD, soil moisture, soil nitrogen availability, and plant  
**1311** functional group as fixed effect coefficients. Two-way interactions between plant  
**1312** functional group and VPD, soil nitrogen availability, or soil moisture were also

1313 included as fixed effect coefficients, in addition to a three-way interaction between  
1314 soil moisture, soil nitrogen availability, and plant functional group. Species were  
1315 included as a random intercept term. We used an information-theoretic model  
1316 selection approach to determine whether 90-, 60-, 30-, 20-, 15-, 10-, 9-, 8-, 7-, 6-,  
1317 5-, 4-, 3-, 2-, or 1-day mean daily VPD conferred the best model fit for  $\chi$  using  
1318 the same approach explained above for the soil moisture effect on  $\beta$ . The soil  
1319 moisture timescale was set to the same timescale that conferred the best fit for  $\beta$ .

1320 To explore environmental drivers of  $N_{\text{area}}$ ,  $N_{\text{mass}}$ , and  $M_{\text{area}}$ , we constructed  
1321 three separate linear mixed effects model that each included  $\chi$ , soil nitrogen avail-  
1322 ability, soil moisture, and plant functional group as fixed effect coefficients. Two-  
1323 way interactions between plant functional group and  $\beta$ ,  $\chi$ , soil nitrogen availability,  
1324 or soil moisture were included as additional fixed effect coefficients, in addition to  
1325 a three-way interaction between soil nitrogen availability, soil moisture, and plant  
1326 functional group. Species were included as a random intercept term, with the soil  
1327 moisture timescale set to the same timescale that conferred the best fit for  $\beta$ .

1328 In all linear mixed-effects models explained above, including those to select  
1329 relevant timescales, we used the 'lmer' function in the 'lme4' R package (Bates  
1330 et al. 2015) to fit each model and the 'Anova' function in the 'car' R package (Fox  
1331 and Weisberg 2019) to calculate Type II Wald's  $\chi^2$  and determine the significance  
1332 level ( $\alpha = 0.05$ ) of each fixed effect coefficient. We also used the 'emmeans'  
1333 R package (Lenth 2019) to conduct post-hoc comparisons using Tukey's tests,  
1334 where degrees of freedom were approximated using the Kenward-Roger approach  
1335 (Kenward and Roger 1997). Trendlines and error ribbons for all plots were drawn  
1336 using a series of 'emmeans' outputs across the range in plotted x-axis values.

Finally, we conducted a path analysis using a piecewise structural equation model to examine direct and indirect pathways that determined variance in  $N_{\text{area}}$ . Seven separate linear mixed effects models were loaded into the piecewise structural equation model. Models were constructed per our *a priori* hypotheses following patterns expected from photosynthetic least-cost theory. The first model regressed  $N_{\text{area}}$  against  $\chi$ ,  $N_{\text{mass}}$ , and  $M_{\text{area}}$ . The second model regressed  $M_{\text{area}}$  against  $\chi$ . The third model regressed  $N_{\text{mass}}$  against  $\chi$  and  $M_{\text{area}}$  (Dong et al. 2017; Dong et al. 2020). The fourth model regressed  $\chi$  against  $\beta$  and VPD. The fifth model regressed  $\beta$  against soil nitrogen availability, soil moisture, ability to associate with symbiotic nitrogen-fixing bacteria, and photosynthetic pathway. The sixth model regressed soil nitrogen availability against soil moisture, while the seventh model regressed VPD against soil moisture (Novick et al. 2016; Sulman et al. 2016). All models included the relevant timescale selected in the individual linear mixed effect models explained above (2-day soil moisture, 4-day vapor pressure deficit). Models also included species as a random intercept term, were built using the ‘lme’ function in the ‘nlme’ R package (Pinheiro and Bates 2022), and subsequently loaded into the piecewise structural equation model using the ‘psem’ function in the ‘piecewiseSEM’ R package (Lefcheck 2016).

## 1355 4.3 Results

### 1356 4.3.1 Cost to acquire nitrogen relative to water ( $\beta$ )

Model selection indicated that 2-day soil moisture was the timescale that conferred the best model fit for  $\beta$  ( $AIC_c = 1227.83$ ; Table S2; Fig. S1). Increasing soil nitrogen availability generally decreased  $\beta$  ( $p < 0.001$ ; Table 2), a

**1360** pattern driven by a negative effect of increasing soil nitrogen availability on  $\beta$  in  
**1361** C<sub>3</sub> nonlegumes (Tukey:  $p < 0.001$ ) and C<sub>3</sub> legumes (Tukey:  $p = 0.004$ ; Fig. 2a).  
**1362** C<sub>4</sub> nonlegumes also demonstrated a negative trend in the effect of increasing soil  
**1363** nitrogen availability on  $\beta$ , but this pattern was not significantly different from  
**1364** zero (Tukey:  $p = 0.307$ ; Fig. 2a). There was no apparent effect of soil moisture  
**1365** on  $\beta$  ( $p = 0.264$ ; Table 1; Fig. 2b). A functional group effect ( $p < 0.001$ ; Ta-  
**1366** ble 1) indicated that C<sub>4</sub> nonlegumes generally had lower  $\beta$  values than both C<sub>3</sub>  
**1367** legumes and C<sub>3</sub> non-legumes when averaged across soil moisture and soil nitrogen  
**1368** availability values (Tukey:  $p < 0.001$  in both cases), while average  $\beta$  values in C<sub>3</sub>  
**1369** legumes did not differ from C<sub>3</sub> nonlegumes (Tukey:  $p = 0.691$ ).

**1370**

placeholder Table 2

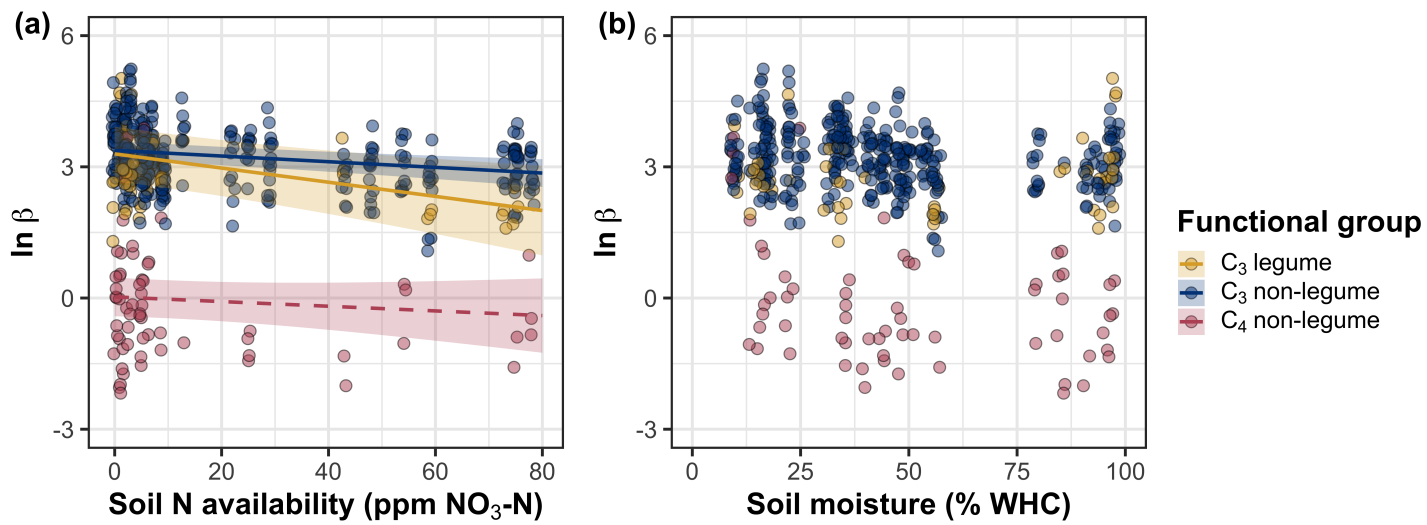


**Figure 4.2.** Effects of soil nitrogen availability (a) and soil moisture (b) on the unit cost ratio  $\beta$ . In (b), soil moisture is represented as a percent of site water holding capacity. Yellow shading and trendlines indicate C<sub>3</sub> legumes, blue shading and trendlines indicate C<sub>3</sub> non-legumes, and red shading and trendlines indicate C<sub>4</sub> non-legumes. Points are jittered for visibility. Variably colored trendlines are only included if there is an interaction between the x-axis and plant functional group, where solid trendlines indicate slopes that are different from zero ( $p < 0.05$ ) and dashed trendlines indicate slopes that are not different from zero ( $p > 0.05$ ). Error ribbons represent the upper and lower 95% confidence intervals of each fitted trendline.

**1371** 4.3.2 *Leaf C<sub>i</sub>:C<sub>a</sub>*

**1372** Model selection indicated that 4-day daily VPD was the timescale that  
**1373** conferred the best model fit for  $\chi$  (AICc = -883.97; Table S1; Fig. S2).

**1374** Variance in  $\chi$  was driven by a series of two-way interactions between func-  
**1375** tional group and VPD ( $p = 0.006$ ; Table 3), soil moisture ( $p = 0.033$ , Table 3),  
**1376** and soil nitrogen availability ( $p = 0.022$ ; Table 3). The interaction between 4-day  
**1377** VPD and functional group revealed that the general negative effect of increasing  
**1378** VPD ( $p < 0.001$ ; Table 3) was driven by a negative effect of increasing VPD  
**1379** on  $\chi$  in C<sub>3</sub> nonlegumes (Tukey:  $p < 0.001$ ) and marginal negative effect in C<sub>3</sub>  
**1380** legumes (Tukey:  $p = 0.074$ ) paired with a positive trending, but insignificant  
**1381** effect of increasing VPD in C<sub>4</sub> nonlegumes (Tukey:  $p = 0.130$ ; Fig. 3a). The  
**1382** interaction between 2-day soil moisture and functional group indicated that the  
**1383** general negative effect of increasing soil moisture on  $\chi$  was driven by a positive  
**1384** effect of increasing soil moisture on  $\chi$  in C<sub>4</sub> nonlegumes (Tukey:  $p = 0.009$ ) de-  
**1385** spite a positive trending but insignificant effect of increasing soil moisture on  $\chi$   
**1386** in C<sub>3</sub> legumes (Tukey:  $p = 0.116$ ) and a null effect of soil moisture on  $\chi$  in C<sub>3</sub>  
**1387** nonlegumes (Tukey:  $p = 0.693$ ; Fig. 3c). The interaction between soil nitrogen  
**1388** availability and plant functional group revealed a weak negative effect of increas-  
**1389** ing soil nitrogen availability on  $\chi$  in C<sub>3</sub> legumes (Tukey:  $p = 0.045$ ), with no  
**1390** apparent effect in C<sub>3</sub> nonlegumes (Tukey:  $p = 0.706$ ) or C<sub>4</sub> nonlegumes (Tukey:  
**1391**  $p = 0.757$ ). Finally, an individual effect of functional group ( $p < 0.001$ ; Table 3)  
**1392** revealed that C<sub>4</sub> nonlegumes generally had lower  $\chi$  than C<sub>3</sub> legumes and C<sub>3</sub> non-  
**1393** legumes (Tukey:  $p < 0.001$  in both cases), with no apparent difference between  
**1394** C<sub>3</sub> legumes and C<sub>3</sub> nonlegumes (Tukey:  $p = 0.831$ ).

**1395**

placeholder Table 3



**1396** 4.3.3 *Leaf nitrogen content*

**1397** An interaction between  $\chi$  and plant functional group ( $p < 0.001$ ; Table  
**1398** 4) revealed that the general negative effect of increasing  $\chi$  on  $N_{\text{area}}$  ( $p < 0.001$ ;  
**1399** Table 4) was driven by a negative effect of increasing  $\chi$  on  $N_{\text{area}}$  in C<sub>3</sub> nonlegumes  
**1400** (Tukey:  $p < 0.001$ ) and C<sub>3</sub> legumes (Tukey:  $p = 0.002$ ) despite a null effect of  $\chi$   
**1401** on  $N_{\text{area}}$  in C<sub>4</sub> nonlegumes (Tukey:  $p = 0.795$ ; Fig. 4a). An interaction between  
**1402** soil nitrogen availability and soil moisture ( $p = 0.028$ ; Table 4) indicated that the  
**1403** marginal positive effect of increasing soil nitrogen availability on  $N_{\text{area}}$  ( $p = 0.091$ ;  
**1404** Table 4) decreased with increasing soil moisture, despite no apparent individual  
**1405** effect of soil moisture on  $N_{\text{area}}$  ( $p = 0.692$ ; Table 4). Finally, a plant functional  
**1406** group effect ( $p < 0.001$ ; Table 4) indicated that C<sub>4</sub> nonlegumes had lower  $N_{\text{area}}$   
**1407** values on average compared to C<sub>3</sub> legumes (Tukey:  $p < 0.001$ ) and C<sub>3</sub> nonlegumes  
**1408** (Tukey:  $p = 0.001$ ), while C<sub>3</sub> legumes had lower average  $N_{\text{area}}$  values compared  
**1409** to C<sub>3</sub> nonlegumes (Tukey:  $p = 0.012$ ).

**1410** A marginal interaction between  $\chi$  and plant functional group ( $p = 0.088$ ;  
**1411** Table 4) revealed that, despite no apparent general effect of  $\chi$  on  $N_{\text{mass}}$  ( $p = 0.273$ ;  
**1412** Table 4), increasing  $\chi$  decreased  $N_{\text{mass}}$  in C<sub>3</sub> nonlegumes (Tukey:  $p = 0.021$ ), but  
**1413** this effect was not apparent in C<sub>4</sub> nonlegumes (Tukey:  $p = 0.693$ ) or C<sub>3</sub> legumes  
**1414** (Tukey:  $p = 0.477$ ). An interaction between soil nitrogen availability and soil  
**1415** moisture ( $p < 0.001$ ; Table 4) indicated that the general positive effect of increas-  
**1416** ing soil nitrogen availability on  $N_{\text{mass}}$  ( $p < 0.001$ ; Table 4) generally decreased  
**1417** with increasing soil moisture, despite an apparent general positive effect of in-  
**1418** creasing soil moisture on  $N_{\text{mass}}$  ( $p < 0.001$ ; Table 4). This interaction indicated  
**1419** that the positive effect of increasing soil nitrogen availability on  $N_{\text{mass}}$  was only

1420 apparent when soil moisture was less than 70% the maximum water holding ca-  
1421 pacity (Tukey:  $p < 0.05$  in all cases) despite a positive effect of increasing soil  
1422 moisture on  $N_{\text{mass}}$  ( $p < 0.001$ ; Table 4). Finally, a plant functional group effect  
1423 ( $p < 0.001$ ; Table 4) indicated that C<sub>4</sub> nonlegumes had lower  $N_{\text{mass}}$  values on  
1424 average compared to C<sub>3</sub> legumes (Tukey:  $p = 0.002$ ) and C<sub>3</sub> nonlegumes (Tukey:  
1425  $p = 0.019$ ), while  $N_{\text{mass}}$  did not differ between C<sub>3</sub> legumes and C<sub>3</sub> nonlegumes  
1426 (Tukey:  $p = 0.149$ ).

1427 An interaction between  $\chi$  and functional group ( $p = 0.005$ ; Table 4) indi-  
1428 cated that the general negative effect of increasing  $\chi$  on  $M_{\text{area}}$  ( $p < 0.001$ ; Table  
1429 4; Fig. 4c) was driven by a negative effect of increasing  $\chi$  on  $M_{\text{area}}$  in C<sub>3</sub> legumes  
1430 and C<sub>3</sub> nonlegumes (Tukey:  $p < 0.001$  in both cases) despite a nonsignificant  
1431 effect of increasing  $\chi$  on  $M_{\text{area}}$  in C<sub>4</sub> nonlegumes (Tukey:  $p = 0.724$ ). An in-  
1432 teraction between soil nitrogen and soil moisture ( $p < 0.001$ ; Table 4) indicated  
1433 that the general negative effect of increasing soil nitrogen availability on  $M_{\text{area}}$  ( $p$   
1434  $< 0.001$ ; Table 4) decreased with increasing soil moisture, despite an apparent  
1435 general negative effect of increasing soil moisture on  $M_{\text{area}}$  ( $p = 0.002$ ; Table 4).  
1436 Specifically, the negative effect of increasing soil nitrogen availability on  $M_{\text{area}}$  was  
1437 only apparent when soil moisture was less than 65% the maximum water holding  
1438 capacity (Tukey:  $p < 0.05$  in all cases). An additional interaction between soil  
1439 nitrogen availability and functional group ( $p = 0.034$ ; Table 4) indicated that the  
1440 general negative effect of increasing soil nitrogen availability on  $M_{\text{area}}$  was driven  
1441 by decreases in C<sub>3</sub> nonlegumes (Tukey:  $p < 0.001$ ) and C<sub>4</sub> nonlegumes (Tukey:  
1442  $p = 0.003$ ), with no apparent effect of soil nitrogen availability on  $M_{\text{area}}$  in C<sub>3</sub>  
1443 legumes (Tukey:  $p = 0.997$ ).

**1444**

placeholder Table 4

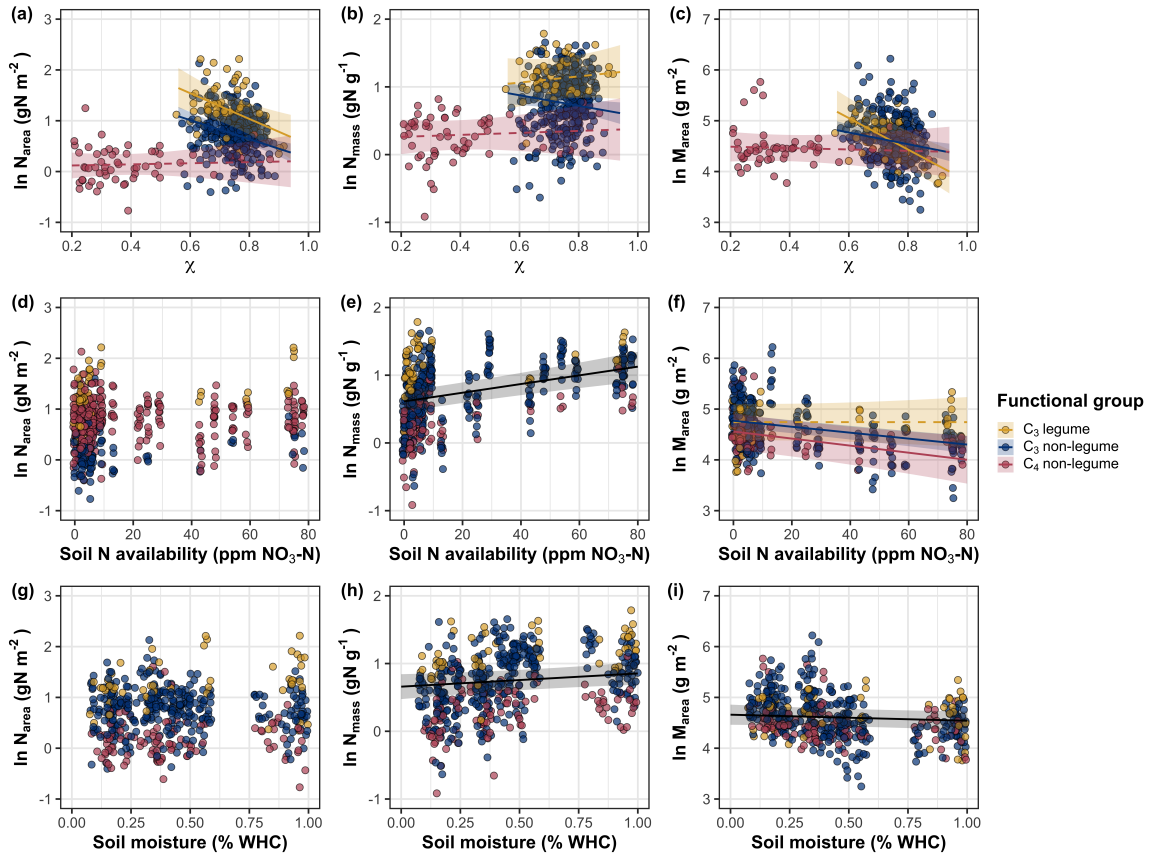


**Figure 4.4.** Effects of  $\chi$  (a-c), soil nitrogen availability (d-f), and soil moisture (g-i) on leaf nitrogen content per unit leaf area (a, d, g), leaf nitrogen content per unit leaf biomass (b, e, h), and leaf mass per area (c, f, i). A solid black trendline indicates the bivariate relationship between the fixed effect the x-axis and response variable on the y-axis and is only included when there is no interaction between the x-axis and plant functional group.

**1445** 4.3.4 *Structural equation model*

**1446** The piecewise structural equation model explained 90%, 54%, 80%, 92%,  
**1447** and 41% of variance in  $N_{\text{area}}$ ,  $N_{\text{mass}}$ ,  $M_{\text{area}}$ ,  $\chi$ , and  $\beta$ , respectively (Table 5; Fig.  
**1448** 5). Variance in  $N_{\text{area}}$  was driven by a negative effect of increasing  $\chi$  ( $p < 0.001$ ;  
**1449** Table 5) paired with positive effects of increasing  $N_{\text{mass}}$  and  $M_{\text{area}}$  ( $p < 0.001$  in  
**1450** both cases; Table 5; Fig. 5). Model results indicated that the negative effect  
**1451** of  $\chi$  on  $N_{\text{area}}$  was driven by a strong reduction in  $M_{\text{area}}$  with increasing  $\chi$  ( $p <$   
**1452** 0.001; Table 5) paired with no change in  $\chi$  due to Nmass ( $p = 0.150$ ; Table 5).  
**1453** However, there was a strong negative effect of increasing  $M_{\text{area}}$  on  $N_{\text{mass}}$  ( $p <$   
**1454** 0.001; Table 5; Fig. 5).  $\chi$  generally increased with increasing  $\beta$  ( $p < 0.001$ ; Table  
**1455** 5) and decreased with increasing VPD ( $p < 0.001$ ; Table 5; Fig. 5). Variance in  $\beta$   
**1456** was driven by a negative effect of increasing soil nitrogen availability ( $p < 0.001$ ;  
**1457** Table 5) and was generally higher in C<sub>3</sub> species ( $p < 0.001$ ; Table 5; Fig. 5).  
**1458** However,  $\beta$  did not change with soil moisture ( $p = 0.332$ ; Table 5) or with ability  
**1459** to acquire nitrogen via symbiotic nitrogen fixation ( $p = 0.546$ ; Table 5). Finally,  
**1460** soil nitrogen availability was positively associated with increasing soil moisture ( $p$   
**1461** < 0.001; Table 5; Fig. 5), while VPD was negatively associated with increasing  
**1462** soil moisture ( $p < 0.001$ ; Table 5; Fig. 5).

**1463**

placeholder Table 5

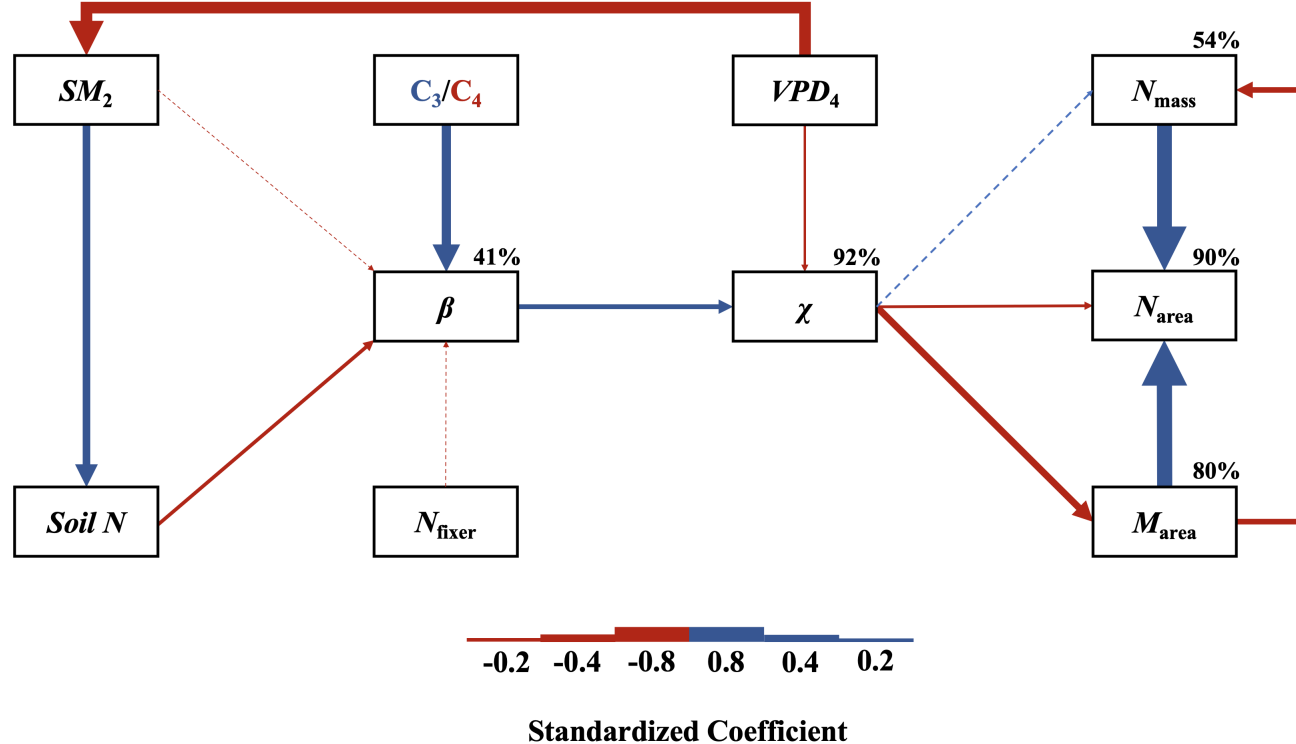


**Figure 4.5.** Structural equation model results exploring direct and indirect drivers of  $N_{area}$ . Boxes indicate measured edaphic factors, climatic factors, and leaf traits. Percentages above boxes indicate conditional  $R^2$  values of each respective leaf trait. Solid arrows indicate bivariate relationships where  $p < 0.05$ , while dashed arrows indicate bivariate relationships where  $p > 0.05$ . Positive model coefficients are indicated through blue arrows, while negative model coefficients are indicated through red arrows. Arrow thickness scales with the standardized model coefficient of each bivariate relationship. A positive coefficient for photosynthetic pathway indicates generally larger values in  $C_3$  species, while a positive coefficient for  $N_{fixer}$  indicates generally larger values in N-fixing species. Standardized model coefficients and associated  $p$ -values are reported in Table 5.

**1464** 4.4 Discussion

1465

## Chapter 5

1466  
1467

### Optimal resource investment to photosynthetic capacity maximizes nutrient allocation to whole plant growth under elevated CO<sub>2</sub>

1468 5.1 Introduction

1469 Terrestrial ecosystems are regulated by complex carbon and nitrogen cy-  
1470 cles. As a result, terrestrial biosphere models, which are beginning to include  
1471 coupled carbon and nitrogen cycles (Shi et al. 2016; Davies-Barnard et al. 2020;  
1472 Braghieri et al. 2022), must accurately represent these cycles under different  
1473 environmental scenarios to reliably simulate carbon and nitrogen atmosphere-  
1474 biosphere fluxes (Hungate et al. 2003; Prentice et al. 2015). While the inclusion  
1475 of coupled carbon and nitrogen cycles tends to reduce model uncertainty (Arora  
1476 et al. 2020), large uncertainty in role of soil nitrogen availability and nitrogen ac-  
1477 quisition strategy on leaf and whole plant acclimation responses to CO<sub>2</sub> remains  
1478 (Smith and Dukes 2013; Terrer et al. 2018; Smith and Keenan 2020). This source  
1479 of uncertainty likely contributes to the widespread divergence in future carbon  
1480 and nitrogen flux simulations across terrestrial biosphere models (Friedlingstein  
1481 et al. 2014; Zaehle et al. 2014; Meyerholt et al. 2020).

1482 Plants grown under elevated CO<sub>2</sub> generally have less leaf nitrogen content  
1483 than those grown under ambient CO<sub>2</sub>, a response that often corresponds with  
1484 reductions in photosynthetic capacity and stomatal conductance at the leaf-level  
1485 and biomass stimulation over time at the whole plant level (Curtis 1996; Drake  
1486 et al. 1997; Ainsworth et al. 2002; Makino 2003; Morgan et al. 2004; Ainsworth  
1487 and Long 2005; Ainsworth and Rogers 2007; Smith and Dukes 2013; Poorter et al.  
1488 2022). As net primary productivity is generally limited by nitrogen availability

**1489** (Vitousek and Howarth 1991; LeBauer and Treseder 2008; Fay et al. 2015), and  
**1490** soil nitrogen availability is often positively correlated with leaf nitrogen content  
**1491** and photosynthetic capacity (Field and Mooney 1986; Evans and Seemann 1989;  
**1492** Evans 1989; Walker et al. 2014; Firn et al. 2019; Liang et al. 2020), some  
**1493** have hypothesized that leaf and whole plant acclimation responses to CO<sub>2</sub> are  
**1494** constrained by soil nitrogen availability. The progressive nitrogen limitation hy-  
**1495** pothesis predicts that elevated CO<sub>2</sub> will increase plant nitrogen demand, which  
**1496** will increase plant nitrogen uptake and progressively deplete soil nitrogen if soil  
**1497** nitrogen supply does not exceed plant nitrogen demand (Luo et al. 2004). The  
**1498** hypothesis predicts that this response should result in strong acute stimulations in  
**1499** whole plant growth and primary productivity that diminish over time as nitrogen  
**1500** becomes more limiting. Assuming a positive relationship between soil nitrogen  
**1501** availability, leaf nitrogen content, and photosynthetic capacity, this hypothesis  
**1502** also implies that progressive reductions in soil nitrogen availability should be the  
**1503** mechanism that drives the downregulation in leaf nitrogen content and photosyn-  
**1504** thetic capacity under elevated CO<sub>2</sub>. This hypothesis has received some support  
**1505** from free air CO<sub>2</sub> enrichment experiments (Reich et al. 2006; Norby et al. 2010),  
**1506** although is not consistently observed across experiments (Finzi et al. 2006; Moore  
**1507** et al. 2006; Liang et al. 2016).

**1508** While possible that progressive nitrogen limitation may determine leaf and  
**1509** whole plant acclimation responses to CO<sub>2</sub>, growing evidence indicates that leaf ni-  
**1510** trogen and photosynthetic capacity are more strongly determined through above-  
**1511** ground growing conditions than by soil resource availability (Dong et al. 2017;  
**1512** Dong et al. 2020; Dong et al. 2022; Smith et al. 2019; Smith and Keenan 2020;

1513 Paillassa et al. 2020; Peng et al. 2021; Querejeta et al. 2022; Westerband et al.  
1514 2023), and satellite-derived chlorophyll fluorescence data indicate that increasing  
1515 atmospheric CO<sub>2</sub> may decrease leaf and canopy demand for nitrogen (Dong et al.  
1516 2022). Together, results from these studies suggest that the downregulation in  
1517 leaf nitrogen content and photosynthetic capacity due to increasing CO<sub>2</sub> may not  
1518 be as tightly linked to progressive nitrogen limitation as previously hypothesized.

1519 A unification of optimal coordination and photosynthetic least-cost the-  
1520 ories predicts that leaves acclimate to elevated CO<sub>2</sub> by downregulating nitrogen  
1521 allocation to Ribulose-1,5-bisphosphate (RuBP) carboxylase/oxygenase (Rubisco)  
1522 to optimize resource use efficiencies at the leaf level, which allows for greater re-  
1523 source allocation to whole plant growth (Drake et al. 1997; Wright et al. 2003;  
1524 Prentice et al. 2014; Smith et al. 2019). The theory predicts that the downregu-  
1525 lation in nitrogen allocation to Rubisco results in a stronger downregulation in the  
1526 maximum rate of Rubisco carboxylation ( $V_{cmax}$ ) than the maximum rate of RuBP  
1527 regeneration ( $J_{max}$ ), which maximizes photosynthetic efficiency by allowing net  
1528 photosynthesis rates to be equally co-limited by Rubisco carboxylation and RuBP  
1529 regeneration (Chen et al. 1993; Maire et al. 2012). This acclimation response  
1530 allows plants to make more efficient use of available light while avoiding overin-  
1531 vestment in Rubisco, which has high nitrogen and energetic costs of building and  
1532 maintaining (Evans 1989; Evans and Clarke 2019). Instead, additional acquired  
1533 resources not needed to optimize leaf photosynthesis are allocated to the mainte-  
1534 nance of structures that support whole plant growth (e.g., total leaf area, whole  
1535 plant biomass, etc.) or to allocation processes not related to leaf photosynthesis  
1536 or growth, such as plant defense mechanisms or leaf structural tissue. Regardless,

**1537** optimized resource allocation at the leaf level should allow for greater resource  
**1538** allocation to whole plant growth. The theory indicates that leaf acclimation re-  
**1539** sponses to CO<sub>2</sub> should be independent of changes in soil nitrogen availability.  
**1540** While this leaf acclimation response maximizes nitrogen allocation to structures  
**1541** that support whole plant growth, the theory suggests that the positive effect of  
**1542** elevated CO<sub>2</sub> on whole plant growth may be further stimulated by soil nitrogen  
**1543** availability through a reduction in the cost of acquiring nitrogen (Bae et al. 2015;  
**1544** Perkowski et al. 2021; Lu et al. 2022).

**1545** Plants acquire nitrogen by allocating photosynthetically derived carbon be-  
**1546** lowground in exchange for nitrogen through different nitrogen acquisition strate-  
**1547** gies. These nitrogen acquisition strategies can include direct uptake pathways  
**1548** such as mass flow or diffusion (Barber 1962), symbioses with mycorrhizal fungi or  
**1549** symbiotic nitrogen-fixing bacteria (Vance and Heichel 1991; Marschner and Dell  
**1550** 1994; Smith and Read 2008; Udvardi and Poole 2013), or through the release  
**1551** of root exudates that prime free-living soil microbial communities (Phillips et al.  
**1552** 2011; Wen et al. 2022). Plants cannot acquire nitrogen without first allocating  
**1553** carbon belowground, which implies an inherent carbon cost to the plant for acquir-  
**1554** ing nitrogen regardless of nitrogen acquisition strategy. Carbon costs to acquire  
**1555** nitrogen often vary in species with different nitrogen acquisition strategies and  
**1556** are dependent on external environmental factors such as atmospheric CO<sub>2</sub>, light  
**1557** availability, and soil nitrogen availability (Brzostek et al. 2014; Terrer et al. 2016;  
**1558** Terrer et al. 2018; Allen et al. 2020; Perkowski et al. 2021; Lu et al. 2022), which  
**1559** suggests that acquisition strategy may be an important factor in determining ef-  
**1560** fects of soil nitrogen availability on leaf and whole plant acclimation responses to

**1561** elevated CO<sub>2</sub>.

**1562** A recent meta-analysis using data across 20 grassland and forest CO<sub>2</sub> en-  
**1563** richment experiments suggested that species which acquire nitrogen from sym-  
**1564** biotic nitrogen-fixing bacteria had reduced costs of nitrogen acquisition under  
**1565** elevated CO<sub>2</sub> (Terrer et al. 2018). Findings from this meta-analysis indicated  
**1566** that reductions in costs of nitrogen acquisition in species that form associations  
**1567** with symbiotic nitrogen-fixing bacteria under elevated CO<sub>2</sub> may drive stronger  
**1568** stimulations in whole plant growth and downregulations in  $V_{cmax}$  than species that  
**1569** associate with arbuscular mycorrhizal fungi (Smith and Keenan 2020), which gen-  
**1570** erally have higher costs of nitrogen acquisition under elevated CO<sub>2</sub> (Terrer et al.  
**1571** 2018). However, plant investments in symbiotic nitrogen fixation generally de-  
**1572** cline with increasing nitrogen availability (Dovrat et al. 2018; Perkowski et al.  
**1573** 2021), a response that has been previously inferred to be the result of a shift in  
**1574** the dominant mode of nitrogen acquisition to direct uptake pathways as costs of  
**1575** direct uptake decrease with increasing soil nitrogen availability (Rastetter et al.  
**1576** 2001; Perkowski et al. 2021). Thus, effects of symbiotic nitrogen fixation on plant  
**1577** acclimation responses to CO<sub>2</sub> should decline with increasing soil nitrogen avail-  
**1578** ability, although manipulative experiments that directly test these patterns are  
**1579** rare.

**1580** Here, we conducted a 7-week growth chamber experiment using *Glycine*  
**1581** *max* L. (Merr.) to examine the effects of soil nitrogen fertilization and inocula-  
**1582** tion with symbiotic nitrogen-fixing bacteria on leaf and whole plant acclimation  
**1583** responses to elevated CO<sub>2</sub>. Following patterns expected from theory, we hypoth-  
**1584** esized that individual leaves should acclimate to elevated CO<sub>2</sub> by more strongly

1585 downregulating  $V_{cmax}$  relative to  $J_{max}$ , allowing leaf photosynthesis to approach  
1586 optimal coordination. We expected this response to correspond with a stronger  
1587 downregulation in leaf nitrogen content than  $V_{cmax}$  and  $J_{max}$ , which would in-  
1588 crease the fraction of leaf nitrogen content allocated to photosynthesis and photo-  
1589 synthetic nitrogen use efficiency. At the whole-plant level, we hypothesized that  
1590 plants would acclimate to elevated CO<sub>2</sub> by stimulating whole plant growth and  
1591 productivity, a response that would be driven by a strong positive response of  
1592 total leaf area and aboveground biomass to elevated CO<sub>2</sub>. We predicted that  
1593 leaf acclimation responses to elevated CO<sub>2</sub> would be independent of soil nitro-  
1594 gen fertilization and inoculation with symbiotic nitrogen-fixing bacteria; however,  
1595 we expected that increasing soil nitrogen fertilization would increase the posi-  
1596 tive effect of elevated CO<sub>2</sub> on measures of whole plant growth due to a stronger  
1597 reduction in the cost of acquiring nitrogen under elevated CO<sub>2</sub> with increasing  
1598 fertilization. We also expected stronger stimulations in whole plant growth due  
1599 to inoculation, but that this effect would only be apparent under low fertilization  
1600 due to a reduction in root nodulation with increasing fertilization.

1601 5.2 Methods

1602 5.2.1 *Seed treatments and experimental design*

1603 *Glycine max* L. (Merr) seeds were planted in 144 6-liter surface sterilized  
1604 pots (NS-600, Nursery Supplies, Orange, CA, USA) containing a steam-sterilized  
1605 70:30 v:v mix of Sphagnum peat moss (Premier Horticulture, Quakertown, PA,  
1606 USA) to sand (Pavestone, subsidiary of Quikrete Companies, Atlanta, GA, USA).  
1607 Before planting, all *G. max* seeds were surface sterilized in 2% sodium hypochlorite

**1608** for 3 minutes, followed by three separate 3-minute washes with ultrapure water  
**1609** (MilliQ 7000; MilliporeSigma, Burlington, MA USA). A subset of surface steril-  
**1610** ized seeds were inoculated with *Bradyrhizobium japonicum* (Verdesian N-Dure™  
**1611** Soybean, Cary, NC, USA) in a slurry following manufacturer recommendations  
**1612** (3.12 g inoculant and 241 g deionized water per 1 kg seed).

**1613** Seventy-two pots were randomly planted with surface-sterilized seeds inoc-  
**1614** ulated with *B. japonicum*, while the remaining 72 pots were planted with surface-  
**1615** sterilized uninoculated seeds. Thirty-six pots within each inoculation treatment  
**1616** were randomly placed in one of two atmospheric CO<sub>2</sub> treatments (ambient and  
**1617** 1000 μmol mol<sup>-1</sup> CO<sub>2</sub>). Pots within each unique inoculation-by-CO<sub>2</sub> treatment  
**1618** combination randomly received one of nine soil nitrogen fertilization treatments  
**1619** equivalent to 0, 35, 70, 105, 140, 210, 280, 350, or 630 ppm N. Nitrogen fertil-  
**1620** ization treatments were created using a modified Hoagland solution (Hoagland  
**1621** and Arnon 1950) designed to keep concentrations of other macronutrients and  
**1622** micronutrients equivalent across treatments (Table S1). Pots received the same  
**1623** fertilization treatment throughout the entire duration experiment, which were ap-  
**1624** plied twice per week in 150 mL doses as topical agents to the soil surface through-  
**1625** out the duration of the experiment. This experimental design yielded a fully  
**1626** factorial experiment with four replicates per unique fertilization-by-inoculation-  
**1627** by-CO<sub>2</sub> combination.

**1628** 5.2.2 *Growth chamber conditions*

**1629** Upon experiment initiation, pots were randomly placed in one of six Per-  
**1630** cival LED-41L2 growth chambers (Percival Scientific Inc., Perry, IA, USA) over

**1631** two experimental iterations due to chamber space limitation. two iterations were  
**1632** conducted such that one iteration included all elevated CO<sub>2</sub> pots and the second  
**1633** iteration included all ambient CO<sub>2</sub> pots. Average ( $\pm$  SD) CO<sub>2</sub> concentrations  
**1634** across chambers throughout the experiment were  $439 \pm 5 \mu\text{mol mol}^{-1}$  for the  
**1635** ambient CO<sub>2</sub> treatment and  $989 \pm 4 \mu\text{mol mol}^{-1}$  for the elevated CO<sub>2</sub> treatment.

**1636** Daytime growing conditions were simulated using a 16-hour photoperiod,  
**1637** with incoming light radiation set to chamber maximum (mean  $\pm$  SD:  $1240 \pm 32$   
**1638**  $\mu\text{mol m}^{-2} \text{s}^{-1}$  across chambers), air temperature set to 25°C, and relative humid-  
**1639** ity set to 50%. The remaining 8 hours simulated nighttime growing conditions,  
**1640** with incoming light radiation set to  $0 \mu\text{mol m}^{-2} \text{s}^{-1}$ , chamber temperature set  
**1641** to 17°C, and relative humidity set to 50%. Transitions between daytime and  
**1642** nighttime growing conditions were simulated by ramping incoming light radiation  
**1643** in 45-minute increments and temperature in 90-minute increments over a 3-hour  
**1644** period (Table S2).

**1645** Including the two, 3-hour ramping periods, pots grew under average ( $\pm$   
**1646** SD) daytime light intensity of  $1049 \pm 27 \mu\text{mol m}^{-2} \text{s}^{-1}$ . In the elevated CO<sub>2</sub>  
**1647** iteration, pots grew under  $24.0 \pm 0.2^\circ\text{C}$  during the day,  $16.4 \pm 0.8^\circ\text{C}$  during the  
**1648** night, and  $51.6 \pm 0.4\%$  relative humidity. In the ambient CO<sub>2</sub> iteration, pots grew  
**1649** under  $23.9 \pm 0.2^\circ\text{C}$  during the day,  $16.0 \pm 1.4^\circ\text{C}$  during the night, and  $50.3 \pm 0.2\%$   
**1650** relative humidity. We accounted for climatic differences across the six chambers  
**1651** by shuffling the same group of pots daily throughout the growth chambers. This  
**1652** process was done by iteratively moving the group of pots on the top rack of a  
**1653** chamber to the bottom rack of the same chamber, while simultaneously moving  
**1654** the group of pots on the bottom rack of a chamber to the top rack of the adjacent

1655 chamber. We moved pots within and across chambers every day throughout the  
1656 course of each experiment iteration.

1657 5.2.3 *Leaf gas exchange measurements*

1658 Gas exchange measurements were collected for all individuals on the sev-  
1659 enth week of development. All gas exchange measurements were collected on  
1660 the center leaf of the most recent fully expanded trifoliate leaf set. Specifi-  
1661 cally, we measured net photosynthesis ( $A_{\text{net}}$ ;  $\mu\text{mol m}^{-2} \text{s}^{-1}$ ), stomatal conduc-  
1662 tance ( $g_{\text{sw}}$ ;  $\text{mol m}^{-2} \text{s}^{-1}$ ), and intercellular  $\text{CO}_2$  ( $C_i$ ;  $\mu\text{mol mol}^{-1}$ ) concentrations  
1663 across a range of atmospheric  $\text{CO}_2$  concentrations (i.e., an  $A_{\text{net}}/C_i$  curve) using the  
1664 Dynamic Assimilation Technique™. The Dynamic Assimilation Technique™ has  
1665 been shown to correspond well with traditional steady-state  $\text{CO}_2$  response curves  
1666 in *G. max* (Saathoff and Welles 2021).  $A_{\text{net}}/C_i$  curves were generated along a  
1667 reference  $\text{CO}_2$  ramp down from  $420 \mu\text{mol mol}^{-1} \text{CO}_2$  to  $20 \mu\text{mol mol}^{-1} \text{CO}_2$ , fol-  
1668 lowed by a ramp up from  $420 \mu\text{mol mol}^{-1} \text{CO}_2$  to  $1620 \mu\text{mol mol}^{-1} \text{CO}_2$  after  
1669 a 90-second wait period at  $420 \mu\text{mol mol}^{-1} \text{CO}_2$ . The ramp rate for each curve  
1670 was set to  $200 \mu\text{mol mol}^{-1} \text{min}^{-1}$ , logging every five seconds, which generated 96  
1671 data points per response curve. All  $A_{\text{net}}/C_i$  curves were generated after  $A_{\text{net}}$  and  
1672  $g_{\text{sw}}$  stabilized in a LI-6800 cuvette set to a  $500 \text{ mol s}^{-1}$ , 10,000 rpm mixing fan  
1673 speed, 1.5 kPa vapor pressure deficit,  $25^\circ\text{C}$  leaf temperature,  $2000 \mu\text{mol m}^{-2} \text{s}^{-1}$   
1674 incoming light radiation, and initial reference  $\text{CO}_2$  set to  $420 \mu\text{mol mol}^{-1}$ .

1675 With the same focal leaf used to generate  $A_{\text{net}}/C_i$  curves, we measured  
1676 dark respiration ( $R_{\text{d25}}$ ;  $\mu\text{mol m}^{-2} \text{s}^{-1}$ ) following at least a 30-minute period of  
1677 darkness. Measurements were collected on a 5-second log interval for 60 seconds

1678 after stabilizing in a LI-6800 cuvette set to a  $500 \text{ mol s}^{-1}$ , 10,000 rpm mixing fan  
1679 speed, 1.5 kPa vapor pressure deficit, 25°C leaf temperature, and  $420 \mu\text{mol mol}^{-1}$   
1680 reference CO<sub>2</sub> concentration (for both CO<sub>2</sub> concentrations), with incoming light  
1681 radiation set to  $0 \mu\text{mol m}^{-2} \text{ s}^{-1}$ . A single dark respiration value was determined  
1682 for each focal leaf by calculating the mean dark respiration value (i.e. the absolute  
1683 value of  $A_{\text{net}}$  during the logging period) across the logging interval.

1684 5.2.4 *Leaf trait measurements*

1685 The focal leaf used to generate  $A_{\text{net}}/C_i$  curves and dark respiration was  
1686 harvested immediately following gas exchange measurements. Images of each focal  
1687 leaf were curated using a flat-bed scanner to determine wet leaf area using the  
1688 'LeafArea' R package (Katabuchi 2015), which automates leaf area calculations  
1689 using ImageJ software (Schneider et al. 2012). Each leaf was dried at 65°C for  
1690 at least 48 hours, and subsequently weighed and ground until homogenized. Leaf  
1691 mass per area ( $M_{\text{area}}$ ; g m<sup>-2</sup>) was calculated as the ratio of dry leaf biomass  
1692 to fresh leaf area. Using subsamples of ground and homogenized leaf tissue, we  
1693 measured leaf nitrogen content ( $N_{\text{mass}}$ ; gN g<sup>-1</sup>) through elemental combustion  
1694 analysis (Costech-4010, Costech, Inc., Valencia, CA, USA). Leaf nitrogen content  
1695 per unit leaf area ( $N_{\text{area}}$ ; gN m<sup>-2</sup>) was calculated by multiplying  $N_{\text{mass}}$  and  $M_{\text{area}}$ .

1696 We extracted chlorophyll content from a second leaf in the same trifoliolate  
1697 leaf set as the focal leaf used to generate  $A_{\text{net}}/C_i$  curves. Prior to chlorophyll  
1698 extraction, we used a cork borer to punch between 3 and 5 0.6 cm<sup>2</sup> disks from  
1699 the leaf. Separate images of each punched leaf and set of leaf disks were curated  
1700 using a flat-bed scanner to determine wet leaf area, again quantified using the

1701 'LeafArea' R package (Katabuchi 2015). The punched leaf was dried and weighed  
1702 after at least 65°C in the drying oven to determine Marea of the chlorophyll leaf.

1703 Leaf disks were shuttled into a test tube containing 10mL dimethyl sul-  
1704 foxide, vortexed, and incubated at 65degreeC for 120 minutes (Barnes et al.  
1705 1992). Incubated test tubes were vortexed again before loaded in 150  $\mu$ L trip-  
1706 licate aliquots to a 96-well plate. Dimethyl sulfoxide was also loaded in a 150  
1707  $\mu$ L triplicate aliquot as a blank. Absorbance measurements at 649.1 nm ( $A_{649.1}$ )  
1708 and 665.1 nm ( $A_{665.1}$ ) were read in each well using a plate reader (Biotek Synergy  
1709 H1; Biotek Instruments, Winooski, VT USA) (Wellburn 1994), with triplicates  
1710 subsequently averaged and corrected by the mean of the blank absorbance value.  
1711 Blank-corrected absorbance values were used to estimate  $Chl_a$  ( $\mu$ g mL $^{-1}$ ) and  
1712  $Chl_b$  ( $\mu$ g mL $^{-1}$ ) following equations from Wellburn (1994):

$$Chl_a = 12.47A_{665.1} - 3.62A_{649.1} \quad (5.1)$$

1713 and

$$Chl_b = 25.06A_{665.1} - 6.50A_{649.1} \quad (5.2)$$

1714  $Chl_a$  and  $Chl_b$  were converted to mmol mL $^{-1}$  using the molar mass of chlorophyll a  
1715 (893.51 g mol $^{-1}$ ) and the molar mass of chlorophyll b (907.47 g mol $^{-1}$ ), then added  
1716 together to calculate total chlorophyll content in the dimethyl sulfoxide extractant  
1717 (mmol mL $^{-1}$ ). Total chlorophyll content was multiplied by the volume of the  
1718 dimethyl sulfoxide extractant (10 mL) and converted to area-based chlorophyll  
1719 content by dividing by the total area of the leaf disks ( $Chl_{area}$ ; mmol m $^{-2}$ ). Mass-  
1720 based chlorophyll content ( $Chl_{mass}$ ; mmol g $^{-1}$ ) was calculated by dividing  $Chl_{area}$

**1721** by the leaf mass per area of the punched leaf.

**1722** 5.2.5 *A/C<sub>i</sub> curve fitting and parameter estimation*

**1723** We fit  $A_{\text{net}}/C_i$  curves of each individual using the ‘fitaci’ function in the  
**1724** ‘plantecophys’ R package (Duursma 2015). This function estimates the maximum  
**1725** rate of Rubisco carboxylation  $V_{\text{cmax}}$ ;  $\mu\text{mol m}^{-2} \text{s}^{-1}$ ) and maximum rate of electron  
**1726** transport for RuBP regeneration ( $J_{\text{max}}$ ;  $\mu\text{mol m}^{-2} \text{s}^{-1}$ ) based on the Farquhar bio-  
**1727** chemical model of C<sub>3</sub> photosynthesis (Farquhar et al. 1980). Triose phosphate  
**1728** utilization (TPU) limitation was included in all curve fits, and all curve fits in-  
**1729** cluded measured dark respiration values. As  $A_{\text{net}}/C_i$  curves were generated using  
**1730** a common leaf temperature, curves were fit using Michaelis-Menton coefficients  
**1731** for Rubisco affinity to CO<sub>2</sub> ( $K_c$ ;  $\mu\text{mol mol}^{-1}$ ) and O<sub>2</sub> ( $K_o$ ;  $\mu\text{mol mol}^{-1}$ ), and the  
**1732** CO<sub>2</sub> compensation point ( $\Gamma^*$ ;  $\mu\text{mol mol}^{-1}$ ) reported in Bernacchi et al. (2001).  
**1733** Specifically,  $K_c$  was set to 404.9  $\mu\text{mol mol}^{-1}$ ,  $K_o$  was set to 278.4  $\mu\text{mol mol}^{-1}$ , and  
**1734**  $\Gamma^*$  was set to 42.75  $\mu\text{mol mol}^{-1}$ . The use of a common leaf temperature across  
**1735** curves and dark respiration measurements also eliminated the need to manually  
**1736** temperature standardize rate estimates. For clarity, we reference  $V_{\text{cmax}}$ ,  $J_{\text{max}}$ , and  
**1737**  $R_d$  estimates throughout the rest of the paper as  $V_{\text{cmax}25}$ ,  $J_{\text{max}25}$ , and  $R_{d25}$ .

**1738** 5.2.6 Stomatal limitation

**1739** We quantified the extent by which stomatal conductance limited photo-  
**1740** synthesis (l; unitless) following equations originally described in Farquhar and  
**1741** Sharkey (1982). Stomatal limitation was calculated as:

$$l = 1 - \frac{A_{net}}{A_{mod}} \quad (5.3)$$

**1742** where  $A_{mod}$  represents the photosynthetic rate where  $C_i = C_a$ .  $A_{mod}$  was calcu-

**1743** lated as:

$$A_{mod} = V_{cmax25} - \frac{420 - \Gamma^*}{420 + K_m} - R_{d25} \quad (5.4)$$

**1744**  $K_m$  is the Michaelis-Menten coefficient for Rubisco-limited photosynthesis, calcu-

**1745** lated as:

$$K_m = K_c \cdot \left(1 + \frac{O_i}{K_o}\right) \quad (5.5)$$

**1746** where  $O_i$  refers to leaf intercellular  $O_2$  concentrations, set to  $210 \mu\text{mol mol}^{-1}$ .

**1747** 5.2.7 *Proportion of leaf nitrogen allocated to photosynthesis and structure*

**1748** We used equations from Niinemets and Tenhunen (1997) to estimate the

**1749** proportion of leaf N content allocated to Rubisco bioenergetics, and light harvest-

**1750** ing proteins. The proportion of leaf N allocated to Rubisco ( $\rho_{rub}$ ;  $\text{gN gN}^{-1}$ ) was

**1751** calculated as a function of  $V_{cmax25}$  and  $N_{area}$ :

$$\rho_{rubisco} = \frac{V_{cmax25} N_r}{V_{cr} N_{area}} \quad (5.6)$$

**1752** where  $N_r$  is the amount of nitrogen in Rubisco, set to  $0.16 \text{ gN (gN in Rubisco)}^{-1}$

**1753** and  $V_{cr}$  is the maximum rate of RuBP carboxylation per unit Rubisco protein,

**1754** set to  $20.5 \mu\text{mol CO}_2 (\text{g Rubisco})^{-1}$ . The proportion of leaf nitrogen allocated to

**1755** bioenergetics ( $\rho_{bioe}$ ;  $\text{gN gN}^{-1}$ ) was similarly calculated as a function of  $J_{max25}$  and

**1756**  $N_{\text{area}}$ :

$$\rho_{\text{bioe}} = \frac{J_{\text{max}25} N_b}{J_{\text{mc}} N_{\text{area}}} \quad (5.7)$$

**1757** where  $N_b$  is the amount of nitrogen in cytochrome f, set to 0.12407 gN ( $\mu\text{mol}$  cytochrome f) $^{-1}$  assuming a constant 1: 1: 1.2 cytochrome f: ferredoxin NADP reductase: coupling factor molar ratio (Evans and Seemann 1989; Niinemets and Tenhunen 1997), and  $J_{\text{mc}}$  is the capacity of electron transport per cytochrome f, set to 156  $\mu\text{mol}$  electron ( $\mu\text{mol}$  cytochrome f) $^{-1}\text{s}^{-1}$ .

**1762** The proportion of leaf nitrogen allocated to light harvesting proteins was calculated as a function of  $Chl_{\text{mass}}$  and  $N_{\text{mass}}$ :

$$\rho_{\text{light}} = \frac{Chl_{\text{mass}}}{N_{\text{mass}} c_b} \quad (5.8)$$

**1764** where  $c_b$  is the stoichiometry of the light-harvesting chlorophyll complexes of photosystem II, set to 2.75 mmol chlorophyll (gN in chlorophyll) $^{-1}$ . We used the  $N_{\text{mass}}$  value of the focal leaf used to generate  $A_{\text{net}}/C_i$  curves instead of the leaf used to extract chlorophyll content, as the two leaves are from the same trifoliolate leaf set and are highly correlated with each other (Figure SX).

**1769** The proportion of leaf nitrogen content allocated to photosynthetic tissue ( $\rho_{\text{photo}}$ ; gN gN $^{-1}$ ) was estimated as the sum of  $\rho_{\text{rubisco}}$ ,  $\rho_{\text{bioe}}$ , and  $\rho_{\text{light}}$ .

**1771** Finally, the proportion of leaf N content allocated to structural tissue ( $\rho_{\text{str}}$ ; gN gN $^{-1}$ ) was estimated as:

$$\rho_{\text{structure}} = \frac{N_{\text{cw}}}{N_{\text{area}}} \quad (5.9)$$

1773 where  $N_{cw}$  is the leaf N content allocated to cell walls ( $\text{gN m}^{-2}$ ), calculated as a  
1774 function of  $M_{area}$  using an empirical equation from Onoda et al. (2017):

$$N_{cw} = 0.000355 * M_{area}^{1.39} \quad (5.10)$$

1775 5.2.8 *Whole plant traits*

1776 Seven weeks after experiment initiation and immediately following gas ex-  
1777 change measurements, we harvested all experimental individuals and separated  
1778 biomass of each experimental individual into major organ types (leaves, stems,  
1779 roots, and nodules when present). Fresh leaf area of all harvested leaves was mea-  
1780 sured using an LI-3100C (Li-COR Biosciences, Lincoln, Nebraska, USA). Total  
1781 fresh leaf area ( $\text{cm}^2$ ) was calculated as the sum of all leaf areas, including the focal  
1782 leaf used to collect gas exchange data and the focal leaf used to extract chlorophyll  
1783 content. All harvested material was dried in an oven set to 65°C for at least 48  
1784 hours, weighed, and ground to homogeneity. Leaves and nodules were manually  
1785 ground either with a mortar and pestle, while stems and roots were ground using  
1786 a Wiley mill (E3300 Mini Mill; Eberbach Corp., MI, USA). Total dry biomass (g)  
1787 was calculated as the sum of dry leaf (including focal leaf for both the  $A_{net}/C_i$   
1788 curve and leaf used to extract chlorophyll content), stem, root, and root nodule  
1789 biomass. We also quantified carbon and nitrogen content of each respective organ  
1790 type through elemental combustion (Costech-4010, Costech, Inc., Valencia, CA,  
1791 USA) using subsamples of ground and homogenized organ tissue.

1792 Following the approach explained in Perkowski et al. (2021), we calcu-  
1793 lated structural carbon costs to acquire nitrogen as the ratio of total belowground

**1794** carbon biomass to whole plant nitrogen biomass ( $N_{\text{cost}}$ ; gC gN<sup>-1</sup>). Belowground  
**1795** carbon biomass ( $C_{\text{bg}}$ ; gC) was calculated as the sum of root carbon biomass  
**1796** and root nodule carbon biomass. Root carbon biomass and root nodule carbon  
**1797** biomass was calculated as the product of the organ biomass and the respective  
**1798** organ carbon content. Whole plant nitrogen biomass ( $N_{\text{wp}}$ ; gN) was similarly  
**1799** calculated as the sum of total leaf, stem, root, and root nodule nitrogen biomass,  
**1800** including the focal leaf used for  $A_{\text{net}}/C_i$  curve and chlorophyll extractions. Leaf,  
**1801** stem, root, and root nodule nitrogen biomass was calculated as the product of  
**1802** the organ biomass and the respective organ nitrogen content. This calculation  
**1803** only quantifies plant structural carbon costs to acquire nitrogen and does not  
**1804** include any additional costs of nitrogen acquisition associated with respiration,  
**1805** root exudation, or root turnover. An explicit explanation of the limitations for  
**1806** interpreting this calculation can be found in Perkowski et al. (2021) and Terrer  
**1807** et al. (2018).

**1808** Finally, plant investments in nitrogen fixation were calculated as the ratio  
**1809** of root nodule biomass to root biomass, where increasing values indicate an in-  
**1810** crease in plant investments to nitrogen fixation (Dovrat et al. 2018; Dovrat et al.  
**1811** 2020; Perkowski et al. 2021). We also calculated the percent of leaf nitrogen  
**1812** acquired from the atmosphere (% $N_{\text{dfa}}$ ) using leaf  $\delta^{15}\text{N}$  and the following equation  
**1813** from Andrews et al. (2011):

$$\%N_{\text{dfa}} = \frac{\delta^{15}N_{\text{reference}} - \delta^{15}N_{\text{sample}}}{\delta^{15}N_{\text{reference}} - B} \quad (5.11)$$

**1814** where  $\delta^{15}\text{N}_{\text{reference}}$  refers to a reference plant that exclusively acquires nitrogen via

1815 direct uptake,  $\delta^{15}\text{N}_{\text{sample}}$  refers to an individual's leaf  $\delta^{15}\text{N}$ , and B refers to individuals that are entirely reliant on nitrogen fixation. Within each unique nitrogen  
1816 fertilization treatment-by-CO<sub>2</sub> treatment combination, we calculated the mean  
1817 leaf  $\delta^{15}\text{N}$  for individuals growing in the non-inoculated treatment for  $\delta^{15}\text{N}_{\text{reference}}$ .  
1818 Any individuals with visual confirmation of root nodule formation or nodule initiation  
1819 were omitted from the calculation of  $\delta^{15}\text{N}_{\text{reference}}$ . Following recommendations  
1820 from Andrews et al. (2011) we calculated B within each CO<sub>2</sub> treatment using the  
1821 mean leaf  $\delta^{15}\text{N}$  of inoculated individuals that received 0 ppm N. We did not calculate  
1822 B within each unique soil nitrogen x CO<sub>2</sub> treatment combination, as previous  
1823 studies suggest decreased reliance on nitrogen fixation with increasing soil nitrogen  
1824 availability (Perkowski et al. 2021). This approach for estimating nitrogen  
1825 fixation standardizes values such that approaching 1 indicates increasing reliance  
1826 on nitrogen fixation.  
1827

1828 5.2.9 *Statistical analyses*

1829 Any uninoculated pots that had substantial root nodule formation (nodule  
1830 biomass: root biomass values greater than 0.05 g g<sup>-1</sup>) were removed from our  
1831 analyses. This was because they were assumed to have been colonized by symbiotic  
1832 nitrogen-fixing bacteria from outside sources. This decision resulted in the removal  
1833 of sixteen pots from our analysis: two pots in the elevated CO<sub>2</sub> treatment that  
1834 received 35 ppm N, three pots in the elevated CO<sub>2</sub> treatment that received 70  
1835 ppm N, one pot in the elevated CO<sub>2</sub> treatment that received 210 ppm N, two pots  
1836 in the elevated CO<sub>2</sub> treatment that received 280 ppm N, two pots in the ambient  
1837 CO<sub>2</sub> treatment that received 0 ppm N, three pots in the ambient CO<sub>2</sub> treatment

1838 that received 70 ppm N, two pots in the ambient CO<sub>2</sub> treatment that received  
1839 105 ppm N, and one pot in the ambient CO<sub>2</sub> treatment that received 280 ppm N.

1840 We built a series of linear mixed effects models to investigate the impacts of  
1841 CO<sub>2</sub> concentration, soil nitrogen fertilization, and inoculation with *B. japonicum*  
1842 on *G. max* gas exchange, tradeoffs between nitrogen and water use, whole plant  
1843 growth, and investment in nitrogen fixation. All models included CO<sub>2</sub> treatment  
1844 as a categorical fixed effect, inoculation treatment as a categorical fixed effect,  
1845 soil nitrogen fertilization as a continuous fixed effect, with interaction terms be-  
1846 tween all three fixed effects. All models also accounted for climatic difference  
1847 between chambers across experiment iterations by including a random intercept  
1848 term that nested starting chamber rack by CO<sub>2</sub> treatment. Models with this  
1849 independent variable structure were created for each of the following dependent  
1850 variables:  $N_{\text{area}}$ ,  $M_{\text{area}}$ ,  $N_{\text{mass}}$ ,  $Chl_{\text{area}}$ ,  $V_{\text{cmax25}}$ ,  $J_{\text{max25}}$ ,  $J_{\text{max25}}:V_{\text{cmax25}}$ ,  $R_{\text{d25}}$ ,  $g_{\text{sw}}$ ,  
1851 stomatal limitation,  $\rho_{\text{rubisco}}$ ,  $\rho_{\text{bioe}}$ ,  $\rho_{\text{light}}$ ,  $\rho_{\text{photo}}$ ,  $\rho_{\text{structure}}$ ,  $N_{\text{cost}}$ ,  $C_{\text{bg}}$ ,  $N_{\text{wp}}$ , total  
1852 biomass, total leaf area, nodule biomass, and the ratio of nodule biomass to root  
1853 biomass.

1854 We used Shapiro-Wilk tests of normality to determine whether linear mixed  
1855 effects models satisfied residual normality assumptions. If residual normality as-  
1856 sumptions were not met (Shapiro-Wilk:  $p < 0.05$ ), then models were fit using  
1857 dependent variables that were natural log transformed. All residual normality  
1858 assumptions that did not originally satisfy residual normality assumptions were  
1859 met with either a natural log or square root data transformation (Shapiro-Wilk:  
1860  $p > 0.05$  in all cases). Specifically, models for  $N_{\text{area}}$ ,  $N_{\text{mass}}$ ,  $Chl_{\text{area}}$ ,  $V_{\text{cmax25}}$ ,  
1861  $J_{\text{max25}}$ ,  $J_{\text{max25}}:V_{\text{cmax25}}$ ,  $g_{\text{sw}}$ , stomatal limitation,  $\rho_{\text{rubisco}}$ ,  $\rho_{\text{bioe}}$ ,  $\rho_{\text{light}}$ ,  $\rho_{\text{photo}}$ , and to-

**1862** tal leaf area satisfied residual normality assumptions without data transformation.

**1863** Models for  $M_{\text{area}}$ ,  $\rho_{\text{structure}}$ ,  $N_{\text{cost}}$ ,  $C_{\text{bg}}$ ,  $N_{\text{wp}}$ , and total biomass satisfied residual

**1864** normality assumptions with a natural log data transformation, while models for

**1865** nodule biomass and nodule biomass: root biomass satisfied residual normality

**1866** assumptions with a square root data transformation.

**1867** In all statistical models, we used the 'lmer' function in the 'lme4' R package

**1868** (Bates et al. 2015) to fit each model and the 'Anova' function in the 'car' R

**1869** package (Fox and Weisberg 2019) to calculate Type II Wald's  $\chi^2$  and determine the

**1870** significance ( $\alpha = 0.05$ ) of each fixed effect coefficient. We then used the 'emmeans'

**1871** R package (Lenth 2019) to conduct post-hoc comparisons using Tukey's tests,

**1872** where degrees of freedom were approximated using the Kenward-Roger approach

**1873** (Kenward and Roger 1997). All analyses and plots were conducted in R version

**1874** 4.2.0 (R Core Team 2021).

**1875** 5.3 Results

**1876** 5.3.1 *Leaf nitrogen content, chlorophyll content, and mass per area*

**1877** Elevated CO<sub>2</sub> reduced  $N_{\text{area}}$ ,  $N_{\text{mass}}$ , and  $Chl_{\text{area}}$  by 29%, 50%, and 31%,

**1878** respectively, and stimulated  $M_{\text{area}}$  by 44% ( $p < 0.001$  in all cases; Table 1). An in-

**1879** teraction between fertilization and CO<sub>2</sub> (CO<sub>2</sub>-by-fertilization interaction:  $p_{N_{\text{area}}} =$

**1880** 0.017,  $p_{N_{\text{mass}}} < 0.001$ ,  $p_{M_{\text{area}}} = 0.006$ ,  $p_{Chl_{\text{area}}} = 0.083$ ; Table 1) indicated that the

**1881** general positive effect of increasing fertilization on  $N_{\text{area}}$ ,  $N_{\text{mass}}$ , and  $Chl_{\text{area}}$  ( $p <$

**1882** 0.001 in all cases; Table 1) was generally stronger under ambient CO<sub>2</sub> (Tukey <sub>$N_{\text{area}}$</sub> :

**1883**  $p = 0.026$ ; Tukey <sub>$N_{\text{mass}}$</sub> :  $p < 0.001$ ; Tukey <sub>$M_{\text{area}}$</sub> :  $p = 0.009$ ; Tukey <sub>$Chl_{\text{area}}$</sub> :  $p = 0.065$ ;

**1884** Table 1; Figs. 1a-d). This pattern resulted in a stronger reduction in  $N_{\text{area}}$ ,  $N_{\text{mass}}$ ,

1885 and  $Chl_{area}$  as well as a stronger stimulation in  $M_{area}$  under elevated CO<sub>2</sub> with  
1886 increasing fertilization. An additional interaction between inoculation and CO<sub>2</sub>  
1887 on  $N_{area}$  (CO<sub>2</sub>-by-inoculation interaction:  $p = 0.030$ ; Table 1) indicated that the  
1888 general positive effect of inoculation on  $N_{area}$  ( $p < 0.001$ ; Table 1) was stronger  
1889 under elevated CO<sub>2</sub> (45% increase; Tukey:  $p < 0.001$ ) than under ambient CO<sub>2</sub>  
1890 (18% increase; Tukey:  $p < 0.001$ ), a result that increased the reduction in  $N_{area}$   
1891 in inoculated pots under elevated CO<sub>2</sub>. Inoculation treatment did not modify the  
1892 downregulation in  $N_{mass}$  (CO<sub>2</sub>-by-inoculation interaction:  $p = 0.148$ ; Table 1) and  
1893  $Chl_{area}$  ( $p = 0.147$ ; Table 1) or the stimulation in  $M_{area}$  ( $p = 0.866$ ; Table 1) un-  
1894 der elevated CO<sub>2</sub>. However, interactions between fertilization and inoculation on  
1895  $N_{area}$  (fertilization-by-inoculation interaction:  $p < 0.001$ ; Table 1; Fig. 1a),  $N_{mass}$   
1896 ( $p = 0.001$ ; Table 1; Fig. 1b),  $M_{area}$  ( $p = 0.025$ ; Table 1; Fig. 1c), and  $Chl_{area}$  ( $p$   
1897  $< 0.001$ ; Table 1; Fig. 1d) indicated that the general positive effect of increasing  
1898 fertilization on each trait was stronger in uninoculated pots (Tukey <sub>$N_{area}$</sub> :  $p <$   
1899 0.001; Tukey <sub>$N_{mass}$</sub> :  $p = 0.001$ ; Tukey <sub>$M_{area}$</sub> :  $p = 0.031$ ; Tukey <sub>$Chl_{area}$</sub> :  $p < 0.001$ ).

**Table 5.1.** Effects of soil nitrogen fertilization, inoculation, and CO<sub>2</sub> treatments on  $N_{\text{area}}$ ,  $N_{\text{mass}}$ ,  $M_{\text{area}}$ , and  $Chl_{\text{area}}$ 

	$N_{\text{area}}$			$N_{\text{mass}}$			$M_{\text{area}}^a$			
	df	Coefficient	$\chi^2$	p	Coefficient	$\chi^2$	p	Coefficient	$\chi^2$	p
(Intercept)	-	1.10E+00	-	-	3.05E-02	-	-	3.64E+00	-	-
CO <sub>2</sub>	1	-5.67E-01	155.908	<0.001	-1.80E-02	272.362	<0.001	3.04E-01	151.319	<0.001
Inoculation (I)	1	6.21E-01	86.029	<0.001	7.54E-03	15.576	<0.001	1.81E-01	19.158	<0.001
Fertilization (N)	1	3.06E-03	316.408	<0.001	5.78E-05	106.659	<0.001	3.10E-04	21.440	<0.001
CO <sub>2</sub> *I	1	2.63E-01	4.729	0.030	3.96E-03	2.025	0.155	-3.37E-02	0.029	0.866
CO <sub>2</sub> *N	1	-3.68E-04	5.723	0.017	-2.85E-05	22.542	<0.001	2.80E-04	7.619	0.006
I*N	1	-1.36E-03	43.381	<0.001	-2.00E-05	11.137	0.001	-3.36E-04	5.022	0.025
CO <sub>2</sub> *I*N	1	-3.23E-04	0.489	0.484	-2.59E-06	0.041	0.839	1.15E-04	0.208	0.649

	$Chl_{\text{area}}$			
	df	Coefficient	$\chi^2$	p
(Intercept)	-	2.13E-02	-	-
CO <sub>2</sub>	1	-1.33E-02	69.233	<0.001
Inoculation (I)	1	1.24E-01	136.341	<0.001
Fertilization (N)	1	3.35E-04	163.111	<0.001
CO <sub>2</sub> *I	1	-3.18E-02	2.102	0.147
CO <sub>2</sub> *N	1	-8.79E-05	2.999	0.083
I*N	1	-2.65E-04	75.769	<0.001
CO <sub>2</sub> *I*N	1	7.68E-05	2.144	0.147

\*Significance determined using Type II Wald  $\chi^2$  tests ( $\alpha = 0.05$ ). P-values  $< 0.05$  are in bold, while p-values between 0.05 and 0.1 are italicized. A superscript “a” is included after trait labels to indicate if models were fit with natural log transformed response variables. Key: df = degrees of freedom,  $N_{\text{area}}$  = leaf nitrogen content per unit leaf area,  $N_{\text{mass}}$  = leaf nitrogen content,  $M_{\text{area}}$  = leaf mass per unit leaf area.

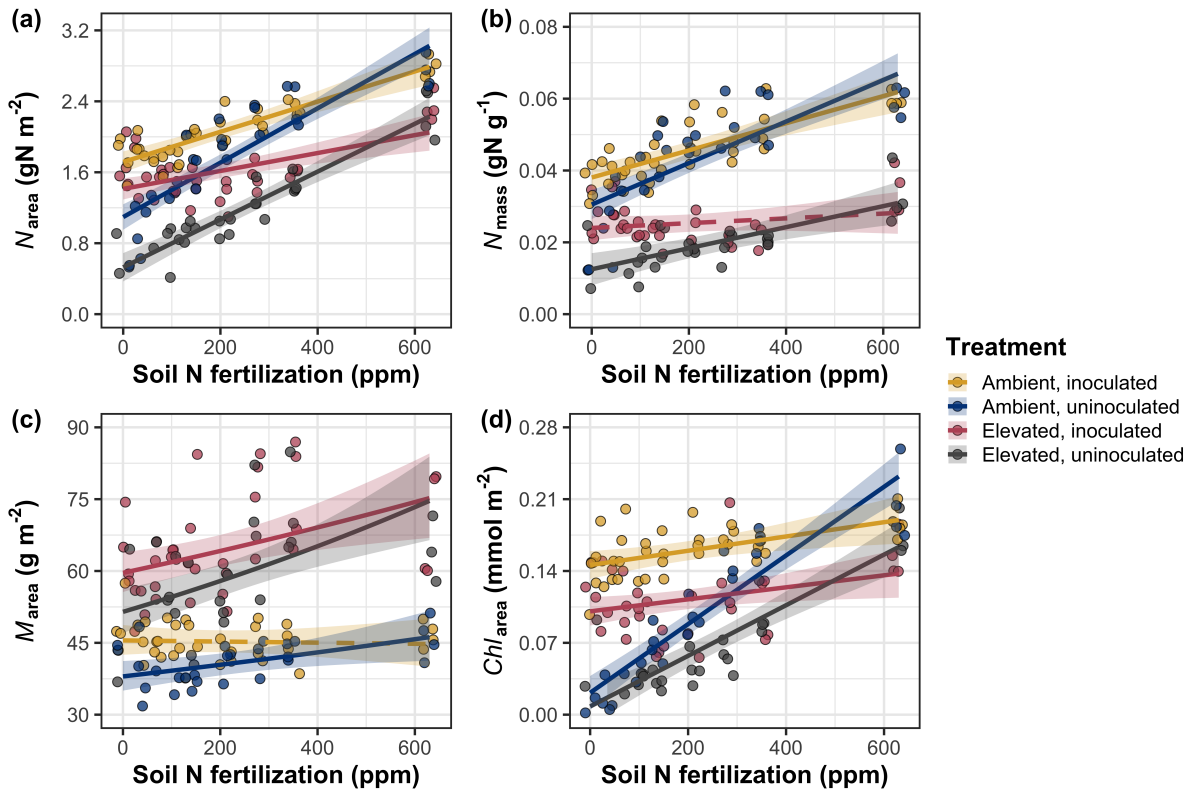


**Figure 5.1.** Effects of CO<sub>2</sub>, fertilization, and inoculation on leaf nitrogen per unit leaf area (a), leaf nitrogen content (b), leaf mass per unit leaf area (c), and chlorophyll content per unit leaf area (d). Soil nitrogen fertilization is represented on the x-axis in all panels. Yellow points and trendlines indicate inoculated individuals grown under ambient CO<sub>2</sub>, blue points and trendlines indicate uninoculated individuals grown under ambient CO<sub>2</sub>, red points and trendlines indicate inoculated individuals grown under elevated CO<sub>2</sub>, and grey points indicate uninoculated individuals grown under elevated CO<sub>2</sub>. Solid trendlines indicate regression slopes that are different from zero ( $p < 0.05$ ), while dashed trendlines indicate slopes that are not distinguishable from zero ( $p > 0.05$ ).

**1900** 5.3.2 *Leaf biochemistry and stomatal conductance*

**1901** Elevated CO<sub>2</sub> resulted in plants with 16% lower  $V_{cmax25}$  ( $p < 0.001$ ; Table  
**1902** 2) and 10% lower  $J_{max25}$  ( $p = 0.014$ ; Table 2) as compared to those grown un-  
**1903** der ambient CO<sub>2</sub>, but did not influence  $R_{d25}$  ( $p = 0.613$ ; Table 2). A relatively  
**1904** stronger downregulation in  $V_{cmax25}$  than  $J_{max25}$  resulted in an 8% stimulation in  
**1905**  $J_{max25}:V_{cmax25}$  under elevated CO<sub>2</sub> ( $p < 0.001$ ; Table 2; Fig. 2E). The downregu-  
**1906** latory effect of CO<sub>2</sub> on  $V_{cmax25}$  and  $J_{max25}$  was not modified across the fertilization  
**1907** gradient (CO<sub>2</sub>-by-fertilization interaction:  $p = 0.185$ ,  $p = 0.389$  for  $V_{cmax25}$  and  
**1908**  $J_{max25}$ , respectively; Table 2; Fig. 2A, 2C) or between inoculation treatments  
**1909** (CO<sub>2</sub>-by-inoculation interaction:  $p = 0.799$  and  $p = 0.714$  for  $V_{cmax25}$  and  $J_{max25}$ ,  
**1910** respectively; Table 2). However, a strong interaction between fertilization and  
**1911** inoculation (fertilization-by-inoculation interaction:  $p \leq 0.001$  in all cases; Table  
**1912** 2) indicated that the general positive effect of increasing fertilization on  $V_{cmax25}$  ( $p$   
**1913**  $< 0.001$ ; Table 2),  $J_{max25}$  ( $p < 0.001$ ; Table 2), and  $R_{d25}$  ( $p = 0.015$ ; Table 2) was  
**1914** only observed in uninoculated pots (Tukey:  $p \leq 0.001$  in all cases), as there was  
**1915** no apparent effect of fertilization on  $V_{cmax25}$  (Tukey:  $p = 0.456$ ),  $J_{max25}$  (Tukey:  $p$   
**1916** = 0.180), or  $R_{d25}$  (Tukey:  $p = 0.443$ ) in inoculated pots (Figs. 2B, 2D, 2F, 2H). A  
**1917** relatively stronger positive effect of increasing fertilization on  $V_{cmax25}$  than  $J_{max25}$   
**1918** resulted in a general reduction in  $J_{max25}:V_{cmax25}$  with increasing fertilization ( $p <$   
**1919** 0.001), though this pattern was only seen in uninoculated pots (Tukey:  $p = 0.003$ )  
**1920** and not inoculated plants (Tukey:  $p > 0.05$ ).

**1921** Elevated CO<sub>2</sub> reduced stomatal conductance by 20% ( $p < 0.001$ ; Table 2)  
**1922** compared to ambient CO<sub>2</sub>, but this downregulation did not influence stomatal  
**1923** limitation of photosynthesis ( $p = 0.355$ ; Table 2). As with  $V_{cmax25}$  and  $J_{max25}$ , the

1924 downregulation of stomatal conductance due to elevated CO<sub>2</sub> was not modified  
1925 across the fertilization gradient (CO<sub>2</sub>-by-fertilization interaction:  $p = 0.141$ ; Table  
1926 2) or between inoculation treatments (CO<sub>2</sub>-by-inoculation interaction:  $p = 0.179$ ;  
1927 Table 2). Fertilization also did not modify the general null effect of CO<sub>2</sub> on stom-  
1928 atal limitation (CO<sub>2</sub>-by-fertilization interaction:  $p = 0.554$ ; Table 2), although  
1929 an interaction between CO<sub>2</sub> and inoculation (CO<sub>2</sub>-by-inoculation interaction:  $p$   
1930 = 0.043; Table 2) indicated that inoculation increased stomatal limitation un-  
1931 der ambient CO<sub>2</sub> (Tukey:  $p = 0.021$ ), but not under elevated CO<sub>2</sub> (Tukey:  $p$   
1932 > 0.999). An interaction between inoculation and fertilization on stomatal con-  
1933 ductance (fertilization-by-inoculation interaction:  $p < 0.001$ ; Table 2) indicated  
1934 that increasing fertilization increased stomatal conductance in uninoculated pots  
1935 (Tukey:  $p = 0.003$ ) but decreased stomatal conductance in inoculated pots (Tukey:  
1936  $p = 0.021$ ). The similar in magnitude, but opposite direction, trend in the effect of  
1937 increasing fertilization on stomatal conductance between inoculation treatments  
1938 likely drove a null general response of stomatal conductance to increasing fertil-  
1939 ization ( $p = 0.642$ ; Table 2).

**Table 5.2.** Effects of soil nitrogen fertilization, inoculation, and CO<sub>2</sub> on leaf biochemistry

	<i>V</i> <sub>cmax25</sub>			<i>J</i> <sub>max25</sub>			<i>R</i> <sub>d25</sub>			
	df	Coefficient	$\chi^2$	p	Coefficient	$\chi^2$	p	Coefficient	$\chi^2$	p
(Intercept)	-	4.36E+01	-	-	8.30E+01	-	-	1.69E+00	-	-
CO <sub>2</sub>	1	-7.05E+00	18.039	<0.001	-9.11E+00	6.042	0.014	4.53E-01	0.256	0.613
Inoculation (I)	1	5.87E+01	98.579	<0.001	9.62E+01	85.064	<0.001	1.04E+00	3.094	0.079
Fertilization (N)	1	1.32E-01	37.053	<0.001	2.09E-01	25.356	<0.001	2.86E-03	5.965	0.015
CO <sub>2</sub> *I	1	-4.65E+00	0.065	0.799	7.84E-01	0.667	0.414	-5.71E-01	2.563	0.109
CO <sub>2</sub> *N	1	-3.58E-02	1.758	0.185	-4.33E-02	0.742	0.389	-1.55E-03	2.675	0.102
I*N	1	-1.35E-01	60.394	<0.001	-2.30E-01	57.410	<0.001	-2.84E-03	12.083	0.001
CO <sub>2</sub> *I*N	1	2.73E-02	0.748	0.387	3.46E-02	0.377	0.539	7.21E-04	0.244	0.622

123

	<i>J</i> <sub>max25</sub> : <i>V</i> <sub>cmax25</sub>			<i>g</i> <sub>sw</sub>			Stomatal limitation			
	df	Coefficient	$\chi^2$	p	Coefficient	$\chi^2$	p	Coefficient	$\chi^2$	p
(Intercept)	-	1.92E+00	-	-	1.95E-01	-	-	2.12E-01	-	-
CO <sub>2</sub>	1	5.71E-02	92.010	<0.001	-6.23E-02	9.718	0.002	3.91E-02	0.856	0.355
Inoculation (I)	1	-1.79E-01	27.768	<0.001	1.30E-01	22.351	<0.001	7.87E-02	4.582	0.032
Fertilization (N)	1	-4.61E-04	28.147	<0.001	2.50E-04	0.066	0.797	2.60E-04	32.218	<0.001
CO <sub>2</sub> *I	1	8.94E-02	2.916	0.088	6.69E-02	1.810	0.179	-7.84E-02	4.093	0.043
CO <sub>2</sub> *N	1	2.35E-04	3.210	0.073	-8.50E-05	2.165	0.141	-1.24E-04	0.350	0.554
I*N	1	3.27E-04	9.607	0.002	-3.09E-04	14.696	<0.001	-1.67E-04	2.547	0.110
CO <sub>2</sub> *I*N	1	-1.66E-04	1.102	0.294	-8.89E-05	0.234	0.629	1.67E-04	2.231	0.135

\*Significance determined using Type II Wald  $\chi^2$  tests ( $\alpha = 0.05$ ). P-values < 0.05 are in bold, while p-values between 0.05 and 0.1 are italicized. Key: *V*<sub>cmax25</sub> – maximum rate of Rubisco carboxylation at 25°C; *J*<sub>max25</sub> – maximum rate of electron transport for RuBP regeneration at 25°C, *R*<sub>d25</sub> - dark respiration at 25°C; *J*<sub>max25</sub>:*V*<sub>cmax25</sub> – the ratio of *J*<sub>max25</sub> to *V*<sub>cmax25</sub>; *g*<sub>sw</sub> - stomatal conductance.

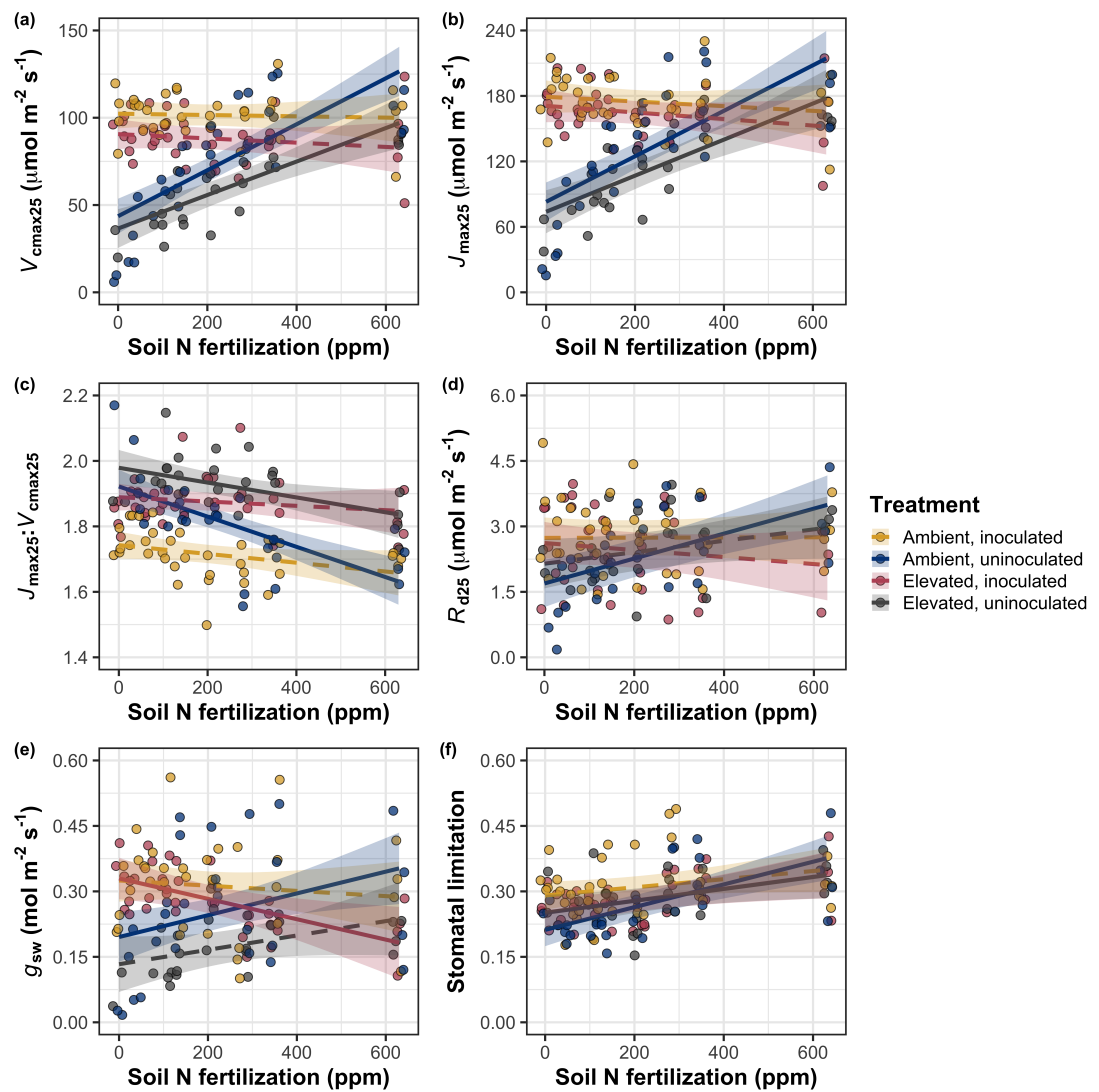


**Figure 5.2.** Effects of CO<sub>2</sub>, fertilization, and inoculation on maximum rate of Rubisco carboxylation (a), the maximum rate of RuBP regeneration (b), and the ratio of the maximum rate of RuBP regeneration to the maximum rate of Rubisco carboxylation leaf mass per unit leaf area (c), dark respiration (d), stomatal conductance (e), and stomatal limitation (f). Soil nitrogen fertilization is represented on the x-axis in all panels. Colored points and trendlines are as explained in Figure 1.

**1940** 5.3.3 *Leaf nitrogen allocation*

**1941** A relatively stronger downregulation in  $N_{\text{area}}$  than  $V_{\text{cmax}25}$  or  $J_{\text{max}25}$  resulted  
**1942** in an 20% and 29% respective stimulation in  $\rho_{\text{rubisco}}$  and  $\rho_{\text{bioe}}$  under elevated CO<sub>2</sub>  
**1943** ( $p < 0.001$  in both cases; Table 3). There was no apparent CO<sub>2</sub> effect on  $\rho_{\text{light}}$   
**1944** ( $p = 0.700$ ; Table 3), but the strong stimulation in  $\rho_{\text{rubisco}}$  and  $\rho_{\text{bioe}}$  resulted  
**1945** in a 21% stimulation of  $\rho_{\text{photo}}$  under elevated CO<sub>2</sub> ( $p < 0.001$ ; Table 3; Fig.  
**1946** 3A). The stimulation of  $\rho_{\text{rubisco}}$ ,  $\rho_{\text{bioe}}$ , and  $\rho_{\text{photo}}$  due to elevated CO<sub>2</sub> was not  
**1947** modified across the fertilization gradient (CO<sub>2</sub>-by-fertilization interaction:  $p_{\text{rubisco}}$   
**1948** = 0.269,  $p_{\text{bioe}} = 0.298$ ,  $p_{\text{photo}} = 0.281$ ; Table 3). A marginal interaction between  
**1949** inoculation and CO<sub>2</sub> on  $\rho_{\text{rubisco}}$  and  $\rho_{\text{photo}}$  (CO<sub>2</sub>-by-inoculation interaction:  $p_{\text{rubisco}}$   
**1950** = 0.057,  $p_{\text{photo}} = 0.057$ ; Table 3) indicated that the general positive effect of  
**1951** inoculation on  $\rho_{\text{rubisco}}$  and  $\rho_{\text{photo}}$  ( $p < 0.001$  in both cases; Table 3) was only  
**1952** apparent under ambient CO<sub>2</sub> (Tukey:  $p < 0.001$  in both cases), with no apparent  
**1953** effect of inoculation under elevated CO<sub>2</sub> (Tukey<sub>rubisco</sub>:  $p = 0.200$ ; Tukey<sub>photo</sub>:  $p$   
**1954** = 0.147). Inoculation did not modify the stimulation of  $\rho_{\text{bioe}}$  under elevated CO<sub>2</sub>  
**1955** (CO<sub>2</sub>-by-inoculation interaction:  $p = 0.122$ ; Table 3) or the null effect of CO<sub>2</sub> on  
**1956**  $\rho_{\text{bioe}}$  (CO<sub>2</sub>-by-inoculation interaction:  $p = 0.298$ ; Table 3). Strong interactions  
**1957** between fertilization and inoculation on  $\rho_{\text{rubisco}}$ ,  $\rho_{\text{bioe}}$ , and  $\rho_{\text{photo}}$  (fertilization-  
**1958** by-inoculation interaction:  $p < 0.001$  in all cases; Table 3) indicated that the  
**1959** general negative effect of increasing fertilization ( $p < 0.001$  in all cases; Table  
**1960** 3) was only observed in inoculated pots (Tukey:  $p < 0.001$  in all cases), with  
**1961** no apparent effect of fertilization on  $\rho_{\text{rubisco}}$  (Tukey:  $p = 0.612$ ),  $\rho_{\text{bioe}}$  (Tukey:  
**1962**  $p = 0.544$ ), or  $\rho_{\text{photo}}$  (Tukey:  $p = 0.521$ ; Fig 3B) in uninoculated pots. An  
**1963** additional interaction between fertilization and inoculation on  $\rho_{\text{light}}$  (fertilization-

**1964** by-inoculation interaction:  $p < 0.001$ ; Table 3) indicated a negative effect of  
**1965** increasing fertilization on  $\rho_{\text{light}}$  in inoculated pots (Tukey:  $p = 0.041$ ), but a  
**1966** positive effect of increasing fertilization in uninoculated pots (Tukey:  $p < 0.001$ ).  
**1967** The stimulation in  $M_{\text{area}}$  resulted in an 133% stimulation of  $\rho_{\text{structure}}$  under  
**1968** elevated CO<sub>2</sub> ( $p < 0.001$ ; Table 3; Fig 3C). An interaction between fertilization  
**1969** and CO<sub>2</sub> (CO<sub>2</sub>-by-fertilization interaction:  $p = 0.039$ ; Table 3) indicated that the  
**1970** general negative effect of increasing fertilization ( $p < 0.001$ ; Table 3) on  $\rho_{\text{structure}}$   
**1971** was marginally stronger under ambient CO<sub>2</sub> (Tukey:  $p = 0.055$ ), resulting in a  
**1972** stronger stimulation in  $\rho_{\text{structure}}$  under elevated CO<sub>2</sub> with increasing fertilization.  
**1973** A marginal interaction between inoculation and CO<sub>2</sub> (CO<sub>2</sub>-by-inoculation inter-  
**1974** action:  $p = 0.057$ ; Table 3) indicated that the general positive effect of inoculation  
**1975** on  $\rho_{\text{structure}}$  ( $p < 0.001$ ; Table 3) was only observed under elevated CO<sub>2</sub> (Tukey:  
**1976**  $p < 0.001$ ), with no apparent inoculation effect observed under ambient CO<sub>2</sub>  
**1977** (Tukey:  $p = 0.513$ ). Finally, an interaction between fertilization and inoculation  
**1978** (fertilization-by-inoculation interaction:  $p < 0.001$ ; Table 3; Fig. 3D) indicated  
**1979** that, while increasing fertilization generally increased  $\rho_{\text{structure}}$  ( $p < 0.001$ ; Table  
**1980** 3), this response was generally stronger in uninoculated pots (Tukey:  $p = 0.001$ ).

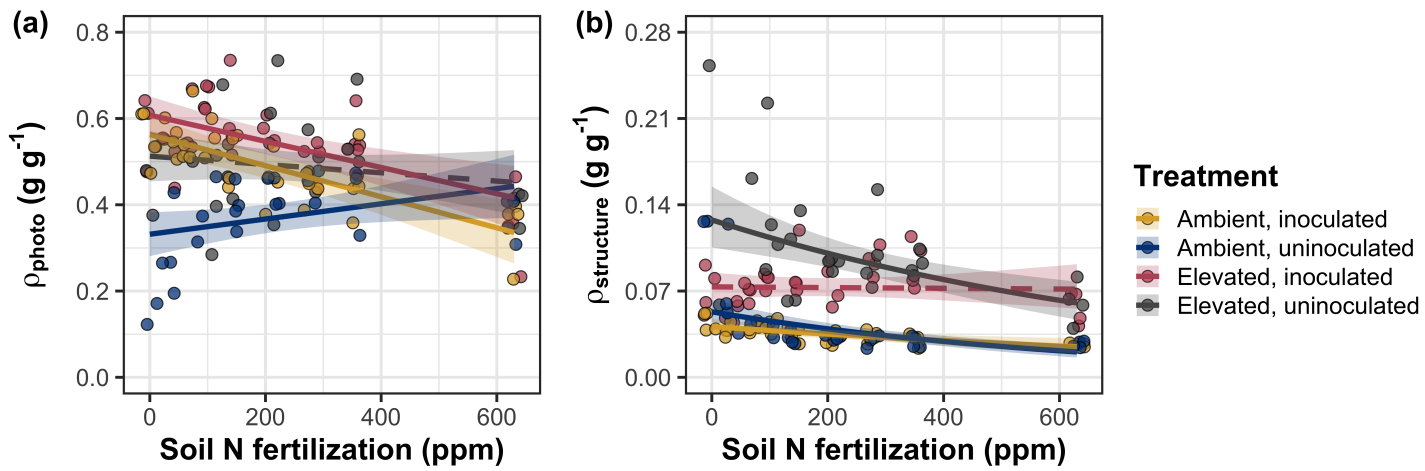
**Table 5.3.** Effects of soil N availability, soil pH, species, and  $N_{\text{area}}$  on leaf nitrogen allocation

	$\rho_{\text{rubisco}}$			$\rho_{\text{bioe}}$			$\rho_{\text{light}}$			
	df	Coefficient	$\chi^2$	p	Coefficient	$\chi^2$	p	Coefficient	$\chi^2$	p
(Intercept)	-	2.70E-01	-	-	5.26E-02	-	-	8.48E-03	-	-
CO <sub>2</sub>	1	1.42E-01	23.510	<b>&lt;0.001</b>	3.00E-02	53.899	<b>&lt;0.001</b>	2.03E-03	0.149	0.700
Inoculation (I)	1	1.83E-01	23.475	<b>&lt;0.001</b>	2.80E-02	13.860	<b>&lt;0.001</b>	2.04E-02	147.234	<b>&lt;0.001</b>
Fertilization (N)	1	1.35E-04	16.609	<b>&lt;0.001</b>	1.22E-05	26.827	<b>&lt;0.001</b>	3.22E-05	19.378	<b>&lt;0.001</b>
CO <sub>2</sub> *I	1	-1.07E-01	3.629	<i>0.057</i>	-1.67E-02	2.390	0.122	-5.33E-03	0.684	0.408
CO <sub>2</sub> *N	1	-2.16E-04	1.223	<i>0.269</i>	-3.59E-05	1.085	0.298	-7.01E-06	0.351	0.553
I*N	1	-4.26E-04	20.045	<b>&lt;0.001</b>	-6.87E-05	15.458	<b>&lt;0.001</b>	-4.37E-05	64.042	<b>&lt;0.001</b>
CO <sub>2</sub> *I*N	1	2.50E-04	3.327	<i>0.068</i>	4.08E-05	2.651	0.103	1.74E-05	3.735	<i>0.053</i>

	$\rho_{\text{photo}}$			$\rho_{\text{structure}}^a$			
	df	Coefficient	$\chi^2$	p	Coefficient	$\chi^2$	p
(Intercept)	-	3.32E-01	-	-	-2.93E+00	-	-
CO <sub>2</sub>	1	1.81E-01	27.651	<b>&lt;0.001</b>	8.77E-01	229.571	<b>&lt;0.001</b>
Inoculation (I)	1	2.31E-01	26.238	<b>&lt;0.001</b>	-2.55E-01	13.872	<b>&lt;0.001</b>
Fertilization (N)	1	1.76E-04	15.899	<b>&lt;0.001</b>	-1.51E-03	38.128	<b>&lt;0.001</b>
CO <sub>2</sub> *I	1	-1.36E-01	3.671	<i>0.055</i>	-2.99E-01	3.622	<i>0.057</i>
CO <sub>2</sub> *N	1	-2.72E-04	1.163	<i>0.281</i>	3.14E-04	4.266	<b>0.039</b>
I*N	1	-5.37E-04	21.355	<b>&lt;0.001</b>	7.00E-04	11.025	<b>0.001</b>
CO <sub>2</sub> *I*N	1	3.29E-04	4.009	<b>0.045</b>	4.52E-04	0.669	0.413

\*Significance determined using Type II Wald  $\chi^2$  tests ( $\alpha = 0.05$ ). P-values  $< 0.05$  are in bold, while p-values between 0.05 and 0.1 are italicized. A superscript “a” is included after trait labels to indicate if models were fit with natural log transformed response variables. Key: df=degrees of freedom,  $\rho_{\text{rubisco}}$  = proportion of leaf N allocated to photosynthesis,  $\rho_{\text{bioe}}$  = proportion of leaf N allocated to bioenergetics,  $\rho_{\text{light}}$ =proportion of leaf N allocated to light harvesting proteins,  $\rho_{\text{photo}}$ =proportion of leaf N allocated to photosynthesis,  $\rho_{\text{structure}}$ =proportion of leaf N allocated to cell wall structural tissue



**Figure 5.3.** Effects of  $\text{CO}_2$ , fertilization, and inoculation on the relative fraction of leaf nitrogen allocated to photosynthesis (a) and the fraction of leaf nitrogen allocated to structure (b). Soil nitrogen fertilization is represented on the x-axis in both panels. Colored points and trendlines are as explained in Figure 1.

**1981** 5.3.4 *Whole plant growth and total leaf area*

**1982** Total leaf area was 51% greater and total biomass was 102% greater un-  
**1983** der elevated CO<sub>2</sub> ( $p < 0.001$  in both cases; Table 4), a pattern that was en-  
**1984** hanced by fertilization (CO<sub>2</sub>-by-fertilization interaction:  $p < 0.001$  in both cases;  
**1985** Table 4; Fig. 4a-b) but was not modified across inoculation treatments (CO<sub>2</sub>-  
**1986** by-inoculation interaction:  $p_{total\_leaf\_area} = 0.151$ ,  $p_{total\_biomass} = 0.472$ ; Table 4).  
**1987** Specifically, the general positive effect of increasing fertilization on total leaf area  
**1988** and whole plant biomass ( $p < 0.001$  in both cases; Table 4) was stronger under  
**1989** elevated CO<sub>2</sub> (Tukey:  $p < 0.001$  in both cases). The general positive effect of  
**1990** increasing fertilization on total leaf area was modified by inoculation treatment  
**1991** (fertilization-by-inoculation interaction:  $p < 0.001$  in both cases; Table 4), in-  
**1992** dicating a stronger positive effect of increasing fertilization in uninoculated pots  
**1993** (Tukey:  $p_{total\_leaf\_area} = 0.002$ ,  $p_{total\_biomass} = 0.001$ ).

**1994** 5.3.5 *Carbon costs to acquire nitrogen*

**1995** A general 62% stimulation in  $N_{cost}$  under elevated CO<sub>2</sub> was modified thr-  
**1996** ough a strong three-way interaction between CO<sub>2</sub>, fertilization, and inoculation  
**1997** (CO<sub>2</sub>-by-inoculation-by-fertilization interaction:  $p < 0.001$ ; Table 4). This in-  
**1998** teraction revealed a general negative effect of increasing fertilization on  $N_{cost}$  ( $p$   
**1999**  $< 0.001$ ; Table 4) that was observed in all treatment combinations (Tukey:  $p <$   
**2000** 0.001 in all cases) except for inoculated pots grown under elevated CO<sub>2</sub> (Tukey:  
**2001**  $p = 0.779$ ; Fig. 5c). This response also resulted in generally stronger negative ef-  
**2002** ffects of increasing fertilization on  $N_{cost}$  in uninoculated pots grown under elevated  
**2003** CO<sub>2</sub> than uninoculated pots grown under ambient CO<sub>2</sub> (Tukey:  $p = 0.001$ ) and

**2004** inoculated pots grown under either ambient CO<sub>2</sub> (Tukey:  $p < 0.001$ ) or elevated  
**2005** CO<sub>2</sub> (Tukey:  $p < 0.001$ ), while uninoculated pots grown under ambient CO<sub>2</sub> had  
**2006** generally stronger negative effects of increasing fertilization on  $N_{\text{cost}}$  than inocu-  
**2007** lated pots grown under elevated CO<sub>2</sub> (Tukey:  $p = 0.002$ ), but not inoculated pots  
**2008** grown under ambient CO<sub>2</sub> (Tukey:  $p = 0.216$ ). The general reduction in  $N_{\text{cost}}$   
**2009** with increasing fertilization and in uninoculated pots were driven by a stronger  
**2010** positive effect of increasing fertilization on  $N_{\text{wp}}$  (denominator of  $N_{\text{cost}}$ ) than  $C_{\text{bg}}$   
**2011** (numerator of  $N_{\text{cost}}$ ), while the general stimulation in  $N_{\text{cost}}$  under elevated CO<sub>2</sub>  
**2012** was driven by a stronger positive effect of elevated CO<sub>2</sub> on  $C_{\text{bg}}$  than  $N_{\text{wp}}$  (Table  
**2013** 4).

**Table 5.4.** Effects of soil N availability, soil pH, species, and  $N_{\text{area}}$  on total leaf area, whole plant biomass, and costs of nitrogen acquisition

	Total leaf area			Total biomass			$N_{\text{cost}}$			
	df	Coefficient	$\chi^2$	p	Coefficient	$\chi^2$	p	Coefficient	$\chi^2$	p
(Intercept)	-	8.78E+01	-	-	9.96E-01	-	-	8.67E+00	-	-
$\text{CO}_2$	1	3.36E+01	69.291	<0.001	5.07E-01	131.477	<0.001	8.75E+00	88.189	<0.001
Inoculation (I)	1	1.88E+02	35.715	<0.001	7.96E-01	34.264	<0.001	-1.68E+00	136.343	<0.001
Fertilization (N)	1	9.35E-01	274.199	<0.001	3.14E-03	269.046	<0.001	-8.50E-03	80.501	<0.001
$\text{CO}_2 * \text{I}$	1	6.44E+01	2.064	0.151	-7.69E-02	0.518	0.472	-8.38E+00	85.237	<0.001
$\text{CO}_2 * \text{N}$	1	5.05E-01	18.655	<0.001	1.61E-03	16.877	<0.001	-9.17E-03	1.050	0.306
$\text{I} * \text{N}$	1	-3.84E-01	10.804	0.001	-1.45E-03	15.779	<0.001	4.20E-03	46.489	<0.001
$\text{CO}_2 * \text{I} * \text{N}$	1	-2.97E-03	<0.001	0.990	-1.14E-04	0.023	0.880	1.32E-02	18.125	<0.001

	$C_{\text{bg}}$			$N_{\text{wp}}$			
	df	Coefficient	$\chi^2$	p	Coefficient	$\chi^2$	p
(Intercept)	-	-1.70E+00	-	-	1.24E-01	-	-
$\text{CO}_2$	1	9.21E-01	84.134	<0.001	-3.41E-03	23.890	<0.001
Inoculation (I)	1	1.18E+00	41.030	<0.001	1.68E-01	134.460	<0.001
N fertilization (N)	1	3.38E-03	152.248	<0.001	6.69E-04	529.021	<0.001
$\text{CO}_2 * \text{I}$	1	-6.18E-01	8.965	0.003	3.68E-02	1.190	0.275
$\text{CO}_2 * \text{N}$	1	-3.66E-05	1.188	0.276	1.58E-04	5.915	0.015
$\text{I} * \text{N}$	1	-2.22E-03	22.648	<0.001	-3.20E-04	55.562	<0.001
$\text{CO}_2 * \text{I} * \text{N}$	1	8.09E-04	1.109	0.292	-7.54E-05	0.620	0.431

\*Significance determined using Type II Wald  $\chi^2$  tests ( $\alpha = 0.05$ ). P-values  $< 0.05$  are in bold, while p-values between 0.05 and 0.1 are italicized. A superscript “a” after trait labels indicates if models were fit using natural log transformed response variables, while a superscript “b” indicates if models were fit using square root transformed variables. Key: df=degrees of freedom

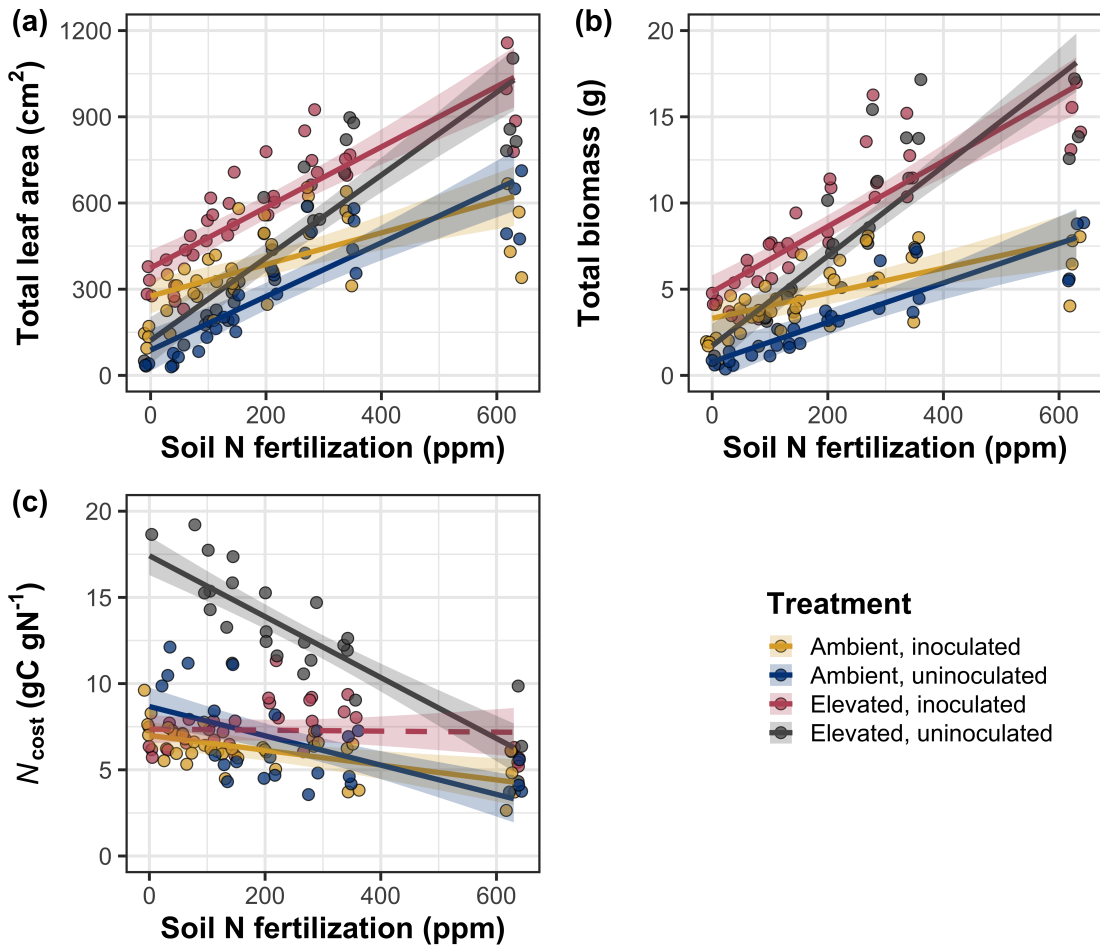


**Figure 5.4.** Effects of  $\text{CO}_2$ , fertilization, and inoculation on total leaf area (a), total biomass (b), and structural carbon costs to acquire nitrogen (c). Soil nitrogen fertilization is represented continuously on the x-axis in all panels. Colored points and trendlines are as explained in Figure 1.

**2014** 5.3.6 *Nitrogen fixation*

**2015** Nodule biomass was stimulated by 30% under elevated CO<sub>2</sub> ( $p < 0.001$ ;  
**2016** Table 5), a pattern that was modified across the fertilization gradient (CO<sub>2</sub>-by-  
**2017** fertilization interaction:  $p = 0.479$ ; Table 5), but not between inoculation treat-  
**2018** ments (CO<sub>2</sub>-by-inoculation interaction:  $p = 0.404$ ; Table 5). Specifically, the  
**2019** general negative effect of increasing fertilization on nodule biomass ( $p < 0.001$ ;  
**2020** Table 5) was stronger under elevated CO<sub>2</sub> than ambient CO<sub>2</sub> (Tukey:  $p < 0.001$ ;  
**2021** Fig. 5a), which reduced the stimulation in nodule biomass under elevated CO<sub>2</sub>  
**2022** with increasing fertilization. A strong interaction between fertilization and inocu-  
**2023** lation (fertilization-by-inoculation interaction:  $p < 0.001$ ; Table 5) was driven by  
**2024** a stronger negative effect of increasing fertilization in inoculated pots (Tukey:  $p$   
**2025**  $< 0.001$ ; Fig. 5a).

**2026** There was no effect of CO<sub>2</sub> on nodule: root biomass ( $p = 0.767$ ; Table 5),  
**2027** although an interaction between CO<sub>2</sub> and inoculation (CO<sub>2</sub>-by-inoculation inter-  
**2028** action:  $p < 0.001$ ; Table 5) indicated that the general positive effect of inoculation  
**2029** on nodule: root biomass ( $p < 0.001$ ; Table 5) was stronger under ambient CO<sub>2</sub>  
**2030** (3129% increase; Tukey:  $p < 0.001$ ) than elevated CO<sub>2</sub> (379% increase; Tukey:  
**2031**  $p < 0.001$ ; Fig. 5b). The null effect of CO<sub>2</sub> on nodule: root biomass was con-  
**2032** sistently observed across the fertilization gradient ( $p = 0.183$ ; Table 5; Fig. 5b).  
**2033** An interaction between fertilization and inoculation (fertilization-by-inoculation  
**2034** interaction:  $p < 0.001$ ; Table 5) indicated that the general negative effect of in-  
**2035** creasing fertilization on nodule: root biomass ( $p < 0.001$ ; Table 5) was stronger  
**2036** in inoculated pots (Tukey:  $p < 0.001$ ; Fig. 5b).  
**2037** There was no effect of CO<sub>2</sub> on %N<sub>dfa</sub> ( $p = 0.472$ ; Table 5), a pattern

**2038** that was not modified by inoculation ( $\text{CO}_2$ -by-inoculation interaction:  $p = 0.156$ ;  
**2039** Table 5) or fertilization ( $\text{CO}_2$ -by-fertilization interaction:  $p = 0.099$ ; Table 5).  
**2040** An interaction between fertilization and inoculation (fertilization-by-inoculation  
**2041** interaction:  $p < 0.001$ ; Table 5) indicated that the general negative effect of  
**2042** increasing fertilization on  $\%N_{\text{dfa}}$  ( $p < 0.001$ ; Table 5) was only observed in inoc-  
**2043** ulated pots (Tukey:  $p < 0.001$ ), with no apparent effect of fertilization on  $\%N_{\text{dfa}}$   
**2044** in uninoculated pots (Tukey:  $p = 0.651$ ; Table 5; Fig. 5c).

**Table 5.5.** Effects of soil N availability, soil pH, species, and  $N_{\text{area}}$  on leaf biochemistry

	df	Root nodule biomass <sup>b</sup>			Root nodule: root biomass <sup>b</sup>			% $N_{\text{dfa}}^b$		
		Coefficient	$\chi^2$	p	Coefficient	$\chi^2$	p	Coefficient	$\chi^2$	p
(Intercept)	-	9.41E-03	-	-	1.33E-02	-	-	7.48E-01	-	-
CO <sub>2</sub>	1	1.20E-01	19.258	<b>&lt;0.001</b>	9.94E-02	0.087	0.768	-1.00E-01	0.518	0.472
Inoculation (I)	1	5.74E-01	755.020	<b>&lt;0.001</b>	5.40E-01	903.691	<b>&lt;0.001</b>	9.01E+00	955.570	<b>&lt;0.001</b>
Fertilization (N)	1	7.71E-06	84.376	<b>&lt;0.001</b>	-5.99E-06	258.099	<b>&lt;0.001</b>	3.64E-04	292.938	<b>&lt;0.001</b>
CO <sub>2</sub> *I	1	-4.68E-02	0.950	0.330	-1.38E-01	20.614	<b>&lt;0.001</b>	-1.44E-01	2.010	0.156
CO <sub>2</sub> *N	1	-1.59E-04	2.106	0.147	-1.73E-04	1.773	0.183	-6.21E-05	2.716	0.099
I*N	1	-5.82E-04	44.622	<b>&lt;0.001</b>	-7.45E-04	133.918	<b>&lt;0.001</b>	-1.58E-02	231.290	<b>&lt;0.001</b>
CO <sub>2</sub> *I*N	1	7.26E-05	0.196	0.658	1.76E-04	2.359	0.125	2.77E-03	2.119	0.145

\*Significance determined using Type II Wald  $\chi^2$  tests ( $\alpha = 0.05$ ). P-values  $< 0.05$  are in bold, while p-values between 0.05 and 0.1 are italicized. Superscript letters indicate model coefficients fit to square-root (<sup>b</sup>) transformed data. Key: % $N_{\text{dfa}}$ =percent nitrogen fixed from the atmosphere.

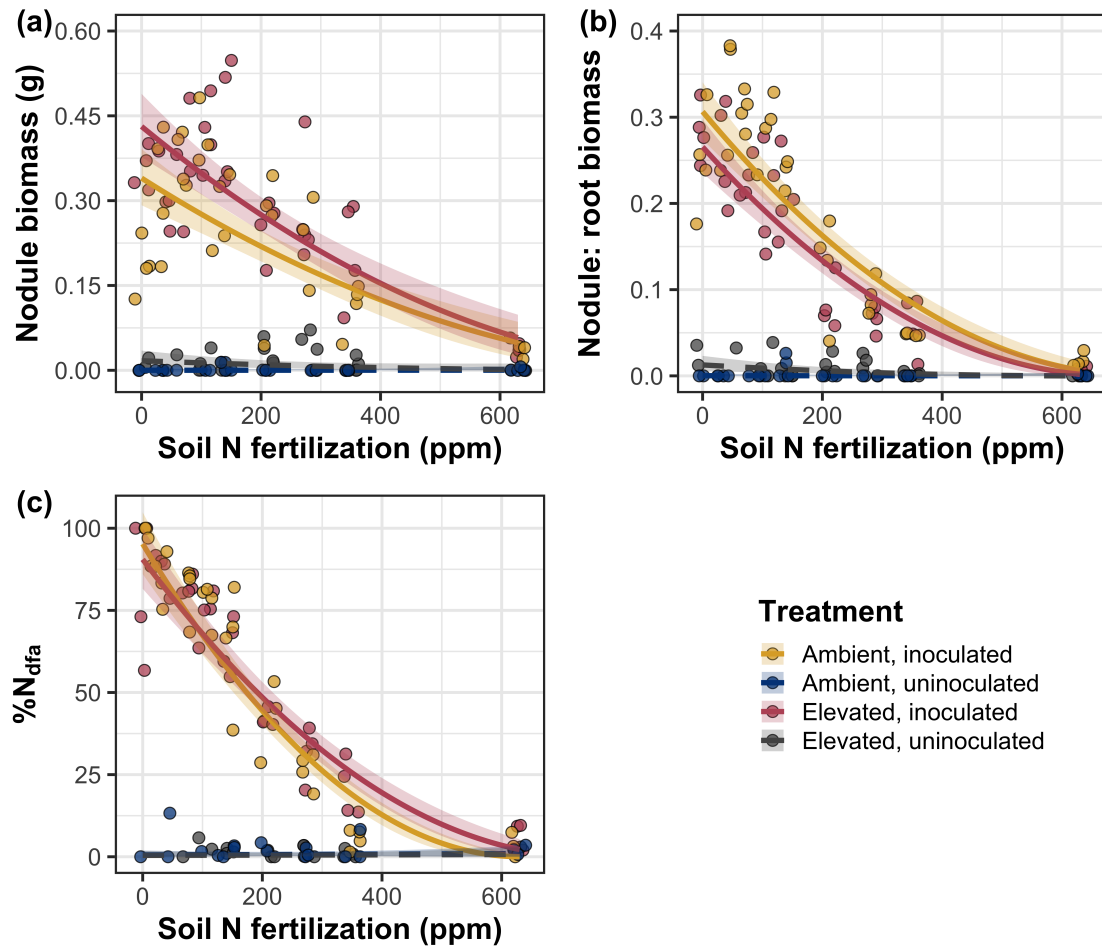


**Figure 5.5.** Effects of  $\text{CO}_2$ , fertilization, and inoculation on nodule biomass (a), nodule: root biomass (b), and percent nitrogen fixed from the atmosphere (c). Soil nitrogen fertilization is represented on the x-axis. Yellow points and trendlines indicate inoculated individuals grown under ambient  $\text{CO}_2$ , blue points and trendlines indicate uninoculated individuals grown under ambient  $\text{CO}_2$ , red points and trendlines indicate inoculated individuals grown under elevated  $\text{CO}_2$ , and grey points indicate uninoculated individuals grown under elevated  $\text{CO}_2$ . Solid trendlines indicate slopes that are different from zero ( $p < 0.05$ ), while dashed trendlines indicate slopes that are not different from zero ( $p > 0.05$ ). Curvilinear trendlines occur as a result of back-transforming models where response variables received either a natural log or square root transformation prior to fitting.

**2045** 5.4 Discussion

**2046** In this study, we determined leaf and whole plant acclimation responses of  
**2047** 7-week *G. max* seedlings grown under two CO<sub>2</sub> concentrations, two inoculation  
**2048** treatments, and nine soil nitrogen fertilization treatments in a full-factorial growth  
**2049** chamber experiment. In support of our hypotheses and patterns expected from  
**2050** theory, elevated CO<sub>2</sub> reduced  $N_{\text{area}}$ ,  $V_{\text{cmax25}}$ , and  $J_{\text{max25}}$ . The relatively stronger  
**2051** downregulation in  $V_{\text{cmax25}}$  than  $J_{\text{max25}}$  under elevated CO<sub>2</sub> resulted in a stimu-  
**2052** lation in  $J_{\text{max25}}:V_{\text{cmax25}}$  under elevated CO<sub>2</sub>. The downregulation of  $V_{\text{cmax25}}$  and  
**2053**  $J_{\text{max25}}$  under elevated CO<sub>2</sub> was similar across fertilization and inoculation treat-  
**2054** ments, indicating that the CO<sub>2</sub> responses were not due to nitrogen limitation.  
**2055** Interestingly, our results indicate that elevated CO<sub>2</sub> increased the fraction of leaf  
**2056** nitrogen allocated to photosynthesis and structure, leading to a stimulation in  
**2057** nitrogen use efficiency under elevated CO<sub>2</sub> despite the apparent downregulation  
**2058** in  $N_{\text{area}}$ ,  $V_{\text{cmax25}}$ , and  $J_{\text{max25}}$ . The downregulation in leaf photosynthetic processes  
**2059** under elevated CO<sub>2</sub> also corresponded with a strong stimulation in total leaf area  
**2060** and total biomass. Strong stimulations in whole plant growth due to elevated CO<sub>2</sub>  
**2061** were generally enhanced with increasing fertilization and were negatively related  
**2062** to structural carbon costs to acquire nitrogen. Inoculation generally did not mod-  
**2063** ify whole plant responses to elevated CO<sub>2</sub> across the fertilization gradient, likely  
**2064** due to a strong reduction in root nodulation with increasing fertilization. However,  
**2065** strong positive effects of inoculation on whole plant growth were observed under  
**2066** low fertilization, consistent with our hypothesis. Overall, observed leaf and whole  
**2067** plant acclimation responses to CO<sub>2</sub> support our hypotheses and patterns expected  
**2068** from photosynthetic least-cost theory, showing that leaf acclimation responses to

2069 CO<sub>2</sub> were decoupled from soil nitrogen availability and ability to acquire nitro-  
2070 gen via symbiotic nitrogen fixation. Instead, leaf and whole plant acclimation  
2071 responses to CO<sub>2</sub> were driven by optimal resource investment to photosynthetic  
2072 capacity, where optimal resource investment at the leaf level maximized nitrogen  
2073 allocation to structures that support whole plant growth.

2074 5.4.1 *Soil nitrogen fertilization has divergent effects on leaf and whole plant*  
2075 *acclimation responses to CO<sub>2</sub>*

2076 Elevated CO<sub>2</sub> reduced  $N_{\text{area}}$ ,  $V_{\text{cmax25}}$ ,  $J_{\text{max25}}$ , and stomatal conductance by  
2077 29%, 16%, 10%, and 20%, respectively (Table 5.2). The larger downregulation in  
2078  $V_{\text{cmax25}}$  than  $J_{\text{max25}}$  led to an 8% stimulation in  $J_{\text{max25}}:V_{\text{cmax25}}$  (Table 5.2), while  
2079 the larger downregulation in  $N_{\text{area}}$  than  $V_{\text{cmax25}}$  resulted in a 21% stimulation  
2080 in the fraction of leaf nitrogen allocated to photosynthesis under elevated CO<sub>2</sub>.  
2081 These acclimation responses are directionally consistent with previous studies that  
2082 have investigated or reviewed leaf acclimation responses to CO<sub>2</sub> (Drake et al.  
2083 1997; Makino et al. 1997; Ainsworth et al. 2002; Ainsworth and Long 2005;  
2084 Ainsworth and Rogers 2007; Smith and Dukes 2013; Smith and Keenan 2020;  
2085 Poorter et al. 2022), and follow patterns expected from photosynthetic least-cost  
2086 theory (Wright et al. 2003; Prentice et al. 2014; Smith et al. 2019; Smith and  
2087 Keenan 2020). Together, the stimulation in  $J_{\text{max25}}:V_{\text{cmax25}}$  and the fraction of leaf  
2088 nitrogen allocated to photosynthesis, and nitrogen use efficiency under elevated  
2089 CO<sub>2</sub> provide strong support for the idea that leaves were downregulating  $V_{\text{cmax25}}$   
2090 in response to elevated CO<sub>2</sub> in order to optimally coordinate photosynthesis such  
2091 that net photosynthesis rates approached becoming equally co-limited by Rubisco

**2092** carboxylation and RuBP regeneration (Chen et al. 1993; Maire et al. 2012).  
**2093** Increasing fertilization and inoculation induced strong positive effects on  
**2094**  $N_{\text{area}}$  (Fig. 1a),  $V_{\text{cmax}25}$  (Fig. 5.2a),  $J_{\text{max}25}$  (Fig. 5.2b). The general positive  
**2095** response of  $N_{\text{area}}$  to increasing fertilization and in inoculated pots was enhanced  
**2096** under ambient  $\text{CO}_2$ , which, paired with the general downregulation in  $N_{\text{area}}$  un-  
**2097** der elevated  $\text{CO}_2$ , resulted in a stronger downregulation of  $N_{\text{area}}$  under elevated  
**2098**  $\text{CO}_2$  with increasing fertilization and in inoculated pots (Fig. 5.1a). These pat-  
**2099** terns suggest that  $N_{\text{area}}$  responses to  $\text{CO}_2$  were at least partially dependent on  
**2100** soil nitrogen fertilization and nitrogen acquisition strategy. However, the general  
**2101** stimulation in the fraction of leaf nitrogen allocated to Rubisco, bioenergetics,  
**2102** or photosynthesis under elevated  $\text{CO}_2$  was not modified across the fertilization  
**2103** gradient and was only marginally enhanced in inoculated pots. These patterns  
**2104** suggest that the increased downregulation of  $N_{\text{area}}$  under elevated  $\text{CO}_2$  with in-  
**2105** creasing fertilization was not associated with a change in relative investment to  
**2106** photosynthetic tissue. Instead, a stronger downregulation in the fraction of leaf  
**2107** nitrogen allocated to structure under ambient  $\text{CO}_2$  resulted in a stronger stim-  
**2108** ulation in  $\rho_{\text{structure}}$  under elevated  $\text{CO}_2$  with increasing fertilization (Fig. 5.3b),  
**2109** indicating that fertilization shifted relative investment in leaf structural tissue un-  
**2110** der elevated  $\text{CO}_2$ . These results, combined with a stimulation in PNUE (Fig. SX)  
**2111** and iWUE (Fig. SX) under elevated  $\text{CO}_2$  that was independent of fertilization  
**2112** or inoculation treatment, provide additional support for the hypothesis that leaf  
**2113** acclimation photosynthetic responses to  $\text{CO}_2$  were independent of fertilization;  
**2114** though fertilization may contribute to changes in leaf morphology under elevated  
**2115**  $\text{CO}_2$  through shifts in  $M_{\text{area}}$  (Onoda et al. 2017; Wang et al. 2017; Dong et al.

**2116** 2022).

**2117** The downregulation in  $N_{\text{area}}$ ,  $V_{\text{cmax25}}$ , and  $J_{\text{max25}}$  under elevated CO<sub>2</sub> cor-  
**2118** responded with a respective 62% and 100% stimulation in total leaf area (Fig.  
**2119** 5.4a) and total biomass (Fig. 5.4b). The stimulation in total leaf area and total  
**2120** biomass under elevated CO<sub>2</sub> also corresponded with generally higher structural  
**2121** carbon costs to acquire nitrogen (Fig. 5.4c), a pattern driven by a stimulation  
**2122** in belowground carbon biomass and reduction in whole plant nitrogen biomass.  
**2123** Alone, this result suggests that elevated CO<sub>2</sub> reduces plant nitrogen uptake effi-  
**2124** ciency, which does not explain why plants grown under elevated CO<sub>2</sub> generally had  
**2125** higher biomass and total leaf area. However, a strong negative effect of increasing  
**2126** fertilization on structural carbon costs to acquire nitrogen, which were generally  
**2127** similar between CO<sub>2</sub> concentrations, was driven by a stronger increase in whole  
**2128** plant nitrogen biomass than belowground carbon biomass. Thus, increases in the  
**2129** positive response of whole plant growth and total leaf area under elevated CO<sub>2</sub>  
**2130** with increasing fertilization were likely driven by an increase in nitrogen uptake  
**2131** efficiency, allowing plants to satisfy any increase in whole plant nitrogen demand  
**2132** associated with increased CO<sub>2</sub>.

**2133** Interestingly, our results indicate that the general stimulation in total leaf  
**2134** area and whole plant growth under elevated CO<sub>2</sub> was not modified by inoculation  
**2135** despite an apparent general negative effect of inoculation on  $N_{\text{cost}}$ . This response  
**2136** could have been due to strong negative effect of increasing fertilization on nodu-  
**2137** lation (Fig. 5.5), which may have caused the strong increase in the positive effect  
**2138** of elevated CO<sub>2</sub> on whole plant growth with increasing fertilization to mask any  
**2139** increase in the positive effect of elevated CO<sub>2</sub> on whole plant growth due to in-

**2140** oculation. Reductions in nodulation with increasing fertilization are commonly  
**2141** observed patterns that have been inferred to be a response that allows species  
**2142** optimize nitrogen uptake efficiency as costs to acquire nitrogen via direct uptake  
**2143** become more similar (Fig. 5.4c) (Gibson and Harper 1985; Rastetter et al. 2001).  
**2144** In this study, pairwise comparisons indicated strong positive effects of inocula-  
**2145** tion on total leaf area and total biomass (158% increase in total leaf area, 119%  
**2146** increase in total biomass) under elevated CO<sub>2</sub> at 0 ppm N, but no observable  
**2147** inoculation effect on total leaf area or total biomass under elevated CO<sub>2</sub> at 350  
**2148** ppm N or 630 ppm N. While these responses did not generally differ from those  
**2149** observed under ambient CO<sub>2</sub>, they do confirm our hypothesis that positive effects  
**2150** of inoculation on whole plant growth responses to elevated CO<sub>2</sub> would decrease  
**2151** with increasing fertilization.

**2152** Combined, results reported here suggest that soil nitrogen availability has  
**2153** a divergent role in modifying leaf and whole plant acclimation responses to CO<sub>2</sub>.  
**2154** Leaf acclimation responses were generally decoupled from fertilization, while whole  
**2155** plant acclimation responses relied heavily on an increase in nitrogen uptake ef-  
**2156** ciency and consequent reduction in costs of acquiring nitrogen associated with  
**2157** increasing fertilization. However, whole plant responses to CO<sub>2</sub> indicated that fer-  
**2158** tilization may play a more important role in determining whole plant acclimation  
**2159** responses to CO<sub>2</sub> than nitrogen acquisition strategy, although these patterns were  
**2160** likely driven by reductions in nodulation with increasing fertilization. Our results  
**2161** suggest that plants acclimate to CO<sub>2</sub> in nitrogen-limited systems by minimizing  
**2162** the number of optimally coordinated leaves, and that the downregulation in leaf  
**2163** nitrogen content under elevated CO<sub>2</sub> is not a direct response to changes in soil

**2164** nitrogen availability as previously implied.

**2165** 5.4.2 *Implications for future model development*

**2166** Many terrestrial biosphere models predict photosynthetic capacity through  
**2167** plant functional group-specific linear regressions between  $N_{\text{area}}$  and  $V_{\text{cmax}}$  (Rogers  
**2168** 2014; Rogers et al. 2017), which assumes that leaf nitrogen-photosynthesis rela-  
**2169** tionships are constant across growing environments. Our results build on previ-  
**2170** ous work suggesting that leaf nitrogen-photosynthesis relationships dynamically  
**2171** change across growing environments (Luo et al. 2021; Dong et al. 2022). Specif-  
**2172** ically, results from this experiment indicate that  $\text{CO}_2$  concentration increased  
**2173** the fraction of leaf nitrogen content allocated to photosynthesis, while a general  
**2174** negative effect of increasing fertilization on the fraction of leaf nitrogen content  
**2175** allocated to photosynthesis was dependent on inoculation treatment. Similar in-  
**2176** creases in  $N_{\text{area}}$ ,  $V_{\text{cmax}25}$ , and  $J_{\text{max}25}$  with increasing fertilization resulted in no  
**2177** change in the fraction of leaf nitrogen allocated to photosynthesis in uninoculated  
**2178** pots, while larger increases in  $N_{\text{area}}$  than  $V_{\text{cmax}25}$  and  $J_{\text{max}25}$  with increasing fertil-  
**2179** ization decreased the fraction of leaf nitrogen allocated to photosynthesis in inoc-  
**2180** ulated pots (Fig. 5.3a). As inoculated pots were able to access less finite supply of  
**2181** nitrogen across the fertilization gradient, these patterns suggest that constant leaf  
**2182** nitrogen-photosynthesis relationships may only apply in environments where ni-  
**2183** trogen is limiting and will likely change with increasing  $\text{CO}_2$  concentrations. Thus,  
**2184** terrestrial biosphere models that parameterize photosynthetic capacity through  
**2185** linear relationships between  $N_{\text{area}}$  and  $V_{\text{cmax}}$  (Rogers 2014; Rogers et al. 2017)  
**2186** may be overestimating photosynthetic capacity in systems where nitrogen is not

**2187** as limiting and may contribute to erroneous model simulations under future CO<sub>2</sub>  
**2188** concentrations.

**2189** Our results also demonstrate that optimal resource investment to photo-  
**2190** synthetic capacity defines leaf acclimation responses to elevated CO<sub>2</sub>, and that  
**2191** these responses were independent of fertilization or inoculation treatment. Cur-  
**2192** rent approaches for simulating photosynthetic responses to CO<sub>2</sub> generally invoke  
**2193** patterns expected from progressive nitrogen limitation, where the downregulation  
**2194** in  $N_{\text{area}}$ , and therefore photosynthetic capacity, due to elevated CO<sub>2</sub> are commonly  
**2195** a function of progressive reductions in soil nitrogen availability. Our results con-  
**2196** tradict this formulation, suggesting that the leaf acclimation response is driven  
**2197** by optimal resource investment to photosynthetic capacity and is independent  
**2198** of soil resource supply. Optimality models that leverage principles from optimal  
**2199** coordination and photosynthetic least-cost theories (Wang et al. 2017; Stocker  
**2200** et al. 2020; Scott and Smith 2022) are capable of capturing such acclimation re-  
**2201** sponses to CO<sub>2</sub> (Smith and Keenan 2020), suggesting that the implementation of  
**2202** these models may improve the simulation of photosynthetic processes in terrestrial  
**2203** biosphere models under increasing CO<sub>2</sub> concentrations.

**2204** 5.4.3 *Study limitations and future directions*

**2205** There are two study limitations that must be addressed to contextualize  
**2206** patterns observed in this study. First, restricting the volume of belowground  
**2207** substrate via a potted experiment does not adequately replicate belowground en-  
**2208** vironments of natural systems, and therefore may modify effects of soil resource  
**2209** availability and inoculation on plant nitrogen uptake, particularly if pot size limits

2210 whole plant growth (Poorter et al. 2012). We attempted to minimize the extent  
2211 of pot size limitation experienced in Perkowski et al. (2021) and account for the  
2212 expected stimulation in whole plant growth under elevated CO<sub>2</sub> by using 6-liter  
2213 pots. Despite attempts to minimize growth limitation imposed by pot volume, fer-  
2214 tilization and CO<sub>2</sub> treatments increased the biomass: pot volume ratio such that  
2215 all treatment combinations to exceed 1 g L<sup>-1</sup> biomass: pot volume under high  
2216 fertilization. The 1 g L<sup>-1</sup> biomass: pot volume recommendation from Poorter  
2217 et al. (2012) was designated to avoid growth limitation imposed by pot volume.  
2218 However, if pot size limitation indeed limited whole plant growth, then structural  
2219 carbon costs to acquire nitrogen, belowground carbon biomass, whole plant ni-  
2220 trogen biomass, and whole plant biomass should each exhibit strong saturation  
2221 points with increasing fertilization, which was not observed here. Additionally,  
2222 a second set of photosynthetic measurements from one week prior to the harvest  
2223 (6 weeks post-germination) revealed ... As pot limitation is expected to de-  
2224 crease net photosynthesis, and focal leaves were of similar ages between the sixth  
2225 and seventh week, one might expect growth limitation induced by constricted  
2226 pot volume to result in a dampened effect of inoculation and fertilization on net  
2227 photosynthesis,  $V_{cmax}$ , and  $J_{max25}$ . Analyses from the sixth week of development  
2228 revealed ... Additionally, analyses revealed a stronger/weaker downregulation in  
2229  $V_{cmax25}$  and  $J_{max25}$  on week 7, though disentangling the causality of this response  
2230 (i.e. whether due to pot size limitation or simply a stronger acclimation response)  
2231 would be difficult.

2232 Second, this study evaluated leaf and whole plant responses to CO<sub>2</sub> in 7-  
2233 week seedlings. Given the long-term scale of the progressive nitrogen limitation

**2234** hypothesis, patterns observed here should be validated in longer-term nitrogen  
**2235** manipulation experiments. Previous work in free air CO<sub>2</sub> enrichment experiments  
**2236** show some support for patterns expected from the progressive nitrogen limitation  
**2237** hypothesis (Reich et al. 2006; Norby et al. 2010), although results are not consis-  
**2238** tent across experimental sites (Finzi et al. 2006; Moore et al. 2006; Liang et al.  
**2239** 2016). We found some support for patterns expected by the progressive nitrogen  
**2240** limitation hypothesis, namely an increase in plant nitrogen uptake under elevated  
**2241** CO<sub>2</sub> (Luo et al. 2004), though leaf acclimation responses to CO<sub>2</sub> were strongly  
**2242** indicative of optimal resource investment to photosynthetic capacity as expected  
**2243** from photosynthetic least-cost theory (Prentice et al. 2014; Smith et al. 2019;  
**2244** Smith and Keenan 2020).

**2245** 5.4.4 *Conclusions*

**2246** This study provides strong evidence suggesting that leaf acclimation re-  
**2247** sponds to elevated CO<sub>2</sub> did not vary with soil nitrogen fertilization or ability  
**2248** to acquire nitrogen through symbiotic nitrogen fixation. However, whole plant  
**2249** acclimation responses to CO<sub>2</sub> were dependent on fertilization, where increasing  
**2250** fertilization increased the positive effect of whole plant growth under elevated  
**2251** CO<sub>2</sub>. Results also indicate that fertilization played a relatively more important  
**2252** role in modifying whole plant responses to CO<sub>2</sub>, perhaps due to a reduction in  
**2253** nodulation across the fertilization gradient. These patterns strongly support the  
**2254** hypothesis that leaf and whole plant acclimation responses are driven by opti-  
**2255** mal resource investment to photosynthetic capacity, and that leaf acclimation  
**2256** responses to CO<sub>2</sub> were not modified by changes in soil nitrogen availability. Ad-

2257 ditionally, strong interactions between fertilization and inoculation on leaf and  
2258 whole plant traits indicated positive effects of fertilization on leaf and whole plant  
2259 traits in uninoculated pots, but null effects of fertilization on leaf and whole plant  
2260 traits in inoculated pots. These results build on previous work suggesting that  
2261 constant leaf nitrogen-photosynthesis relationships are dynamic and change across  
2262 growing environments, calling the use of constant relationships by terrestrial bio-  
2263 sphere models into question.

**2264**

## Chapter 6

**2265**

### Conclusions

**2266** Experiments included in this dissertation leverage patterns expected from  
**2267** photosynthetic least-cost theory to investigate effects of soil resource availability  
**2268** and aboveground climate on costs of nitrogen acquisition, leaf nitrogen-water use  
**2269** tradeoffs, and plant acclimation responses to elevated CO<sub>2</sub>. Photosynthetic least-  
**2270** cost theory provides a contemporary framework for understanding impacts of  
**2271** climatic and edaphic characteristics on plant ecophysiological processes, namely  
**2272** leaf nitrogen allocation and photosynthetic capacity. When I began planning  
**2273** experiments for this dissertation in August 2018,, empirical tests of the theory  
**2274** were sparse and model development was just beginning with a goal of eventually  
**2275** implementing the theory in terrestrial biosphere models. At the time, it was  
**2276** critical that experimentation be done to test underlying assumptions of the theory  
**2277** and validate its suitability for implementing in terrestrial biosphere models.

**2278** Early iterations of model development held the unit cost of acquiring ni-  
**2279** trogen relative to water constant (Wang et al. 2017), in part because limited data  
**2280** existed to evaluate how this parameter changes across spatiotemporal scales and  
**2281** different environmental gradients. However, the Fixation and Uptake of Nitrogen  
**2282** model (Fisher et al. 2010; Brzostek et al. 2014) indicates that costs of nitro-  
**2283** gen acquisition decreased with increasing soil nitrogen availability and varies in  
**2284** species with different nitrogen acquisition strategies, suggesting that the unit cost  
**2285** of acquiring nitrogen relative to water should change across nitrogen availability  
**2286** gradients. Additionally,

**2287** All experimental chapters in this dissertation provide strong and consist-  
**2288** ent support for patterns expected from the theory across different experimental  
**2289** approaches, spatiotemporal scales, and different plant functional groups. In this  
**2290** chapter, I first summarize experimental approaches and primary findings of each  
**2291** experimental chapter. Then, I use findings from the four experimental chapters  
**2292** to synthesize recommendations for future photosynthetic least-cost theory model  
**2293** development, and propose experiments that will allow for further understanding  
**2294** of mechanisms that drive patterns expected from photosynthetic least-cost theory  
**2295** across environmental gradients.

**2296**

## References

- 2297** Abrams, M. D. and S. A. Mostoller (1995). Gas exchange, leaf structure and  
**2298** nitrogen in contrasting successional tree species growing in open and under-  
**2299** story sites during a drought. *Tree Physiology* 15(6), 361–370.
- 2300** Adams, M. A., T. L. Turnbull, J. I. Sprent, and N. Buchmann (2016). Legumes  
**2301** are different: Leaf nitrogen, photosynthesis, and water use efficiency. *Pro-  
**2302** ceedings of the National Academy of Sciences of the United States of Amer-  
**2303** ica* 113(15), 4098–4103.
- 2304** Ainsworth, E. A., P. A. Davey, C. J. Bernacchi, O. C. Dermody, E. A. Heaton,  
**2305** D. J. Moore, P. B. Morgan, S. L. Naidu, H. S. Y. Ra, X. G. Zhu, P. S. Curtis,  
**2306** and S. P. Long (2002). A meta-analysis of elevated [CO<sub>2</sub>] effects on soybean  
**2307** (*Glycine max*) physiology, growth and yield. *Global Change Biology* 8(8),  
**2308** 695–709.
- 2309** Ainsworth, E. A. and S. P. Long (2005). What have we learned from 15 years of  
**2310** free-air CO<sub>2</sub> enrichment (FACE)? A meta-analytic review of the responses  
**2311** of photosynthesis, canopy properties and plant production to rising CO<sub>2</sub>.  
**2312** *New Phytologist* 165(2), 351–372.
- 2313** Ainsworth, E. A. and A. Rogers (2007). The response of photosynthesis and  
**2314** stomatal conductance to rising [CO<sub>2</sub>]: mechanisms and environmental in-  
**2315** teractions. *Plant, Cell and Environment* 30(3), 258–270.
- 2316** Allen, K., J. B. Fisher, R. P. Phillips, J. S. Powers, and E. R. Brzostek (2020).  
**2317** Modeling the carbon cost of plant nitrogen and phosphorus uptake across  
**2318** temperate and tropical forests. *Frontiers in Forests and Global Change* 3,

- 2319 1–12.
- 2320 Allison, S. D., C. I. Czimczik, and K. K. Treseder (2008). Microbial activity  
2321 and soil respiration under nitrogen addition in Alaskan boreal forest. *Global  
2322 Change Biology* 14(5), 1156–1168.
- 2323 Andersen, M. K., H. Hauggaard-Nielsen, P. Ambus, and E. S. Jensen (2005).  
2324 Biomass production, symbiotic nitrogen fixation and inorganic N use in dual  
2325 and tri-component annual intercrops. *Plant and Soil* 266(1-2), 273–287.
- 2326 Andrews, M., E. K. James, J. I. Sprent, R. M. Boddey, E. Gross, and F. B. dos  
2327 Reis (2011). Nitrogen fixation in legumes and actinorhizal plants in natural  
2328 ecosystems: Values obtained using  $^{15}\text{N}$  natural abundance. *Plant Ecology  
2329 and Diversity* 4(2-3), 117–130.
- 2330 Arndal, M. F., A. Tolver, K. S. Larsen, C. Beier, and I. K. Schmidt (2018). Fine  
2331 root growth and vertical distribution in response to elevated CO<sub>2</sub>, warming  
2332 and drought in a mixed heathland–grassland. *Ecosystems* 21(1), 15–30.
- 2333 Arnone, J. A. (1997). Indices of plant N availability in an alpine grassland under  
2334 elevated atmospheric CO<sub>2</sub>. *Plant and Soil* 190(1), 61–66.
- 2335 Arora, V. K., A. Katavouta, R. G. Williams, C. D. Jones, V. Brovkin,  
2336 P. Friedlingstein, J. Schwinger, L. Bopp, O. Boucher, P. Cadule, M. A.  
2337 Chamberlain, J. R. Christian, C. Delire, R. A. Fisher, T. Hajima, T. Ilyina,  
2338 E. Joetzjer, M. Kawamiya, C. D. Koven, J. P. Krasting, R. M. Law, D. M.  
2339 Lawrence, A. Lenton, K. Lindsay, J. Pongratz, T. Raddatz, R. Séférian,  
2340 K. Tachiiri, J. F. Tjiputra, A. Wiltshire, T. Wu, and T. Ziehn (2020).  
2341 Carbon-concentration and carbon-climate feedbacks in CMIP6 models and  
2342 their comparison to CMIP5 models. *Biogeosciences* 17(16), 4173–4222.

- 2343 Bae, K., T. J. Fahey, R. D. Yanai, and M. Fisk (2015). Soil nitrogen availabil-  
2344 ity affects belowground carbon allocation and soil respiration in northern  
2345 hardwood forests of New Hampshire. *Ecosystems* 18(7), 1179–1191.
- 2346 Barber, S. A. (1962). A diffusion and mass-flow concept of soil nutrient avail-  
2347 ability. *Soil Science* 93(1), 39–49.
- 2348 Barnes, J. D., L. Balaguer, E. Manrique, S. Elvira, and A. W. Davison (1992).  
2349 A reappraisal of the use of DMSO for the extraction and determination  
2350 of chlorophylls a and b in lichens and higher plants. *Environmental and*  
2351 *Experimental Botany* 32(2), 85–100.
- 2352 Bates, D., M. Mächler, B. Bolker, and S. Walker (2015). Fitting linear mixed-  
2353 effects models using lme4. *Journal of Statistical Software* 67(1), 1–48.
- 2354 Beaudette, D., J. Skovlin, S. Roeker, and A. Brown (2022). soilDB: Soil  
2355 Database Interface.
- 2356 Bengtson, P., J. Barker, and S. J. Grayston (2012). Evidence of a strong cou-  
2357 pling between root exudation, C and N availability, and stimulated SOM  
2358 decomposition caused by rhizosphere priming effects. *Ecology and Evolu-*  
2359 *tion* 2(8), 1843–1852.
- 2360 Bernacchi, C. J., E. L. Singsaas, C. Pimentel, A. R. Portis, and S. P. Long  
2361 (2001). Improved temperature response functions for models of Rubisco-  
2362 limited photosynthesis. *Plant, Cell and Environment* 24(2), 253–259.
- 2363 Bialic-Murphy, L., N. G. Smith, P. Voothuluru, R. M. McElderry, M. D.  
2364 Roche, S. T. Cassidy, S. N. Kivlin, and S. Kalisz (2021). Invasion-induced  
2365 root–fungal disruptions alter plant water and nitrogen economies. *Ecology*

- 2366** *Letters* 24(6), 1145–1156.
- 2367** Bloom, A. J., F. S. Chapin, and H. A. Mooney (1985). Resource limitation  
**2368** in plants - an economic analogy. *Annual Review of Ecology and Systemat-*  
**2369** *ics* 16(1), 363–392.
- 2370** Bloomfield, K. J., B. D. Stocker, T. F. Keenan, and I. C. Prentice (2022).  
**2371** Environmental controls on the light use efficiency of terrestrial gross primary  
**2372** production. *Global Change Biology*, 0–2.
- 2373** Bonan, G. B., M. D. Hartman, W. J. Parton, and W. R. Wieder (2013). Evaluat-  
**2374** ing litter decomposition in earth system models with long-term litterbag ex-  
**2375** periments: an example using the Community Land Model version 4 (CLM4).  
**2376** *Global Change Biology* 19(3), 957–974.
- 2377** Bonan, G. B., P. J. Lawrence, K. W. Oleson, S. Levis, M. Jung, M. Reich-  
**2378** stein, D. M. Lawrence, and S. C. Swenson (2011). Improving canopy pro-  
**2379** cesses in the Community Land Model version 4 (CLM4) using global flux  
**2380** fields empirically inferred from FLUXNET data. *Journal of Geophysical Re-*  
**2381** *search* 116(G2), G02014.
- 2382** Booth, B. B. B., C. D. Jones, M. Collins, I. J. Totterdell, P. M. Cox, S. Sitch,  
**2383** C. Huntingford, R. A. Betts, G. R. Harris, and J. Lloyd (2012). High sen-  
**2384** sitivity of future global warming to land carbon cycle processes. *Environ-*  
**2385** *mental Research Letters* 7(2), 024002.
- 2386** Borer, E. T., W. S. Harpole, P. B. Adler, E. M. Lind, J. L. Orrock, E. W.  
**2387** Seabloom, and M. D. Smith (2014). Finding generality in ecology: A model  
**2388** for globally distributed experiments. *Methods in Ecology and Evolution* 5(1),  
**2389** 65–73.

- 2390** Braghieri, R. K., J. B. Fisher, K. Allen, E. Brzostek, M. Shi, X. Yang, D. M.  
**2391** Ricciuto, R. A. Fisher, Q. Zhu, and R. P. Phillips (2022). Modeling global  
**2392** carbon costs of plant nitrogen and phosphorus acquisition. *Journal of Ad-*  
**2393** *vances in Modeling Earth Systems* 14(8), 1–23.
- 2394** Brix, H. (1971). Effects of nitrogen fertilization on photosynthesis and respi-  
**2395** ration in Douglas-fir. *Forest Science* 17(4), 407–414.
- 2396** Brzostek, E. R., J. B. Fisher, and R. P. Phillips (2014). Modeling the carbon  
**2397** cost of plant nitrogen acquisition: Mycorrhizal trade-offs and multipath  
**2398** resistance uptake improve predictions of retranslocation. *Journal of Geo-*  
**2399** *physical Research: Biogeosciences* 119, 1684–1697.
- 2400** Bubier, J. L., R. Smith, S. Juutinen, T. R. Moore, R. Minocha, S. Long, and  
**2401** S. Minocha (2011). Effects of nutrient addition on leaf chemistry, morphol-  
**2402** ogy, and photosynthetic capacity of three bog shrubs. *Oecologia* 167(2),  
**2403** 355–368.
- 2404** Cernusak, L. A., N. Ubierna, K. Winter, J. A. M. Holtum, J. D. Marshall, and  
**2405** G. D. Farquhar (2013). Environmental and physiological determinants of  
**2406** carbon isotope discrimination in terrestrial plants. *New Phytologist* 200(4),  
**2407** 950–965.
- 2408** Chen, J.-L., J. F. Reynolds, P. C. Harley, and J. D. Tenhunen (1993). Coor-  
**2409** dination theory of leaf nitrogen distribution in a canopy. *Oecologia* 93(1),  
**2410** 63–69.
- 2411** Clark, D. B., L. M. Mercado, S. Sitch, C. D. Jones, N. Gedney, M. J. Best,  
**2412** M. Pryor, G. G. Rooney, R. L. H. Essery, E. Blyth, O. Boucher, R. J.  
**2413** Harding, C. Huntingford, and P. M. Cox (2011). The Joint UK Land Envi-

- 2414 ronment Simulator (JULES), model description. Part 2: Carbon fluxes and  
2415 vegetation dynamics. *Geoscientific Model Development* 4(3), 701–722.
- 2416 Cornwell, W. K., J. H. C. Cornelissen, K. Amatangelo, E. Dorrepaal, V. T.  
2417 Eviner, O. Godoy, S. E. Hobbie, B. Hoorens, H. Kurokawa, N. Pérez-  
2418 Harguindeguy, H. M. Quested, L. S. Santiago, D. A. Wardle, I. J. Wright,  
2419 R. Aerts, S. D. Allison, P. van Bodegom, V. Brovkin, A. Chatain, T. V.  
2420 Callaghan, S. Díaz, E. Garnier, D. E. Gurvich, E. Kazakou, J. A. Klein,  
2421 J. Read, P. B. Reich, N. A. Soudzilovskaia, M. V. Vaieretti, and M. Westoby  
2422 (2008). Plant species traits are the predominant control on litter decompo-  
2423 sition rates within biomes worldwide. *Ecology Letters* 11(10), 1065–1071.
- 2424 Cornwell, W. K., I. J. Wright, J. Turner, V. Maire, M. M. Barbour, L. A.  
2425 Cernusak, T. E. Dawson, D. S. Ellsworth, G. D. Farquhar, H. Griffiths,  
2426 C. Keitel, A. Knohl, P. B. Reich, D. G. Williams, R. Bhaskar, J. H. C. Cor-  
2427 nelissen, A. Richards, S. Schmidt, F. Valladares, C. Körner, E.-D. Schulze,  
2428 N. Buchmann, and L. S. Santiago (2018). Climate and soils together regulate  
2429 photosynthetic carbon isotope discrimination within C<sub>3</sub> plants worldwide.  
2430 *Global Ecology and Biogeography* 27(9), 1056–1067.
- 2431 Cramer, W. and I. C. Prentice (1988). Simulation of regional soil moisture  
2432 deficits on a European scale. *Norsk Geografisk Tidsskrift - Norwegian Jour-*  
2433 *nal of Geography* 42(2-3), 149–151.
- 2434 Curtis, P. S. (1996). A meta-analysis of leaf gas exchange and nitrogen in trees  
2435 grown under elevated carbon dioxide. *Plant, Cell and Environment* 19(2),  
2436 127–137.
- 2437 Daly, C., M. Halbleib, J. I. Smith, W. P. Gibson, M. K. Doggett, G. H. Taylor,

- 2438** J. Curtis, and P. P. Pasteris (2008). Physiographically sensitive mapping  
**2439** of climatological temperature and precipitation across the conterminous  
**2440** United States. *International Journal of Climatology* 28(15), 2031–2064.
- 2441** Davies-Barnard, T., J. Meyerholt, S. Zaehle, P. Friedlingstein, V. Brovkin,  
**2442** Y. Fan, R. A. Fisher, C. D. Jones, H. Lee, D. Peano, B. Smith, D. Wårlind,  
**2443** and A. J. Wiltshire (2020). Nitrogen cycling in CMIP6 land surface models:  
**2444** progress and limitations. *Biogeosciences* 17(20), 5129–5148.
- 2445** Davis, T. W., I. C. Prentice, B. D. Stocker, R. T. Thomas, R. J. Whitley,  
**2446** H. Wang, B. J. Evans, A. V. Gallego-Sala, M. T. Sykes, and W. Cramer  
**2447** (2017). Simple process-led algorithms for simulating habitats (SPLASH  
**2448** v.1.0): robust indices of radiation, evapotranspiration and plant-available  
**2449** moisture. *Geoscientific Model Development* 10, 689–708.
- 2450** Delaire, M., E. Frak, M. Sigogne, B. Adam, F. Beaujard, and X. Le Roux  
**2451** (2005). Sudden increase in atmospheric CO<sub>2</sub> concentration reveals strong  
**2452** coupling between shoot carbon uptake and root nutrient uptake in young  
**2453** walnut trees. *Tree Physiology* 25(2), 229–235.
- 2454** Doane, T. A. and W. R. Horwáth (2003). Spectrophotometric determination of  
**2455** nitrate with a single reagent. *Analytical Letters* 36(12), 2713–2722.
- 2456** Dong, N., I. C. Prentice, B. J. Evans, S. Caddy-Retalic, A. J. Lowe, and I. J.  
**2457** Wright (2017). Leaf nitrogen from first principles: field evidence for adaptive  
**2458** variation with climate. *Biogeosciences* 14(2), 481–495.
- 2459** Dong, N., I. C. Prentice, I. J. Wright, B. J. Evans, H. F. Togashi, S. Caddy-  
**2460** Retalic, F. A. McInerney, B. Sparrow, E. Leitch, and A. J. Lowe (2020).  
**2461** Components of leaf-trait variation along environmental gradients. *New Phy-*

- 2462** *tologist* 228(1), 82–94.
- 2463** Dong, N., I. C. Prentice, I. J. Wright, H. Wang, O. K. Atkin, K. J. Bloomfield,
- 2464** T. F. Domingues, S. M. Gleason, V. Maire, Y. Onoda, H. Poorter, and N. G.
- 2465** Smith (2022). Leaf nitrogen from the perspective of optimal plant function.
- 2466** *Journal of Ecology* 110(11), 2585–2602.
- 2467** Dong, N., I. J. Wright, J. M. Chen, X. Luo, H. Wang, T. F. Keenan, N. G.
- 2468** Smith, and I. C. Prentice (2022). Rising CO<sub>2</sub> and warming reduce global
- 2469** canopy demand for nitrogen. *New Phytologist* 235(5), 1692–1700.
- 2470** Dovrat, G., H. Bakhshian, T. Masci, and E. Sheffer (2020). The nitrogen eco-
- 2471** nomic spectrum of legume stoichiometry and fixation strategy. *New Phytol-*
- 2472** *ogist* 227(2), 365–375.
- 2473** Dovrat, G., T. Masci, H. Bakhshian, E. Mayzlish Gati, S. Golan, and E. Shef-
- 2474** fer (2018). Drought-adapted plants dramatically downregulate dinitrogen
- 2475** fixation: Evidences from Mediterranean legume shrubs. *Journal of Ecol-*
- 2476** *ogy* 106(4), 1534–1544.
- 2477** Drake, B. G., M. A. Gonzàlez-Meler, and S. P. Long (1997). More efficient
- 2478** plants: a consequence of rising atmospheric CO<sub>2</sub>? *Annual Review of Plant*
- 2479** *Biology* 48, 609–639.
- 2480** Duursma, R. A. (2015). Plantecophys - An R Package for Analysing and Mod-
- 2481** elling Leaf Gas Exchange Data. *PLOS ONE* 10(11), e0143346.
- 2482** Eastman, B. A., M. B. Adams, E. R. Brzostek, M. B. Burnham, J. E. Carrara,
- 2483** C. Kelly, B. E. McNeil, C. A. Walter, and W. T. Peterjohn (2021). Altered
- 2484** plant carbon partitioning enhanced forest ecosystem carbon storage after 25

- 2485 years of nitrogen additions. *New Phytologist* 230(4), 1435–1448.
- 2486 Ellsworth, D. S. and P. B. Reich (1996). Photosynthesis and leaf nitrogen in five  
2487 Amazonian tree species during early secondary succession. *Ecology* 77(2),  
2488 581–594.
- 2489 Espelta, J. M., P. Cortés, M. Mangirón, and J. Retana (2005). Differences in  
2490 biomass partitioning, leaf nitrogen content, and water use efficiency d13C  
2491 result in similar performance of seedlings of two Mediterranean oaks with  
2492 contrasting leaf habit. *Ecoscience* 12(4), 447–454.
- 2493 Evans, J. R. (1989). Photosynthesis and nitrogen relationships in leaves of C<sub>3</sub>  
2494 plants. *Oecologia* 78(1), 9–19.
- 2495 Evans, J. R. and V. C. Clarke (2019). The nitrogen cost of photosynthesis.  
2496 *Journal of Experimental Botany* 70(1), 7–15.
- 2497 Evans, J. R. and H. Poorter (2001). Photosynthetic acclimation of plants to  
2498 growth irradiance: the relative importance of specific leaf area and nitrogen  
2499 partitioning in maximizing carbon gain. *Plant, Cell and Environment* 24(8),  
2500 755–767.
- 2501 Evans, J. R. and J. R. Seemann (1989). The allocation of protein nitrogen in  
2502 the photosynthetic apparatus: costs, consequences, and control. *Photosyn-*  
2503 *thesis* 8, 183–205.
- 2504 Exbrayat, J.-F., A. A. Bloom, P. Falloon, A. Ito, T. L. Smallman, and  
2505 M. Williams (2018). Reliability ensemble averaging of 21<sup>st</sup> century projec-  
2506 tions of terrestrial net primary productivity reduces global and regional  
2507 uncertainties. *Earth System Dynamics* 9(1), 153–165.

- 2508 Farquhar, G. D., J. R. Ehleringer, and K. T. Hubick (1989). Carbon Isotope  
2509 Discrimination and Photosynthesis. *Annual Review of Plant Physiology and*  
2510 *Plant Molecular Biology* 40(1), 503–537.
- 2511 Farquhar, G. D. and T. D. Sharkey (1982). Stomatal conductance and photo-  
2512 synthesis. *Annual Review of Plant Physiology* 33(1), 317–345.
- 2513 Farquhar, G. D., S. von Caemmerer, and J. A. Berry (1980). A biochemical  
2514 model of photosynthetic CO<sub>2</sub> assimilation in leaves of C<sub>3</sub> species.  
2515 *Planta* 149(1), 78–90.
- 2516 Fay, P. A., S. M. Prober, W. S. Harpole, J. M. H. Knops, J. D. Bakker, E. T.  
2517 Borer, E. M. Lind, A. S. MacDougall, E. W. Seabloom, P. D. Wragg, P. B.  
2518 Adler, D. M. Blumenthal, Y. M. Buckley, C. Chu, E. E. Cleland, S. L.  
2519 Collins, K. F. Davies, G. Du, X. Feng, J. Firn, D. S. Gruner, N. Hagenah,  
2520 Y. Hautier, R. W. Heckman, V. L. Jin, K. P. Kirkman, J. A. Klein, L. M.  
2521 Ladwig, Q. Li, R. L. McCulley, B. A. Melbourne, C. E. Mitchell, J. L. Moore,  
2522 J. W. Morgan, A. C. Risch, M. Schütz, C. J. Stevens, D. A. Wedin, and  
2523 L. H. Yang (2015). Grassland productivity limited by multiple nutrients.  
2524 *Nature Plants* 1(7), 15080.
- 2525 Feng, X. (1999). Trends in intrinsic water-use efficiency of natural trees for the  
2526 past 100-200 years: A response to atmospheric CO<sub>2</sub> concentration. *Geochim-  
2527 ica et Cosmochimica Acta* 63(13-14), 1891–1903.
- 2528 Field, C. B. and H. A. Mooney (1986). The photosynthesis-nitrogen relationship  
2529 in wild plants. In T. J. Givnish (Ed.), *On the Economy of Plant Form and*  
2530 *Function*, pp. 25–55. Cambridge: Cambridge University Press.
- 2531 Finzi, A. C., D. J. P. Moore, E. H. DeLucia, J. Lichter, K. S. Hofmockel, R. B.

- 2532 Jackson, H. S. Kim, R. Matamala, H. R. McCarthy, R. Oren, J. S. Pippen,  
2533 and W. H. Schlesinger (2006). Progressive nitrogen limitation of ecosystem  
2534 processes under elevated CO<sub>2</sub> in a warm-temperate forest. *Ecology* 87(1),  
2535 15–25.
- 2536 Firn, J., J. M. McGree, E. Harvey, H. Flores Moreno, M. Schutz, Y. M. Buckley,  
2537 E. T. Borer, E. W. Seabloom, K. J. La Pierre, A. M. MacDougall, S. M.  
2538 Prober, C. J. Stevens, L. L. Sullivan, E. Porter, E. Ladouceur, C. Allen,  
2539 K. H. Moromizato, J. W. Morgan, W. S. Harpole, Y. Hautier, N. Eisen-  
2540 hauer, J. P. Wright, P. B. Adler, C. A. Arnillas, J. D. Bakker, L. Biederman,  
2541 A. A. D. Broadbent, C. S. Brown, M. N. Bugalho, M. C. Caldeira, E. E. Cle-  
2542 land, A. Ebeling, P. A. Fay, N. Hagenah, A. R. Kleinhesselink, R. Mitchell,  
2543 J. L. Moore, C. Nogueira, P. L. Peri, C. Roscher, M. D. Smith, P. D. Wragg,  
2544 and A. C. Risch (2019). Leaf nutrients, not specific leaf area, are consistent  
2545 indicators of elevated nutrient inputs. *Nature Ecology and Evolution* 3(3),  
2546 400–406.
- 2547 Fisher, J. B., S. Sitch, Y. Malhi, R. A. Fisher, C. Huntingford, and S.-Y. Tan  
2548 (2010). Carbon cost of plant nitrogen acquisition: A mechanistic, globally  
2549 applicable model of plant nitrogen uptake, retranslocation, and fixation.  
2550 *Global Biogeochemical Cycles* 24(1), 1–17.
- 2551 Fox, J. and S. Weisberg (2019). *An R companion to applied regression* (Third  
2552 edit ed.). Thousand Oaks, California: Sage.
- 2553 Franklin, O., R. E. McMurtrie, C. M. Iversen, K. Y. Crous, A. C. Finzi, D. Tis-  
2554 sue, D. S. Ellsworth, R. Oren, and R. J. Norby (2009). Forest fine-root  
2555 production and nitrogen use under elevated CO<sub>2</sub>: contrasting responses

- 2556 in evergreen and deciduous trees explained by a common principle. *Global*  
2557 *Change Biology* 15(1), 132–144.
- 2558 Friedlingstein, P., M. Meinshausen, V. K. Arora, C. D. Jones, A. Anav, S. K.  
2559 Liddicoat, and R. Knutti (2014). Uncertainties in CMIP5 climate projections  
2560 due to carbon cycle feedbacks. *Journal of Climate* 27(2), 511–526.
- 2561 Friel, C. A. and M. L. Friesen (2019). Legumes modulate allocation to rhizobial  
2562 nitrogen fixation in response to factorial light and nitrogen manipulation.  
2563 *Frontiers in Plant Science* 10, 1316.
- 2564 Fujikake, H., A. Yamazaki, N. Ohtake, K. Sueoshi, S. Matsuhashi, T. Ito,  
2565 C. Mizuniwa, T. Kume, S. Hoshimoto, N.-S. Ishioka, S. Watanabe, A. Osa,  
2566 T. Sekine, H. Uchida, A. Tsuji, and T. Ohyama (2003). Quick and reversible  
2567 inhibition of soybean root nodule growth by nitrate involves a decrease in  
2568 sucrose supply to nodules. *Journal of Experimental Botany* 54(386), 1379–  
2569 1388.
- 2570 Ghimire, B., W. J. Riley, C. D. Koven, J. Kattge, A. Rogers, P. B. Reich, and  
2571 I. J. Wright (2017). A global trait-based approach to estimate leaf nitro-  
2572 gen functional allocation from observations:. *Ecological Applications* 27(5),  
2573 1421–1434.
- 2574 Giardina, C. P., M. D. Coleman, J. E. Hancock, J. S. King, E. A. Lilleskov,  
2575 W. M. Loya, K. S. Pregitzer, M. G. Ryan, and C. C. Trettin (2005). The  
2576 response of belowground carbon allocation in forests to global change. In  
2577 D. Binkley and O. Manyailo (Eds.), *Tree Species Effects on Soils: Implica-*  
2578 *tions for Global Change* (Volume 55 ed.), Chapter Chapter 7, pp. 119–154.  
2579 Berlin/Heidelberg: Springer-Verlag.

- 2580 Gibson, A. H. and J. E. Harper (1985). Nitrate effect on nodulation of soybean  
2581 by *Bradyrhizobium japonicum*. *Crop Science* 25(3), 497–501.
- 2582 Gill, A. L. and A. C. Finzi (2016). Belowground carbon flux links biogeochemical  
2583 cycles and resource-use efficiency at the global scale. *Ecology Letters* 19(12),  
2584 1419–1428.
- 2585 Goll, D. S., V. Brovkin, B. R. Parida, C. H. Reick, J. Kattge, P. B. Reich, P. M.  
2586 van Bodegom, and Ü. Niinemets (2012). Nutrient limitation reduces land  
2587 carbon uptake in simulations with a model of combined carbon, nitrogen  
2588 and phosphorus cycling. *Biogeosciences Discussions* 9(3), 3173–3232.
- 2589 Gregory, L. M., A. M. McClain, D. M. Kramer, J. D. Pardo, K. E. Smith, O. L.  
2590 Tessmer, B. J. Walker, L. G. Ziccardi, and T. D. Sharkey (2021, oct). The  
2591 triose phosphate utilization limitation of photosynthetic rate: Out of global  
2592 models but important for leaf models. *Plant, Cell and Environment* 44(10),  
2593 3223–3226.
- 2594 Guerrieri, R., M. Mencuccini, L. J. Sheppard, M. Saurer, M. P. Perks, P. Levy,  
2595 M. A. Sutton, M. Borghetti, and J. Grace (2011). The legacy of enhanced  
2596 N and S deposition as revealed by the combined analysis of  $\delta^{13}\text{C}$ ,  $\delta^{18}\text{O}$  and  
2597  $\delta^{15}\text{N}$  in tree rings. *Global Change Biology* 17(5), 1946–1962.
- 2598 Gulmon, S. L. and C. C. Chu (1981). The effects of light and nitrogen on pho-  
2599 tosynthesis, leaf characteristics, and dry matter allocation in the chaparral  
2600 shrub, <i>Diplacus aurantiacus</i>. *Oecologia* 49(2), 207–212.
- 2601 Gutschick, V. P. (1981). Evolved strategies in nitrogen acquisition by plants.  
2602 *The American Naturalist* 118(5), 607–637.

- 2603** Hallik, L., Ü. Niinemets, and I. J. Wright (2009). Are species shade and drought  
**2604** tolerance reflected in leaf-level structural and functional differentiation in  
**2605** Northern Hemisphere temperate woody flora? *New Phytologist* 184(1), 257–  
**2606** 274.
- 2607** Harrison, M. T., E. J. Edwards, G. D. Farquhar, A. B. Nicotra, and J. R.  
**2608** Evans (2009). Nitrogen in cell walls of sclerophyllous leaves accounts for  
**2609** little of the variation in photosynthetic nitrogen-use efficiency. *Plant, Cell*  
**2610** and *Environment* 32(3), 259–270.
- 2611** Harrison, S. P., W. Cramer, O. Franklin, I. C. Prentice, H. Wang,  
**2612** Å. Bränström, H. de Boer, U. Dieckmann, J. Joshi, T. F. Keenan,  
**2613** A. Lavergne, S. Manzoni, G. Mengoli, C. Morfopoulos, J. Peñuelas,  
**2614** S. Pietsch, K. T. Rebel, Y. Ryu, N. G. Smith, B. D. Stocker, and I. J.  
**2615** Wright (2021). Eco-evolutionary optimality as a means to improve vegeta-  
**2616** tion and land-surface models. *New Phytologist* 231(6), 2125–2141.
- 2617** Henneron, L., P. Kardol, D. A. Wardle, C. Cros, and S. Fontaine (2020). Rhizo-  
**2618** sphere control of soil nitrogen cycling: a key component of plant economic  
**2619** strategies. *New Phytologist* 228(4), 1269–1282.
- 2620** Hijmans, R. J. (2022). terra: Spatial Data Analysis.
- 2621** Hikosaka, K. and A. Shigeno (2009). The role of Rubisco and cell walls in the  
**2622** interspecific variation in photosynthetic capacity. *Oecologia* 160(3), 443–  
**2623** 451.
- 2624** Hoagland, D. R. and D. I. Arnon (1950). The water culture method for growing  
**2625** plants without soil. *California Agricultural Experiment Station: 347* 347(2),  
**2626** 1–32.

- 2627** Hobbie, E. A. (2006). Carbon allocation to ectomycorrhizal fungi correlates  
**2628** with belowground allocation in culture studies. *Ecology* 87(3), 563–569.
- 2629** Hobbie, E. A. and J. E. Hobbie (2008). Natural abundance of  $^{15}\text{N}$  in nitrogen-  
**2630** limited forests and tundra can estimate nitrogen cycling through mycorrhizal  
**2631** fungi: a review. *Ecosystems* 11(5), 815–830.
- 2632** Hoek, T. A., K. Axelrod, T. Biancalani, E. A. Yurtsev, J. Liu, and J. Gore  
**2633** (2016). Resource availability modulates the cooperative and competitive na-  
**2634** nature of a microbial cross-feeding mutualism. *PLOS Biology* 14(8), e1002540.
- 2635** Höglberg, M. N., M. J. I. Briones, S. G. Keel, D. B. Metcalfe, C. Campbell, A. J.  
**2636** Midwood, B. Thornton, V. Hurry, S. Linder, T. Näsholm, and P. Höglberg  
**2637** (2010). Quantification of effects of season and nitrogen supply on tree below-  
**2638** ground carbon transfer to ectomycorrhizal fungi and other soil organisms in  
**2639** a boreal pine forest. *New Phytologist* 187(2), 485–493.
- 2640** Höglberg, P., M. N. Höglberg, S. G. Göttlicher, N. R. Betson, S. G. Keel, D. B.  
**2641** Metcalfe, C. Campbell, A. Schindlbacher, V. Hurry, T. Lundmark, S. Linder,  
**2642** and T. Näsholm (2008). High temporal resolution tracing of photosynthate  
**2643** carbon from the tree canopy to forest soil microorganisms. *New Phytolo-*  
**2644** *gist* 177(1), 220–228.
- 2645** Houlton, B. Z., Y.-P. Wang, P. M. Vitousek, and C. B. Field (2008). A uni-  
**2646** fying framework for dinitrogen fixation in the terrestrial biosphere. *Nature*  
**2647** 454(7202), 327–330.
- 2648** Huber, M. L., R. A. Perkins, A. Laesecke, D. G. Friend, J. V. Sengers, M. J.  
**2649** Assael, I. N. Metaxa, E. Vogel, R. Mareš, and K. Miyagawa (2009). New  
**2650** international formulation for the viscosity of H<sub>2</sub>O. *Journal of Physical and*

- 2651** *Chemical Reference Data* 38(2), 101–125.
- 2652** Hungate, B. A., J. S. Dukes, M. R. Shaw, Y. Luo, and C. B. Field (2003).
- 2653** Nitrogen and climate change. *Science* 302(5650), 1512–1513.
- 2654** IPCC (2021). *Climate Change 2021: The Physical Science Basis. Contribution of Working Group I to the Sixth Assessment Report of the Intergovernmental Panel on Climate Change*. Cambridge University Press.
- 2655**
- 2656**
- 2657** Johnson, N. C., J. H. Graham, and F. A. Smith (1997). Functioning of mycorrhizal associations along the mutualism-parasitism continuum. *New Phytologist* 135(4), 575–585.
- 2658**
- 2659**
- 2660** Kachurina, O. M., H. Zhang, W. R. Raun, and E. G. Krenzer (2000). Simultaneous determination of soil aluminum, ammonium- and nitrate- nitrogen using 1 M potassium chloride. *Communications in Soil Science and Plant Analysis* 31(7-8), 893–903.
- 2661**
- 2662**
- 2663**
- 2664** Kaiser, C., M. R. Kilburn, P. L. Clode, L. Fuchsleger, M. Koranda, J. B. Cliff, Z. M. Solaiman, and D. V. Murphy (2015). Exploring the transfer of recent plant photosynthates to soil microbes: mycorrhizal pathway vs direct root exudation. *New Phytologist* 205(4), 1537–1551.
- 2665**
- 2666**
- 2667**
- 2668** Katabuchi, M. (2015). LeafArea: An R package for rapid digital analysis of leaf area. *Ecological Research* 30(6), 1073–1077.
- 2669**
- 2670** Kattge, J. and W. Knorr (2007). Temperature acclimation in a biochemical model of photosynthesis: a reanalysis of data from 36 species. *Plant, Cell and Environment* 30(9), 1176–1190.
- 2671**
- 2672**
- 2673** Kattge, J., W. Knorr, T. Raddatz, and C. Wirth (2009). Quantifying photosyn-

- 2674**      thetic capacity and its relationship to leaf nitrogen content for global-scale  
**2675**      terrestrial biosphere models. *Global Change Biology* 15(4), 976–991.
- 2676**      Kayler, Z., A. Gessler, and N. Buchmann (2010). What is the speed of link  
**2677**      between aboveground and belowground processes? *New Phytologist* 187(4),  
**2678**      885–888.
- 2679**      Kayler, Z., C. Keitel, K. Jansen, and A. Gessler (2017). Experimental evi-  
**2680**      dence of two mechanisms coupling leaf-level C assimilation to rhizosphere  
**2681**      CO<sub>2</sub> release. *Environmental and Experimental Botany* 135,  
**2682**      21–26.
- 2683**      Keeling, C. D., W. G. Mook, and P. P. Tans (1979, jan). Recent trends in the  
**2684**      <sup>13</sup>C/<sup>12</sup>C ratio of atmospheric carbon dioxide.  
**2685**      *Nature* 277(5692), 121–123.
- 2686**      Kenward, M. G. and J. H. Roger (1997). Small sample inference for fixed effects  
**2687**      from restricted maximum likelihood. *Biometrics* 53(3), 983.
- 2688**      Knapp, A. K., M. L. Avolio, C. Beier, C. J. W. Carroll, S. L. Collins, J. S.  
**2689**      Dukes, L. H. Fraser, R. J. Griffin-Nolan, D. L. Hoover, A. Jentsch, M. E.  
**2690**      Loik, R. P. Phillips, A. K. Post, O. E. Sala, I. J. Slette, L. Yahdjian, and  
**2691**      M. D. Smith (2017). Pushing precipitation to the extremes in distributed  
**2692**      experiments: recommendations for simulating wet and dry years. *Global  
Change Biology* 23(5), 1774–1782.
- 2694**      Knorr, W. (2000). Annual and interannual CO<sub>2</sub> exchanges of the  
**2695**      terrestrial biosphere: process-based simulations and uncertainties. *Global  
Ecology and Biogeography* 9(3), 225–252.

- 2697 Knorr, W. and M. Heimann (2001). Uncertainties in global terrestrial biosphere  
2698 modeling: 1. A comprehensive sensitivity analysis with a new photosynthesis  
2699 and energy balance scheme. *Global Biogeochemical Cycles* 15(1), 207–225.
- 2700 Kulmatiski, A., P. B. Adler, J. M. Stark, and A. T. Tredennick (2017). Water  
2701 and nitrogen uptake are better associated with resource availability than  
2702 root biomass. *Ecosphere* 8(3), e01738.
- 2703 Lavergne, A., D. Sandoval, V. J. Hare, H. Graven, and I. C. Prentice (2020).  
2704 Impacts of soil water stress on the acclimated stomatal limitation of pho-  
2705 tosynthesis: Insights from stable carbon isotope data. *Global Change Biol-*  
2706 *ogy* 26(12), 7158–7172.
- 2707 Lawrence, D. M., R. A. Fisher, C. D. Koven, K. W. Oleson, S. C. Swen-  
2708 son, G. B. Bonan, N. Collier, B. Ghimire, L. Kamphout, D. Kennedy,  
2709 E. Kluzeck, P. J. Lawrence, F. Li, H. Li, D. L. Lombardozzi, W. J. Riley,  
2710 W. J. Sacks, M. Shi, M. Vertenstein, W. R. Wieder, C. Xu, A. A. Ali,  
2711 A. M. Badger, G. Bisht, M. Broeke, M. A. Brunke, S. P. Burns, J. Buzan,  
2712 M. Clark, A. Craig, K. M. Dahlin, B. Drewniak, J. B. Fisher, M. Flanner,  
2713 A. M. Fox, P. Gentine, F. M. Hoffman, G. Keppel-Aleks, R. Knox, S. Ku-  
2714 mar, J. Lenaerts, L. R. Leung, W. H. Lipscomb, Y. Lu, A. Pandey, J. D.  
2715 Pelletier, J. Perket, J. T. Randerson, D. M. Ricciuto, B. M. Sanderson,  
2716 A. Slater, Z. M. Subin, J. Tang, R. Q. Thomas, M. Val Martin, and X. Zeng  
2717 (2019). The Community Land Model Version 5: description of new features,  
2718 benchmarking, and impact of forcing uncertainty. *Journal of Advances in*  
2719 *Modeling Earth Systems* 11(12), 4245–4287.
- 2720 LeBauer, D. S. and K. K. Treseder (2008). Nitrogen limitation of net primary

- 2721 productivity. *Ecology* 89(2), 371–379.
- 2722 Lefcheck, J. S. (2016). piecewiseSEM: Piecewise structural equation modelling  
2723 in r for ecology, evolution, and systematics. *Methods in Ecology and Evolution*  
2724 7(5), 573–579.
- 2725 Lenth, R. (2019). emmeans: estimated marginal means, aka least-squares  
2726 means.
- 2727 Li, W., H. Zhang, G. Huang, R. Liu, H. Wu, C. Zhao, and N. G. McDowell  
2728 (2020). Effects of nitrogen enrichment on tree carbon allocation: A global  
2729 synthesis. *Global Ecology and Biogeography* 29(3), 573–589.
- 2730 Liang, J., X. Qi, L. Souza, and Y. Luo (2016). Processes regulating progressive  
2731 nitrogen limitation under elevated carbon dioxide: a meta-analysis. *Biogeosciences*  
2732 13(9), 2689–2699.
- 2733 Liang, X., T. Zhang, X. Lu, D. S. Ellsworth, H. BassiriRad, C. You, D. Wang,  
2734 P. He, Q. Deng, H. Liu, J. Mo, and Q. Ye (2020). Global response patterns of  
2735 plant photosynthesis to nitrogen addition: A meta-analysis. *Global Change  
2736 Biology* 26(6), 3585–3600.
- 2737 Lu, J., J. Yang, C. Keitel, L. Yin, P. Wang, W. Cheng, and F. A. Dijkstra  
2738 (2022). Belowground Carbon Efficiency for Nitrogen and Phosphorus Ac-  
2739 quisition Varies Between *Lolium perenne* and *Trifolium repens* and Depends  
2740 on Phosphorus Fertilization. *Frontiers in Plant Science* 13, 1–9.
- 2741 Luo, X., T. F. Keenan, J. M. Chen, H. Croft, I. C. Prentice, N. G. Smith,  
2742 A. P. Walker, H. Wang, R. Wang, C. Xu, and Y. Zhang (2021). Global  
2743 variation in the fraction of leaf nitrogen allocated to photosynthesis. *Nature*

- 2744** *Communications* 12(1), 4866.
- 2745** Luo, Y., W. S. Currie, J. S. Dukes, A. C. Finzi, U. A. Hartwig, B. A. Hungate,
- 2746** R. E. McMurtrie, R. Oren, W. J. Parton, D. E. Pataki, R. M. Shaw, D. R.
- 2747** Zak, and C. B. Field (2004). Progressive nitrogen limitation of ecosystem
- 2748** responses to rising atmospheric carbon dioxide. *BioScience* 54(8), 731–739.
- 2749** Maire, V., P. Martre, J. Kattge, F. Gastal, G. Esser, S. Fontaine, and J.-F.
- 2750** Soussana (2012). The coordination of leaf photosynthesis links C and N
- 2751** fluxes in C<sub>3</sub> plant species. *PLoS ONE* 7(6), e38345.
- 2752** Makino, A. (2003). Rubisco and nitrogen relationships in rice: leaf photosyn-
- 2753** thesis and plant growth. *Soil Science and Plant Nutrition* 49(3), 319–327.
- 2754** Makino, A., M. Harada, T. Sato, H. Nakano, and T. Mae (1997). Growth and N
- 2755** Allocation in Rice Plants under CO<sub>2</sub> Enrichment. *Plant Physiology* 115(1),
- 2756** 199–203.
- 2757** Markham, J. H. and C. Zekveld (2007). Nitrogen fixation makes biomass al-
- 2758** location to roots independent of soil nitrogen supply. *Canadian Journal of*
- 2759** *Botany* (9), 787–793.
- 2760** Marschner, H. and B. Dell (1994). Nutrient uptake in mycorrhizal symbiosis.
- 2761** *Plant and Soil* 159(1), 89–102.
- 2762** Matamala, R. and W. H. Schlesinger (2000). Effects of elevated atmospheric
- 2763** CO<sub>2</sub> on fine root production and activity in an intact tem-
- 2764** perate forest ecosystem. *Global Change Biology* 6(8), 967–979.
- 2765** Medlyn, B. E., E. Dreyer, D. S. Ellsworth, M. Forstreuter, P. C. Harley,
- 2766** M. U. F. Kirschbaum, X. Le Roux, P. Montpied, J. Strassmeyer, A. Wal-

- 2767 croft, K. Wang, and D. Loustau (2002). Temperature response of parameters  
2768 of a biochemically based model of photosynthesis. II. A review of experimen-  
2769 tal data. *Plant, Cell and Environment* 25(9), 1167–1179.
- 2770 Menge, D. N. L., S. A. Levin, and L. O. Hedin (2008). Evolutionary tradeoffs can  
2771 select against nitrogen fixation and thereby maintain nitrogen limitation.  
2772 *Proceedings of the National Academy of Sciences* 105(5), 1573–1578.
- 2773 Menne, M. J., I. Durre, R. S. Vose, B. E. Gleason, and T. G. Houston (2012).  
2774 An overview of the global historical climatology network-daily database.  
2775 *Journal of Atmospheric and Oceanic Technology* 29(7), 897–910.
- 2776 Meyerholt, J., K. Sickel, and S. Zaehle (2020). Ensemble projections elucidate  
2777 effects of uncertainty in terrestrial nitrogen limitation on future carbon up-  
2778 take. *Global Change Biology* 26(7), 3978–3996.
- 2779 Meyerholt, J., S. Zaehle, and M. J. Smith (2016). Variability of pro-  
2780 jected terrestrial biosphere responses to elevated levels of atmospheric  
2781 CO<sub>2</sub> due to uncertainty in biological nitrogen fixation. *Bio-*  
2782 *geosciences* 13(5), 1491–1518.
- 2783 Minocha, R., S. Long, A. H. Magill, J. D. Aber, and W. H. McDowell (2000).  
2784 Foliar free polyamine and inorganic ion content in relation to soil and soil  
2785 solution chemistry in two fertilized forest stands at the Harvard Forest,  
2786 Massachusetts. *Plant and Soil* 222(1-2), 119–137.
- 2787 Moore, D. J., S. Aref, R. M. Ho, J. S. Pippen, J. G. Hamilton, and E. H. De  
2788 Lucia (2006). Annual basal area increment and growth duration of *Pinus*  
2789 *taeda* in response to eight years of free-air carbon dioxide enrichment. *Global*  
2790 *Change Biology* 12(8), 1367–1377.

- 2791 Morgan, J. A., D. E. Pataki, C. Körner, H. Clark, S. J. Del Grosso, J. M.  
2792 Grünzweig, A. K. Knapp, A. R. Mosier, P. C. D. Newton, P. A. Niklaus,  
2793 J. B. Nippert, R. S. Nowak, W. J. Parton, H. W. Polley, and M. R. Shaw  
2794 (2004). Water relations in grassland and desert ecosystems exposed to ele-  
2795 vated atmospheric CO<sub>2</sub>. *Oecologia* 140(1), 11–25.
- 2796 Muñoz, N., X. Qi, M. W. Li, M. Xie, Y. Gao, M. Y. Cheung, F. L. Wong, and  
2797 H.-M. Lam (2016). Improvement in nitrogen fixation capacity could be part  
2798 of the domestication process in soybean. *Heredity* 117(2), 84–93.
- 2799 Nadelhoffer, K. J. and J. W. Raich (1992). Fine root production estimates and  
2800 belowground carbon allocation in forest ecosystems. *Ecology* 73(4), 1139–  
2801 1147.
- 2802 Niinemets, Ü. and J. D. Tenhunen (1997). A model separating leaf struc-  
2803 tural and physiological effects on carbon gain along light gradients for the  
2804 shade-tolerant species <i>Acer saccharum</i>. *Plant, Cell and Environ-  
2805 ment* 20(7), 845–866.
- 2806 Norby, R. J., J. Ledford, C. D. Reilly, N. E. Miller, and E. G. O'Neill  
2807 (2004). Fine-root production dominates response of a deciduous forest to  
2808 atmospheric CO<sub>2</sub> enrichment. *Proceedings of the National Academy of Sci-  
2809 ences* 101(26), 9689–9693.
- 2810 Norby, R. J., J. M. Warren, C. M. Iversen, B. E. Medlyn, and R. E. Mc-  
2811 Murtrie (2010). CO<sub>2</sub> enhancement of forest productivity constrained by  
2812 limited nitrogen availability. *Proceedings of the National Academy of Sci-  
2813 ences* 107(45), 19368–19373.
- 2814 Novick, K. A., D. L. Ficklin, P. C. Stoy, C. A. Williams, G. Bohrer, A. C.

- 2815** Oishi, S. A. Papuga, P. D. Blanken, A. Noormets, B. N. Sulman, R. L.  
**2816** Scott, L. Wang, and R. P. Phillips (2016). The increasing importance of  
**2817** atmospheric demand for ecosystem water and carbon fluxes. *Nature Climate  
Change* 6(11), 1023–1027.
- 2819** Noyce, G. L., M. L. Kirwan, R. L. Rich, and J. P. Megonigal (2019). Asyn-  
**2820** chronous nitrogen supply and demand produce nonlinear plant allocation  
**2821** responses to warming and elevated CO<sub>2</sub>. *Proceedings of the  
National Academy of Sciences* 116(43), 21623–21628.
- 2823** Onoda, Y., K. Hikosaka, and T. Hirose (2004). Allocation of nitrogen to  
**2824** cell walls decreases photosynthetic nitrogen-use efficiency. *Functional Ecol-  
ogy* 18(3), 419–425.
- 2826** Onoda, Y., I. J. Wright, J. R. Evans, K. Hikosaka, K. Kitajima, Ü. Niinemets,  
**2827** H. Poorter, T. Tosens, and M. Westoby (2017). Physiological and structural  
**2828** tradeoffs underlying the leaf economics spectrum. *New Phytologist* 214(4),  
**2829** 1447–1463.
- 2830** Oreskes, N., K. Shrader-Frechette, and K. Belitz (1994). Verification, vali-  
**2831** dation, and confirmation of numerical models in the Earth sciences. *Sci-  
ence* 263(5147), 641–646.
- 2833** Paillassa, J., I. J. Wright, I. C. Prentice, S. Pepin, N. G. Smith, G. Ethier,  
**2834** A. C. Westerband, L. J. Lamarque, H. Wang, W. K. Cornwell, and V. Maire  
**2835** (2020). When and where soil is important to modify the carbon and water  
**2836** economy of leaves. *New Phytologist* 228(1), 121–135.
- 2837** Parvin, S., S. Uddin, S. Tausz Posch, R. Armstrong, and M. Tausz (2020). Car-  
**2838** bon sink strength of nodules but not other organs modulates photosynthesis

- 2839 of faba bean (*i>Vicia faba</i> ) grown under elevated [CO<sub>2</sub>] and different  
2840 water supply. *New Phytologist* 227(1), 132–145.*
- 2841 Peng, Y., K. J. Bloomfield, L. A. Cernusak, T. F. Domingues, and I. C. Prentice (2021). Global climate and nutrient controls of photosynthetic capacity.  
2842 *Communications Biology* 4(1), 462.
- 2843 Perkowski, E. A., E. F. Waring, and N. G. Smith (2021). Root mass carbon  
2844 costs to acquire nitrogen are determined by nitrogen and light availability  
2845 in two species with different nitrogen acquisition strategies. *Journal of*  
2846 *Experimental Botany* 72(15), 5766–5776.
- 2847 Phillips, R. P., E. R. Brzostek, and M. G. Midgley (2013). The mycorrhizal-  
2848 associated nutrient economy: a new framework for predicting carbon-  
2849 nutrient couplings in temperate forests. *New Phytologist* 199(1), 41–51.
- 2850 Phillips, R. P., A. C. Finzi, and E. S. Bernhardt (2011). Enhanced root ex-  
2851 udation induces microbial feedbacks to N cycling in a pine forest under  
2852 long-term CO<sub>2</sub> fumigation. *Ecology Letters* 14(2), 187–194.
- 2853 Pinheiro, J. and D. Bates (2022). nlme: linear and nonlinear mixed effects  
2854 models.
- 2855 Poggio, L., L. M. De Sousa, N. H. Batjes, G. B. M. Heuvelink, B. Kempen,  
2856 E. Ribeiro, and D. Rossiter (2021). SoilGrids 2.0: Producing soil information  
2857 for the globe with quantified spatial uncertainty. *Soil* 7(1), 217–240.
- 2858 Pons, T. L. and R. W. Pearcy (1994). Nitrogen reallocation and photosynthetic  
2859 acclimation in response to partial shading in soybean plants. *Physiologia*  
2860 *Plantarum* 92(4), 636–644.

- 2862 Poorter, H., J. Bühler, D. Van Dusschoten, J. Climent, and J. A. Postma (2012).
- 2863 Pot size matters: A meta-analysis of the effects of rooting volume on plant
- 2864 growth. *Functional Plant Biology* 39(11), 839–850.
- 2865 Poorter, H., O. Knopf, I. J. Wright, A. A. Temme, S. W. Hogewoning, A. Graf,
- 2866 L. A. Cernusak, and T. L. Pons (2022). A meta-analysis of responses of C<sub>3</sub>
- 2867 plants to atmospheric CO<sub>2</sub>: dose–response curves for 85 traits ranging from
- 2868 the molecular to the whole-plant level. *New Phytologist* 233(4), 1560–1596.
- 2869 Prentice, I. C., N. Dong, S. M. Gleason, V. Maire, and I. J. Wright (2014).
- 2870 Balancing the costs of carbon gain and water transport: testing a new theo-
- 2871 retical framework for plant functional ecology. *Ecology Letters* 17(1), 82–91.
- 2872 Prentice, I. C., X. Liang, B. E. Medlyn, and Y.-P. Wang (2015). Reliable, ro-
- 2873 bust and realistic: The three R's of next-generation land-surface modelling.
- 2874 *Atmospheric Chemistry and Physics* 15, 5987–6005.
- 2875 Priestley, C. H. B. and R. J. Taylor (1972). On the Assessment of Surface
- 2876 Heat Flux and Evaporation Using Large-Scale Parameters. *Monthly Weather*
- 2877 *Review* 100(2), 81–92.
- 2878 Querejeta, J. I., I. Prieto, C. Armas, F. Casanoves, J. S. Diémé, M. Diouf,
- 2879 H. Yossi, B. Kaya, F. I. Pugnaire, and G. M. Rusch (2022). Higher leaf
- 2880 nitrogen content is linked to tighter stomatal regulation of transpiration
- 2881 and more efficient water use across dryland trees. *New Phytologist* 235(4),
- 2882 1351–1364.
- 2883 R Core Team (2021). R: A language and environment for statistical computing.
- 2884 Raich, J. W., D. A. Clark, L. Schwendenmann, and T. E. Wood (2014). Above-

- 2885 ground tree growth varies with belowground carbon allocation in a tropical  
2886 rainforest environment. *PLoS ONE* 9(6), e100275.
- 2887 Rastetter, E. B., P. M. Vitousek, C. B. Field, G. R. Shaver, D. Herbert, and  
2888 G. I. Ågren (2001). Resource optimization and symbiotic nitrogen fixation.  
2889 *Ecosystems* 4(4), 369–388.
- 2890 Reich, P. B. (2014). The world-wide 'fast-slow' plant economics spectrum: a  
2891 traits manifesto. *Journal of Ecology* 102(2), 275–301.
- 2892 Reich, P. B., S. E. Hobbie, T. Lee, D. S. Ellsworth, J. B. West, D. Tilman,  
2893 J. M. H. Knops, S. Naeem, and J. Trost (2006). Nitrogen limitation con-  
2894 strains sustainability of ecosystem response to CO<sub>2</sub>. *Nature* 440(7086), 922–925.
- 2895 Rhine, E. D., R. L. Mulvaney, E. J. Pratt, and G. K. Sims (1998). Improving  
2896 the Berthelot reaction for determining ammonium in soil extracts and water.  
2897 *Soil Science Society of America Journal* 62(2), 473.
- 2898 Rogers, A. (2014). The use and misuse of  $V_{cmax}$  in Earth System Models. *Pho-*  
2899 *tosynthesis Research* 119(1-2), 15–29.
- 2900 Rogers, A., B. E. Medlyn, J. S. Dukes, G. B. Bonan, S. Caemmerer, M. C.  
2901 Dietze, J. Kattge, A. D. B. Leakey, L. M. Mercado, Ü. Niinemets, I. C.  
2902 Prentice, S. P. Serbin, S. Sitch, D. A. Way, and S. Zaehle (2017). A roadmap  
2903 for improving the representation of photosynthesis in Earth system models.  
2904 *New Phytologist* 213(1), 22–42.
- 2905 Saathoff, A. J. and J. Welles (2021). Gas exchange measurements in the un-  
2906 steady state. *Plant Cell and Environment* 44(11), 3509–3523.

- 2908** Saleh, A. M., M. Abdel-Mawgoud, A. R. Hassan, T. H. Habeeb, R. S. Yehia,  
**2909** and H. AbdElgawad (2020). Global metabolic changes induced by arbuscular  
**2910** mycorrhizal fungi in oregano plants grown under ambient and elevated levels  
**2911** of atmospheric CO<sub>2</sub>. *Plant Physiology and Biochemistry* 151, 255–263.
- 2912** Saxton, K. E. and W. J. Rawls (2006). Soil water characteristic estimates by  
**2913** texture and organic matter for hydrologic solutions. *Soil Science Society of  
2914 America Journal* 70(5), 1569–1578.
- 2915** Schaefer, K., C. R. Schwalm, C. Williams, M. A. Arain, A. Barr, J. M. Chen,  
**2916** K. J. Davis, D. Dimitrov, T. W. Hilton, D. Y. Hollinger, E. Humphreys,  
**2917** B. Poulter, B. M. Racza, A. D. Richardson, A. Sahoo, P. Thornton, R. Var-  
**2918** gas, H. Verbeeck, R. Anderson, I. Baker, T. A. Black, P. Bolstad, J. Chen,  
**2919** P. S. Curtis, A. R. Desai, M. C. Dietze, D. Dragoni, C. M. Gough, R. F.  
**2920** Grant, L. Gu, A. K. Jain, C. Kucharik, B. E. Law, S. Liu, E. Lokipitiya,  
**2921** H. A. Margolis, R. Matamala, J. H. McCaughey, R. Monson, J. W. Munger,  
**2922** W. Oechel, C. Peng, D. T. Price, D. Ricciuto, W. J. Riley, N. Roulet,  
**2923** H. Tian, C. Tonitto, M. Torn, E. Weng, and X. Zhou (2012). A model-  
**2924** data comparison of gross primary productivity: Results from the North  
**2925** American Carbon Program site synthesis. *Journal of Geophysical Research:  
2926 Biogeosciences* 117(G3), G03010.
- 2927** Schneider, C. A., W. S. Rasband, and K. W. Eliceiri (2012). NIH Image to  
**2928** ImageJ: 25 years of image analysis. *Nature Methods* 9(7), 671–675.
- 2929** Scott, H. G. and N. G. Smith (2022). A Model of C4 Photosynthetic Acclimation  
**2930** Based on Least-Cost Optimality Theory Suitable for Earth System Model  
**2931** Incorporation. *Journal of Advances in Modeling Earth Systems* 14(3), 1–16.

- 2932 Shi, M., J. B. Fisher, E. R. Brzostek, and R. P. Phillips (2016). Carbon cost  
2933 of plant nitrogen acquisition: Global carbon cycle impact from an improved  
2934 plant nitrogen cycle in the Community Land Model. *Global Change Biology*  
2935 *22*(3), 1299–1314.
- 2936 Shi, M., J. B. Fisher, R. P. Phillips, and E. R. Brzostek (2019). Neglecting  
2937 plant–microbe symbioses leads to underestimation of modeled climate im-  
2938 pacts. *Biogeosciences* *16*(2), 457–465.
- 2939 Smith, B., D. Wärllind, A. Arneth, T. Hickler, P. Leadley, J. Siltberg, and  
2940 S. Zaehle (2014). Implications of incorporating N cycling and N limitations  
2941 on primary production in an individual-based dynamic vegetation model.  
2942 *Biogeosciences* *11*(7), 2027–2054.
- 2943 Smith, N. G. and J. S. Dukes (2013). Plant respiration and photosynthesis in  
2944 global-scale models: incorporating acclimation to temperature and CO<sub>2</sub>.  
2945 *Global Change Biology* *19*(1), 45–63.
- 2946 Smith, N. G. and T. F. Keenan (2020). Mechanisms underlying leaf photosyn-  
2947 thetic acclimation to warming and elevated CO<sub>2</sub> as inferred from least-cost  
2948 optimality theory. *Global Change Biology* *26*(9), 5202–5216.
- 2949 Smith, N. G., T. F. Keenan, I. C. Prentice, H. Wang, I. J. Wright, Ü. Niinemets,  
2950 K. Y. Crous, T. F. Domingues, R. Guerrieri, F. oko Ishida, J. Kattge, E. L.  
2951 Kruger, V. Maire, A. Rogers, S. P. Serbin, L. Tarvainen, H. F. Togashi,  
2952 P. A. Townsend, M. Wang, L. K. Weerasinghe, and S.-X. Zhou (2019).  
2953 Global photosynthetic capacity is optimized to the environment. *Ecology*  
2954 *Letters* *22*(3), 506–517.
- 2955 Smith, N. G., D. L. Lombardozzi, A. Tawfik, G. B. Bonan, and J. S. Dukes

- 2956 (2017). Biophysical consequences of photosynthetic temperature acclimation  
2957 for climate. *Journal of Advances in Modeling Earth Systems* 9(1), 536–547.
- 2958 Smith, N. G., S. L. Malyshev, E. Shevliakova, J. Kattge, and J. S. Dukes  
2959 (2016). Foliar temperature acclimation reduces simulated carbon sensitivity  
2960 to climate. *Nature Climate Change* 6(4), 407–411.
- 2961 Smith, S. E. and D. J. Read (2008). *Mycorrhizal Symbiosis*. Academic Press.
- 2962 Soil Survey Staff (2022). Web Soil Survey.
- 2963 Soudzilovskaia, N. A., J. C. Douma, A. A. Akhmetzhanova, P. M. van Bode-  
2964 gom, W. K. Cornwell, E. J. Moens, K. K. Treseder, and J. H. C. Cornelissen  
2965 (2015). Global patterns of plant root colonization intensity by mycorrhizal  
2966 fungi explained by climate and soil chemistry. *Global Ecology and Biogeog-  
2967 raphy* 24(3), 371–382.
- 2968 Stocker, B. D., H. Wang, N. G. Smith, S. P. Harrison, T. F. Keenan, D. San-  
2969 doval, T. Davis, and I. C. Prentice (2020). P-model v1.0: An optimality-  
2970 based light use efficiency model for simulating ecosystem gross primary pro-  
2971 duction. *Geoscientific Model Development* 13(3), 1545–1581.
- 2972 Stocker, B. D., J. Zscheischler, T. F. Keenan, I. C. Prentice, J. Peñuelas, and  
2973 S. I. Seneviratne (2018). Quantifying soil moisture impacts on light use  
2974 efficiency across biomes. *New Phytologist* 218(4), 1430–1449.
- 2975 Sulman, B. N., D. T. Roman, K. Yi, L. Wang, R. P. Phillips, and K. A.  
2976 Novick (2016). High atmospheric demand for water can limit forest car-  
2977 bon uptake and transpiration as severely as dry soil. *Geophysical Research  
2978 Letters* 43(18), 9686–9695.

- 2979 Sulman, B. N., E. Shevliakova, E. R. Brzostek, S. N. Kivlin, S. L. Malyshev,  
2980 D. N. L. Menge, and X. Zhang (2019). Diverse mycorrhizal associations  
2981 enhance terrestrial C storage in a global model. *Global Biogeochemical Cy-*  
2982 *cles* 33(4), 501–523.
- 2983 Sweet, S. K., D. W. Wolfe, A. DeGaetano, and R. Benner (2017). Anatomy  
2984 of the 2016 drought in the Northeastern United States: Implications for  
2985 agriculture and water resources in humid climates. *Agricultural and Forest*  
2986 *Meteorology* 247, 571–581.
- 2987 Taylor, B. N. and D. N. L. Menge (2018). Light regulates tropical symbiotic  
2988 nitrogen fixation more strongly than soil nitrogen. *Nature Plants* 4(9), 655–  
2989 661.
- 2990 Terrer, C., S. Vicca, B. A. Hungate, R. P. Phillips, and I. C. Prentice (2016).  
2991 Mycorrhizal association as a primary control of the CO<sub>2</sub> fertilization effect.  
2992 *Science* 353(6294), 72–74.
- 2993 Terrer, C., S. Vicca, B. D. Stocker, B. A. Hungate, R. P. Phillips, P. B. Reich,  
2994 A. C. Finzi, and I. C. Prentice (2018). Ecosystem responses to elevated CO<sub>2</sub>  
2995 governed by plant–soil interactions and the cost of nitrogen acquisition. *New*  
2996 *Phytologist* 217(2), 507–522.
- 2997 Thieurmel, B. and A. Elmarhraoui (2019). suncalc: Compute sun position,  
2998 sunlight phases, moon position, and lunar phase.
- 2999 Thomas, R. Q., E. N. J. Brookshire, and S. Gerber (2015). Nitrogen limita-  
3000 tion on land: how can it occur in Earth system models? *Global Change*  
3001 *Biology* 21(5), 1777–1793.

- 3002** Thomas, R. Q., S. Zaehle, P. H. Templer, and C. L. Goodale (2013). Global patterns of nitrogen limitation: confronting two global biogeochemical models  
**3003**  
**3004** with observations. *Global Change Biology* 19(10), 2986–2998.
- 3005** Thornton, P. E., J.-F. Lamarque, N. A. Rosenbloom, and N. M. Mahowald  
**3006** (2007). Influence of carbon-nitrogen cycle coupling on land model response  
**3007** to CO<sub>2</sub> fertilization and climate variability. *Global Biogeochemical Cycles* 21(4), GB4018.
- 3008**  
**3009** Tingey, D. T., D. L. Phillips, and M. G. Johnson (2000). Elevated CO<sub>2</sub> and  
**3010** conifer roots: effects on growth, life span and turnover. *New Phytologist* 147(1), 87–103.  
**3011**
- 3012** Udvardi, M. and P. S. Poole (2013). Transport and metabolism in legume-  
**3013** rhizobia symbioses. *Annual Review of Plant Biology* 64, 781–805.
- 3014** USDA NRCS (2022). The PLANTS Database.
- 3015** Uselman, S. M., R. G. Qualls, and R. B. Thomas (2000). Effects of increased  
**3016** atmospheric CO<sub>2</sub>, temperature, and soil N availability on root exudation of  
**3017** dissolved organic carbon by a N-fixing tree (*Robinia pseudoacacia* L.). *Plant*  
**3018** and *Soil* 222, 191–202.
- 3019** van Diepen, L. T. A., E. A. Lilleskov, K. S. Pregitzer, and R. M. Miller (2007).  
**3020** Decline of arbuscular mycorrhizal fungi in northern hardwood forests ex-  
**3021** posed to chronic nitrogen additions. *New Phytologist* 176(1), 175–183.
- 3022** Vance, C. P. and G. H. Heichel (1991). Carbon in N<sub>2</sub> fixation: Limitation or  
**3023** exquisite adaptation. *Annual Review of Plant Physiology and Plant Molec-*  
**3024** *ular Biology* 42(1), 373–392.

- 3025** Viet, H. D., J.-H. Kwak, K.-S. Lee, S.-S. Lim, M. Matsushima, S. X. Chang,  
**3026** K.-H. Lee, and W.-J. Choi (2013). Foliar chemistry and tree ring  $\delta^{13}\text{C}$  of  
**3027** *Pinus densiflora* in relation to tree growth along a soil pH gradient. *Plant*  
**3028** and *Soil* 363(1-2), 101–112.
- 3029** Vitousek, P. M., K. Cassman, C. C. Cleveland, T. Crews, C. B. Field, N. B.  
**3030** Grimm, R. W. Howarth, R. Marino, L. Martinelli, E. B. Rastetter, and  
**3031** J. I. Sprent (2002). Towards an ecological understanding of biological nitro-  
**3032** gen fixation. In *The Nitrogen Cycle at Regional to Global Scales*, pp. 1–45.  
**3033** Springer Netherlands.
- 3034** Vitousek, P. M. and R. W. Howarth (1991). Nitrogen limitation on land and in  
**3035** the sea: How can it occur? *Biogeochemistry* 13(2), 87–115.
- 3036** Vitousek, P. M., S. Porder, B. Z. Houlton, and O. A. Chadwick (2010).  
**3037** Terrestrial phosphorus limitation: mechanisms, implications, and nitro-  
**3038** gen–phosphorus interactions. *Ecological Applications* 20(1), 5–15.
- 3039** Walker, A. P., A. P. Beckerman, L. Gu, J. Kattge, L. A. Cernusak, T. F.  
**3040** Domingues, J. C. Scales, G. Wohlfahrt, S. D. Wullschleger, and F. I. Wood-  
**3041** ward (2014). The relationship of leaf photosynthetic traits -  $V_{cmax}$  and  $J_{max}$   
**3042** - to leaf nitrogen, leaf phosphorus, and specific leaf area: a meta-analysis  
**3043** and modeling study. *Ecology and Evolution* 4(16), 3218–3235.
- 3044** Wang, H., I. C. Prentice, T. F. Keenan, T. W. Davis, I. J. Wright, W. K.  
**3045** Cornwell, B. J. Evans, and C. Peng (2017). Towards a universal model for  
**3046** carbon dioxide uptake by plants. *Nature Plants* 3(9), 734–741.
- 3047** Wang, W., Y. Wang, G. Hoch, Z. Wang, and J. Gu (2018). Linkage of root mor-  
**3048** phology to anatomy with increasing nitrogen availability in six temperate

- 3049** tree species. *Plant and Soil* 425(1-2), 189–200.
- 3050** Weatherburn, M. W. (1967). Phenol-hypochlorite reaction for determination of
- 3051** ammonia. *Analytical Chemistry* 39(8), 971–974.
- 3052** Wellburn, A. R. (1994). The spectral determination of chlorophylls a and b, as
- 3053** well as total carotenoids, using various solvents with spectrophotometers of
- 3054** different resolution. *Journal of Plant Physiology* 144(3), 307–313.
- 3055** Wen, Z., P. J. White, J. Shen, and H. Lambers (2022). Linking root exuda-
- 3056** tion to belowground economic traits for resource acquisition. *New Phytolo-*
- 3057** *gist* 233(4), 1620–1635.
- 3058** Westerband, A. C., I. J. Wright, V. Maire, J. Paillassa, I. C. Prentice, O. K.
- 3059** Atkin, K. J. Bloomfield, L. A. Cernusak, N. Dong, S. M. Gleason, C. Guil-
- 3060** herme Pereira, H. Lambers, M. R. Leishman, Y. Malhi, and R. H. Nolan
- 3061** (2023). Coordination of photosynthetic traits across soil and climate gradi-
- 3062** ents. *Global Change Biology* 29(3), 1–29.
- 3063** Wieder, W. R., C. C. Cleveland, W. K. Smith, and K. Todd-Brown (2015).
- 3064** Future productivity and carbon storage limited by terrestrial nutrient avail-
- 3065** ability. *Nature Geoscience* 8(6), 441–444.
- 3066** Wieder, W. R., D. M. Lawrence, R. A. Fisher, G. B. Bonan, S. J. Cheng, C. L.
- 3067** Goodale, A. S. Grandy, C. D. Koven, D. L. Lombardozzi, K. W. Oleson,
- 3068** and R. Q. Thomas (2019). Beyond static benchmarking: using experimental
- 3069** manipulations to evaluate land model assumptions. *Global Biogeochemical*
- 3070** *Cycles* 33(10), 1289–1309.
- 3071** Wright, I. J., P. B. Reich, and M. Westoby (2003). Least-cost input mixtures

- 3072 of water and nitrogen for photosynthesis. *The American Naturalist* 161(1),  
3073 98–111.
- 3074 Wright, I. J., P. B. Reich, M. Westoby, D. D. Ackerly, Z. Baruch, F. Bongers,  
3075 J. Cavender-Bares, T. Chapin, J. H. C. Cornelissen, M. Diemer, J. Flexas,  
3076 E. Garnier, P. K. Groom, J. Gulias, K. Hikosaka, B. B. Lamont, T. Lee,  
3077 W. Lee, C. Lusk, J. J. Midgley, M.-L. Navas, Ü. Niinemets, J. Oleksyn,  
3078 N. Osada, H. Poorter, P. Poot, L. Prior, V. I. Pyankov, C. Roumet, S. C.  
3079 Thomas, M. G. Tjoelker, E. J. Veneklaas, and R. Villar (2004). The world-  
3080 wide leaf economics spectrum. *Nature* 428(6985), 821–827.
- 3081 Xu-Ri and I. C. Prentice (2017). Modelling the demand for new nitrogen fixation  
3082 by terrestrial ecosystems. *Biogeosciences* 14(7), 2003–2017.
- 3083 Zaehle, S., B. E. Medlyn, M. G. De Kauwe, A. P. Walker, M. C. Dietze, T. Hick-  
3084 ler, Y. Luo, Y. P. Wang, B. El-Masri, P. Thornton, A. Jain, S. Wang,  
3085 D. Warlind, E. Weng, W. Parton, C. M. Iversen, A. Gallet-Budynek, H. Mc-  
3086 carthy, A. C. Finzi, P. J. Hanson, I. C. Prentice, R. Oren, and R. J. Norby  
3087 (2014). Evaluation of 11 terrestrial carbon-nitrogen cycle models against  
3088 observations from two temperate Free-Air CO<sub>2</sub> Enrichment studies. *New*  
3089 *Phytologist* 202(3), 803–822.
- 3090 Zaehle, S., S. Sitch, B. Smith, and F. Hatterman (2005). Effects of parame-  
3091 ter uncertainties on the modeling of terrestrial biosphere dynamics. *Global*  
3092 *Biogeochemical Cycles* 19(3), GB3020.
- 3093 Zhu, Q., W. J. Riley, J. Tang, N. Collier, F. M. Hoffman, X. Yang, and G. Bisht  
3094 (2019). Representing nitrogen, phosphorus, and carbon interactions in the  
3095 E3SM land model: development and global benchmarking. *Journal of Ad-*

- 3096** *vances in Modeling Earth Systems* 11(7), 2238–2258.
- 3097** Ziegler, C., M. E. Dusenge, B. Nyirambangutse, E. Zibera, G. Wallin, and  
**3098** J. Uddling (2020). Contrasting Dependencies of Photosynthetic Capacity  
**3099** on Leaf Nitrogen in Early- and Late-Successional Tropical Montane Tree  
**3100** Species. *Frontiers in Plant Science* 11, 1–12.
- 3101** Ziehn, T., J. Kattge, W. Knorr, and M. Scholze (2011). Improving the pre-  
**3102** dictability of global CO<sub>2</sub> assimilation rates under climate change. *Geophys-  
**3103** ical Research Letters* 38(10), L10404.